UNITED NATIONS UNIVERSITY

UNU-GTP

ORKUSTOFNUN

Silica rich waters in Köldulaugagil, Hengill area, SW-Iceland

Tufwane Mwagomba

PRELIMINARY TECHNICAL AND ECONOMIC FEASIBILITY STUDY OF BINARY POWER PLANT FOR CHIWETA GEOTHERMAL FIELD, MALAWI

Report 1
February 2016

UNITED NATIONS UNIVERSITY
UNU-GTP
Geothermal Training Programme

Orkustofnun, Grensasvegur 9,
IS-108 Reykjavik, Iceland

Reports 2016
Number 1

PRELIMINARY TECHNICAL AND ECONOMIC FEASIBILITY STUDY OF BINARY POWER PLANT FOR CHIWETA GEOTHERMAL FIELD, MALAWI

MSc thesis
Iceland School of Energy
School of Science and Engineering
Reykjavik University

by

Tufwane Mwagomba
Malawi Energy Regulatory Authority - MERA
Private Bag B-496
Lilongwe 3
MALAWI
tufwane@gmail.com

United Nations University
Geothermal Training Programme
Reykjavík, Iceland
Published in February 2016

ISBN 978-9979-68-379-7
ISSN 1670-7427

This MSc thesis has also been published in January 2016 by the
Iceland School of Energy – School of Science and Engineering
Reykjavik University

INTRODUCTION

The Geothermal Training Programme of the United Nations University (UNU) has operated in Iceland since 1979 with six month annual courses for professionals from developing countries. The aim is to assist developing countries with significant geothermal potential to build up groups of specialists that cover most aspects of geothermal exploration and development. During 1979-2015, 613 scientists and engineers from 59 developing countries have completed the six month courses, or similar. They have come from Africa (37%), Asia (37%), Central America (15%), Europe (10%), and Oceania (1%). There is a steady flow of requests from all over the world for the six-month training and we can only meet a portion of the requests. Most of the trainees are awarded UNU Fellowships financed by the Government of Iceland.

Candidates for the six-month specialized training must have at least a BSc degree and a minimum of one year practical experience in geothermal work in their home countries prior to the training. Many of our trainees have already completed their MSc or PhD degrees when they come to Iceland, but many excellent students with only BSc degrees have made requests to come again to Iceland for a higher academic degree. From 1999 UNU Fellows have also been given the chance to continue their studies and study for MSc degrees in geothermal science or engineering in co-operation with the University of Iceland. An agreement to this effect was signed with the University of Iceland. A similar agreement was also signed with Reykjavik University in 2013. The six-month studies at the UNU Geothermal Training Programme form a part of the graduate programme.

It is a pleasure to introduce the 46th UNU Fellow to complete the MSc studies under a UNU-GTP Fellowship and the first one to do his studies at Reykjavik University. Tufwane Mwagomba, BSc in Electrical Engineering from Malawi Energy Regulatory Authority - MERA, completed the six-month specialized training in Geothermal Utilization at UNU Geothermal Training Programme in October 2013. His research report was entitled: *Comparative analysis of geothermal power plant designs suitable for Malawi's Chiweta geothermal field.* After one year of geothermal energy work in Malawi, he came back to Iceland for MSc studies at Iceland School of Energy – School of Science and Engineering, Reykjavik University in August 2014. In December 2015, he defended his MSc thesis presented here, entitled: *Preliminary technical and economic feasibility study of binary power plant for Chiweta geothermal field, Malawi.* His studies in Iceland were financed by the Government of Iceland through a UNU-GTP Fellowship from the UNU Geothermal Training Programme. We congratulate him on his achievements and wish him all the best for the future. We thank the Iceland School of Energy – School of Science and Engineering, Reykjavik University for the co-operation, and his supervisors for the dedication.

Finally, I would like to mention that Tufwane´s MSc thesis with the figures in colour is available for downloading on our website *www.unugtp.is*, under publications.

With warmest greetings from Iceland,

Lúdvík S. Georgsson, director
United Nations University
Geothermal Training Programme

ACKNOWLEDGEMENTS

I sincerely thank the UNU-GTP for offering me an opportunity to undertake my studies under this course in Iceland. The UNU-GTP members of staff led by the program director Lúdvík S. Georgsson were so supportive to make both my stay and studies as comfortable as possible. Being a first fellow under the arrangement with my University, it meant the UNU had to learn and do some things for the first time. And it has all made what I have become today.

A special thanks my supervisor Einar Jón Ásbjörnsson for the guidance and support during the thesis and making sure that I was focused. The scheduled weekly meetings always reminded me to have a new thing for the next meeting and this helped to accelerate my work.

Inputs to this work came from a number of individuals and corporates. I appreciate the support from Dr. Páll Valdimarsson who assisted in this work selflessly, I was challenged. The engineers from EFLA Consulting firm for HS Orka at Svartsengi power plant for assisting with practical understanding of binary power plants. Friends from ISE class of 2016 made the way throughout the course to be lighter, and Ximena was just exceptional. UNU fellows both in Iceland and away made contributions in one way or the other, thank you guys.

Thanks to my employer, MERA for releasing me for the studies and much appreciation to all the members of staff who played a role in assisting me pursue this study.

Finally I thank my family for the moral support and belief in me that I can do more, especially my wife and daughter who had to release me and endure with my long absence at a critical time. No words can appreciate your sacrifice.

DEDICATION

I dedicate this thesis work to my wife, daughter and family.

ABSTRACT

Insufficient electricity generation capacity that is failing to meet the ever increasing electricity demand coupled with low electrification rate and low per capita consumption of electricity in Malawi are some of the reasons causing Malawi to search for alternative sources of energy to complement the current predominantly hydro generation capacity. Having manifestation of geothermal in some parts of the country, geothermal energy is being considered for development in line with having a diverse national energy mix.

By virtue of its location in the western branch of the East African Rift System, which is relatively cooler than the eastern branch due to its lower geothermal temperature gradient, developing geothermal in Malawi for electricity generation can focus on utilizing binary technology until such a time when subsurface studies proves otherwise. The field of focus that has high promising geothermal potential in Malawi with the highest geothermal water surface temperature measured so far, is Chiweta geothermal field measuring 79°C.

Technical and economic analysis of four binary power plant models has been done using Engineering Equations Solver software as a technical analysis tool and NPV, IRR and Discounted Payback Period as economic analysis tools. Technical and economic performance of all the four models is satisfactory with wet cooled recuperative binary model emerging the best performer in both analyses. However, due to issues of pressure drop in heat exchangers and the fact that the model's performance is similar to a wet cooled basic binary, it is recommended for Malawi to develop a wet cooled basic binary for its promising Chiweta field which would generate a net power of 10 MW at a total development capital cost of approximately US $49.5 million. The capital cost can be recovered in 17 years at a discount rate of 12% while selling electricity at the prescribed tariff of US $0.105/kWh as informed by Malawi's Feed-in Tariff policy.

TABLE OF CONTENTS

Page

Page

LIST OF FIGURES

Page

LIST OF TABLES

1. INTRODUCTION

As country defined as a growing economy, demand for electricity is ever increasing in Malawi. The current electricity supply industry generates about 351 MW, predominantly from hydro, against a 2014 forecasted maximum demand of 441 MW (MCC-Malawi, 2015), thereby posing an insufficient generation capacity challenge. To cope with the situation, the electricity supply company implements a daily power rationing program that highly affects electricity users and subsequently slowing down the economy of the nation.

To improve the situation, government of Malawi, through the department of energy affairs, is reviewing the Malawi energy policy. The policy under review provided some guidelines to developing energy in Malawi after noting that the country was predominantly relying on biomass as a source of energy (DoE, 2003). The policy sought for alternative ways of diversifying energy sources other than heavily depending on biomass which leads to environmental degradation. As the review is going on, the policy analysis is focusing on what has been done and how best to move Malawi from where it is in terms of energy status. With the intermittent electricity supply, it is evident that electricity supply deserves more attention in the energy policy review. As such Malawi is looking forward to exploiting alternative electricity sources that will complement hydro and geothermal is one of them.

Located within the East African Rift System, Malawi manifests its geothermal resource through hot springs with surface temperatures recorded at 79°C in Chiweta geothermal prospect (GDC, 2010). The resource has not been exploited yet and this report therefore looks at how geothermal in Chiweta, which is one of Malawi's geothermal fields, can be used for electricity generation in order to complement the current hydro generation capacity.

The objectives of this study therefore are:

i. To present binary power plant as the most suitable technology for Chiweta geothermal development,
ii. To conduct a technical analysis of the binary power plant with different options,
iii. To perform an economic analysis of the different binary models as analysed technically,
iv. To propose an economically and technically feasible binary option for development in Chiweta.

The methodology that this study uses include:

i. Literature review,
ii. EES program modelling for technical analysis,
iii. Ratio economic analysis.

This work therefore seeks to present preliminary technical and economic assessment of developing a binary power plant in Chiweta geothermal field in Malawi.

2. BACKGROUND

This chapter is about the geothermal in Malawi in terms of geology, how Malawi is linked to the East African Rift System, and the manifestation of geothermal in Malawi. The chapter further describes the highest temperature field in Malawi and then discusses general utilization of geothermal with focus on electricity generation and the current electricity supply in Malawi.

2.1 Geothermal in Malawi

Malawi is in south-eastern part of Africa and is located between latitudes 9° and 18°S, and longitudes 32° and 36°E. The country is bordered by Zambia to the northwest, Tanzania to the northeast and Mozambique to the southeast, south and southwest. The country lies within the southern part of the western branch of the East African Rift System (EARS), with a total land of 118,000 km^2. Malawi has Lake Malawi as a result of EARS along a bigger part of the east side of the country which is about 580 km long with a maximum width of 75 km. The lake drains its water at the southern end into River Shire, the river on which the major hydro power stations in Malawi are built.

2.1.1 Geology of Malawi

The general geology of Malawi is predominantly underlain by crystalline basement complex rocks of Precambrian to lower Palaeozoic of medium to high grade metamorphism (Chorowicz, 2005). These basement rocks have pelitic and semi-pelitic affinities which are intercalated with calc-silicate gneisses and marble, amphibolites and basic/utrabasic assemblages like pyroxenites and metagabbros (Dulanya et al., 2010). Permian to early Triassic Karoo sedimentary sequences occupy a number of small fault bounded basins within the Precambrian framework, mainly in the North and South-West of the country (Chorowicz, 2005). These are rocks such as sandstones, limestones and mudstones with coal formation. The Jurassic to lower Cretaceous alkaline igneous rocks including granites, syenites, carbonatites, agglomerates, foidolites and associated alkaline dykes interrupted the older sequences especially in the south of Malawi. The alluvial and lacustrine sediments of the Tertiary and Quaternary dominate most of the Lake Malawi shores and major plains in Malawi (GDC, 2010).

Structural control of Lake Malawi Rift is believed to be dominated by a series of segmented N – S rift controlling normal faults (Gondwe et al., 2012), signifying the propagation of the EARS in the N – S direction across the country. Despite the country not being affected by Neogene volcanism, there are some localised sequence of Neogene tuffs (Pleistocene volcanicity) in the northern Malawi. These correlate with the eruption of one of the active volcanoes of south west Tanzania some 10,000 years ago (Gondwe et al., 2012) and the area is believed to be an extension of the Rungwe volcanic province in Tanzania (Dulanya et al., 2010) which is part of the East African Rift System. Map of Malawi showing the geology is presented in Figure 1 below.

The East African Rift System, which is causing the continent of Africa to experience a divergent plate boundary along the rift, extends from Afar triple junction in Djibouti to Beira in Mozambique and is divided into three branches; the eastern branch, the western branch and the south-eastern branch (Figure 2). Malawi lies at the southern end of the western branch of the rift system.

The East African rift system is a series of several thousand kilometres long aligned successions of adjacent individual tectonic basins (rift valleys), separated from each other by relative shoals or uplifted ridges and generally bordered by uplifted shoulders (Hardarson, 2014). The eastern branch has been studied to be more volcanically active than the western branch which is paucity of volcanism (Omenda, 2013). The Western branch runs over a distance of 2100 km from Lake Albert in the north, to Lake Malawi in the south with several segments: the northern segment includes Lake Albert, Lake Edward and Lake Kivu basins; the central segment with the basins of lakes Tanganyika and Rukwa whilst the southern segment corresponds mainly to Lake Malawi and small basins further to the south (Hardarson, 2014). Each segment or basin is controlled by faults and forms a subsiding graben or trough. Limited studies have been done on the south-eastern branch, located on the coast of Indian Ocean in the

east of Tanzania and Mozambique. EARS has exhibited traits of early stages of evolution of passive continental margins preceding oceanic opening and thus it is considered that the East African rift system is an intra-continental ridge system, comprising an axial rift, prelude of oceanic opening (Gondwe et al., 2012).

The EARS can therefore be taken as the beginning of opening of an ocean, between two large continental blocks drifting apart, thus separating the main African plate and the Somalian plate. The EARS continues to propagate southward at a mean rate between 2.5 cm/year and 5 cm/year with evidence of seismic activity creating tension and heat (Chorowicz, 2005).

Recent seismic activities experienced on some border faults in Malawi indicate that the rift-controlling fault system of the Lake Malawi trough is still active (Eliyasi, 2015). Figure 2 shows the East African Rift System.

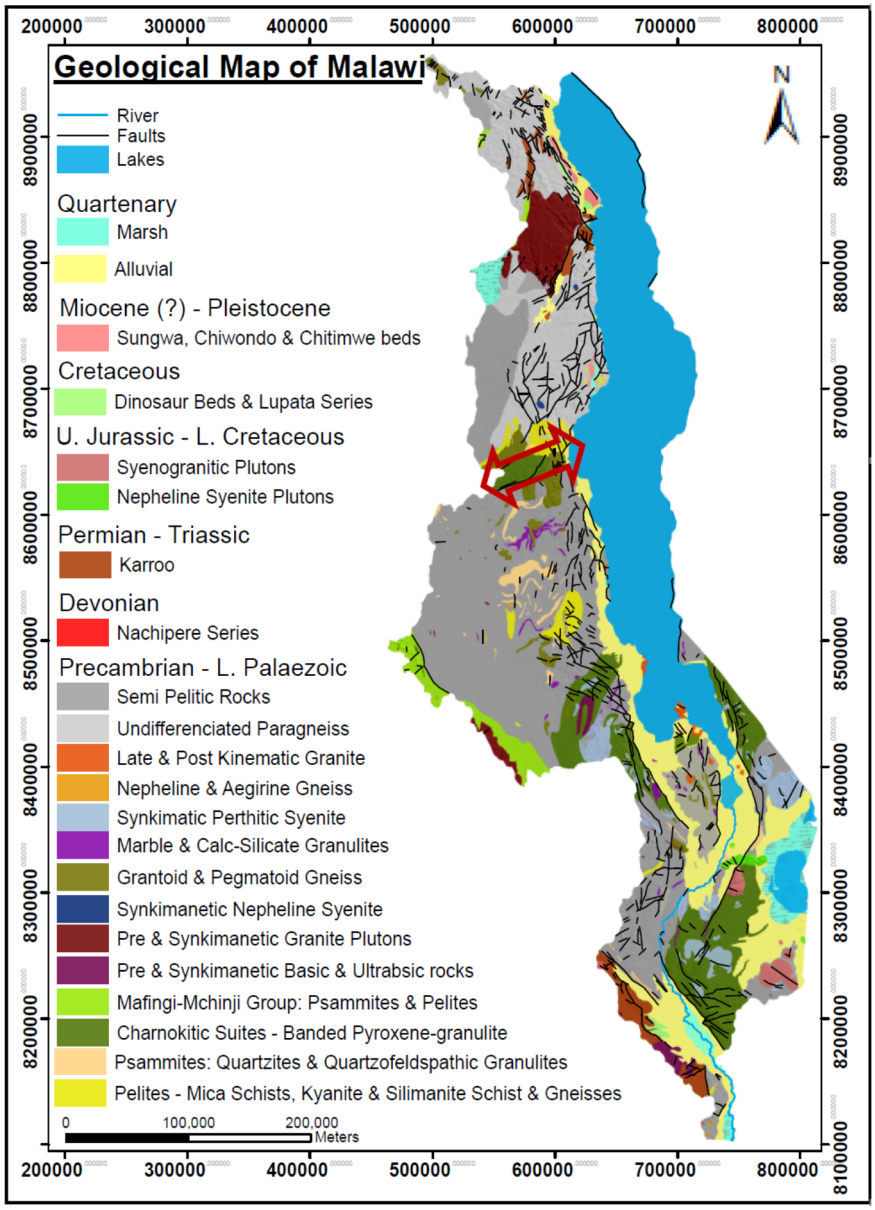

FIGURE 1: Geological map of Malawi. Source: (Mdala, 2015)

The magnitude of movements on the rift-controlling faults suggests that significant thicknesses of Neogene deposits could exist in the rift lowlands bordering Lake Malawi, so aquifers may occur at considerable depth. Geothermal gradients in the EARS vary along the length of the rift system depending on degree of crustal thinning and volcanic activity (Gondwe et al., 2012).

The EARS crustal thinning is related to the lithospheric opening that is occurring in the African continent, which in terms of plate tectonics results from the divergence of large, regional-scale blocks. The rift is at an early stage of development creating some empty basins, some filled with sediments of about 3000 m thick and more, while others filled with volcanic rocks with signs of asthenospheric intrusion (Chorowicz, 2005).

The asthenospheric intrusions in the lithosphere are pronounced along the rift system and are responsible for negative bouguer anomaly along the rift. However, the intrusion is more pronouncing in the north and less pronouncing along the line of EARS propagation towards the south where Malawi is. In Afar region, the crust thickness is around 5 km and the region has high manifestation of geothermal, while moving down south the crust thickness reaches as much as 35 km with sparse geothermal manifestation

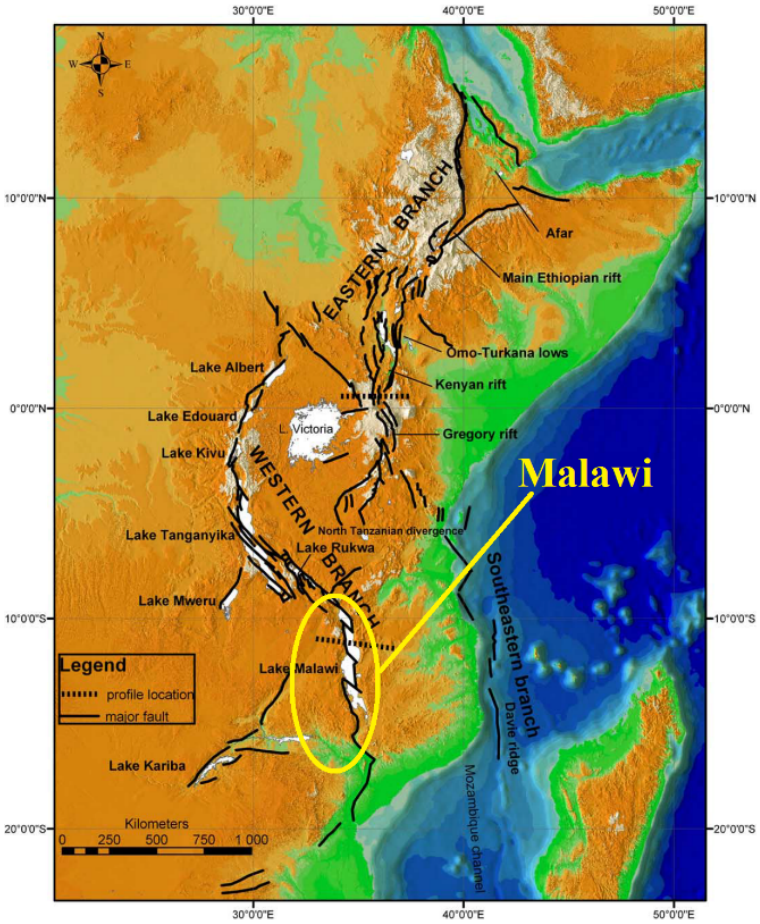

FIGURE 2: The East African Rift System. Source (Chorowicz, 2005)

when compared to the north (Omenda, 2013). The level of upwelling of the asthenosphere coupled with magmatic bodies close to the earth‘s surface relates to the level of geothermal gradient along the rift, and this is partly the reason why the north, i.e. the eastern branch, of the rift system has higher geothermal gradient than the south of the rift system i.e. western branch. Figure 3 shows the principle of the asthesnospheric intrusion along the EARS in relation to crust thinness.

In the volcanically active part of the EARS, where the asthenosphere intrusion is advanced, geothermal gradients of the order of 200°C/km have been estimated on the basis of heat flow measurements (Gondwe et al., 2012). As a result, some of the subsurface temperatures recorded at about 2 km depth for the eastern branch of the EARS include: Alid volcanic centre in Eritrea recording 250°C; Aluto-Langano and Tendaho in Ethiopia recording 350 and 270°C, respectively; and various fields in Kenya recording from 200 to over 300°C (Omenda, 2013;

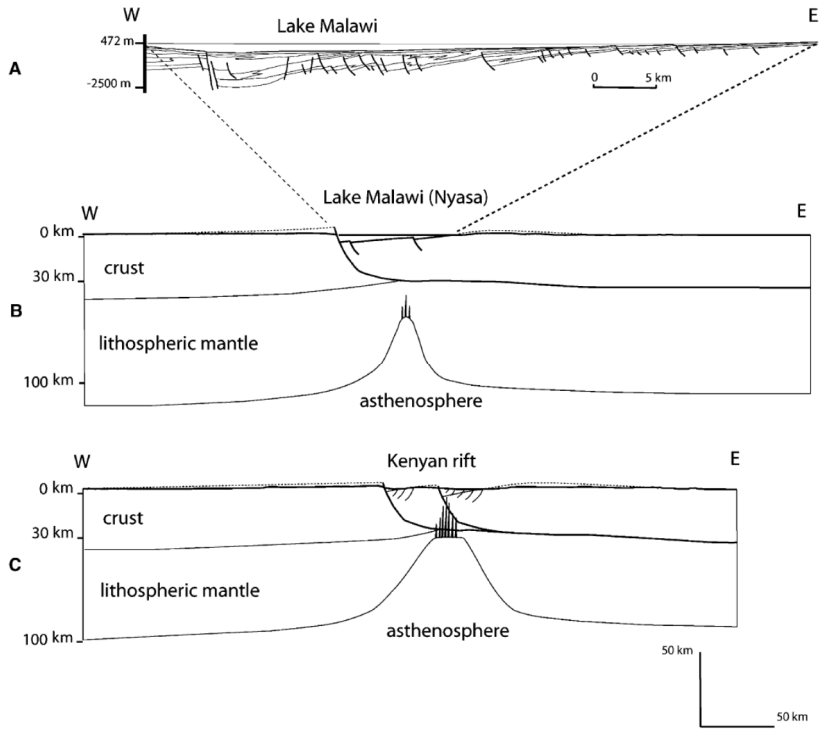

FIGURE 3: Showing (A) seismic reflection profile for L. Malawi, (B) and (C) Inferred lithospheric cross-section of Malawi and Kenya. Source: (Chorowicz, 2005)

Simiyu, 2010). Relatively, the volcanically paucity western branch of the EARS has geothermal gradients ranging from 30 to 140°C/km (Gondwe et al., 2012). Studies conducted in the northern prospect of Rungwe volcanic province in Tanzania, which is one of the few volcanic centres in the western branch, have suggested a geothermal gradient of 95°C/km and even lower gradient in the southern prospects going towards Malawi (Kraml et al., 2010). Some of the estimated subsurface temperatures recorded along the western branch of the EARS include: Barunga and Kibiro in Uganda, 150 and 200°C respectively; Karisimbi in Rwanda, 210°C; and Mbeya in Tanzania >200°C (Omenda, 2013). Gondwe et al. (2012) suggested that geothermal gradient of at least 100°C/km might be expected in the northern sector of the Malawi Rift. With limited studies done to assess the geothermal resource in Malawi, the foregoing concludes that Malawi system has lower geothermal gradient and hence a medium to low temperature geothermal system. Detailed studies are however recommended to be more certain of the kind of resource that Malawi has for appropriate development.

2.1.2 Geothermal manifestation and studies done

Manifestation of geothermal in majority of the sites in Malawi is through hot springs. Studies for Malawi's geothermal have been going on for quite a while, however not much details are yet known about the resource. Most of the studies have concentrated on reconnaissance surveys. There are over 60 hot springs documented in Malawi with some of them having their water studied for geochemistry to understand the nature of reservoir, their temperature and the origin of the water in the system. Most of the work done on the thermal springs focused on mapping litho-structural control and the physio-chemical characteristics of the hot springs (Dulanya et al., 2010). Such studies have revealed that location of the hot springs tend to be along or near the intersection of major faults within the rift valley, in other words the springs are controlled by the faults.

The recorded surface temperatures of the hot springs are between 28 and 79°C (GDC, 2010) with some anticipation of beyond 80°C in some cases. Field report submitted to Geological Surveys Department of Malawi by the Geothermal Development Company of Kenya about the hot springs' geochemistry suggests that most of the water are immature and have not attained equilibrium thereby presenting some degree of uncertainty in geothermometry (GDC, 2010). The immaturity of the water may be either as a result of thermal water mixing with ground fresh water or that the system is permeable and fast recharging. However, subsurface temperature studies done using sodium potassium (Na-K) geothermometers have indicated a temperature range of 169^0 - 249^0C (GDC, 2010). The Na-K geothermometry gives a good indication for surface exploration that there is a resource in Malawi. However, more study is encouraged to truly ascertain the details of the resource in terms of actual resource temperature, depth and size of the resource for appropriate utilization.

The majority of hotter springs in Malawi are located in the northern part of the country and this includes the most promising field (Chiweta) which records the highest measured surface temperature. Most of the springs have basic pH signifying that they are weak to affect alteration in their host rocks. Most of the springs are also overlain by sedimentary rocks thereby the absence of alteration (Eliyasi, 2015). In tandem with the studies conducted in the western branch of EARS, utilization of the geothermal resource in this region is suggested through binary electricity power generation and other direct uses (Hardarson, 2014) due to its low temperature geothermal gradient.

2.2 Description of Chiweta geothermal field

Located at coordinates 10°13´S and 34°16´ E at an altitude of about 480 m a.s.l., is Chiweta one of local trading centres in the northern part of Malawi. Chiweta is located within the deep seated border fault which acts as a conduit for geothermal water (Eliyasi, 2015) and it hosts the hottest geothermal hot springs recorded so far in Malawi (GDC, 2010) which are located to the immediate north of North Rumphi river, at the edge of Mkerakera hill. Within a distance of 1.5 km to the east of the hot springs lie Lake Malawi as shown in Figure 4 below.

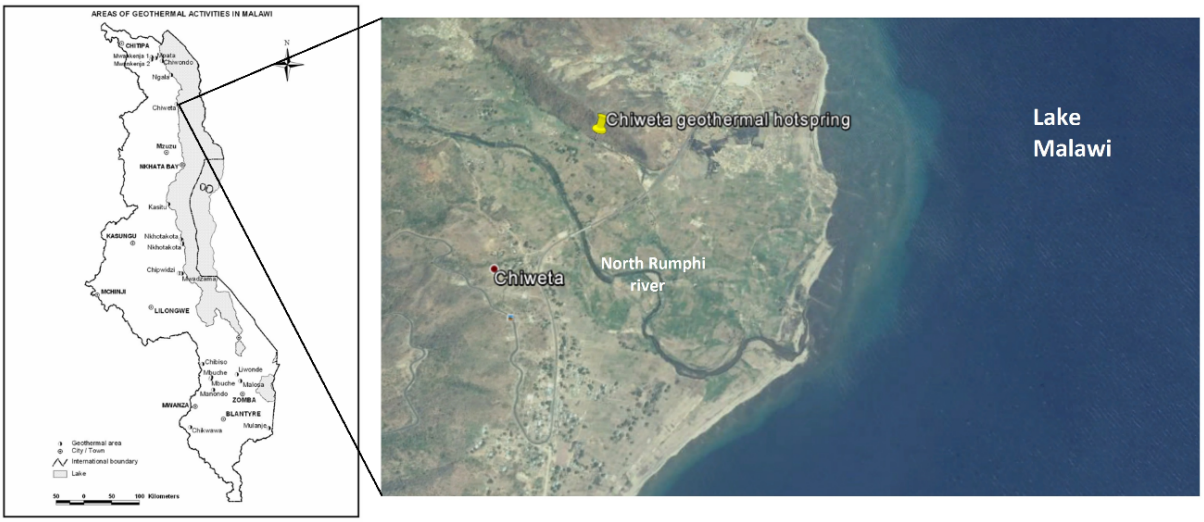

FIGURE 4: Location of Chiweta hot spring. Source: adapted from (Dulanya et al., 2010)

The area experiences tropical climate and receives more rainfall in the months of November to April than the rest of the year. The annual average temperatures experienced in the area are around 24.4°C with highest temperatures experienced in November and lowest temperature in July (Climate Data, 2015). The area receives an average annual rainfall of 1081 mm. The climate summary is depicted in Figure 5.

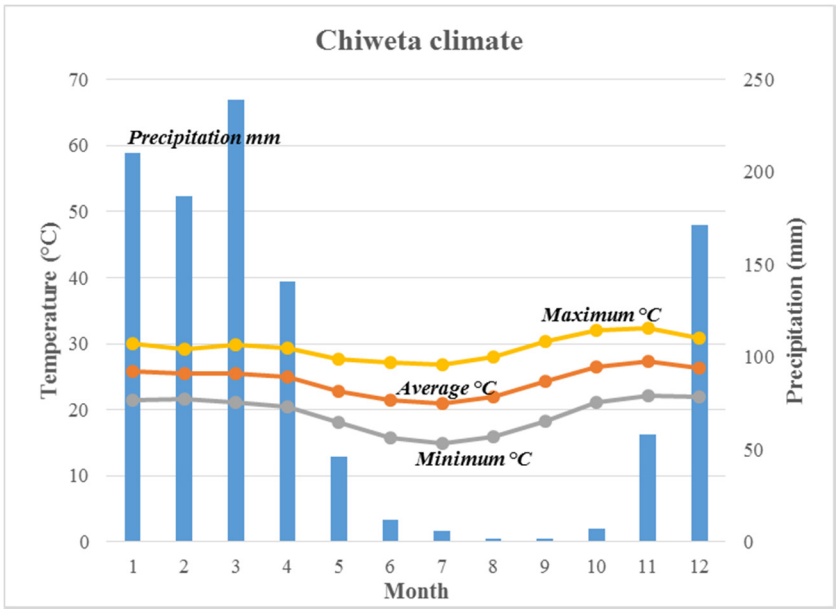

FIGURE 5: Chiweta climate showing temperature and precipitation. Source: adapted from (Climate Data, 2015)

The local geology of Chiweta has an underlain of gneisses, schist and granites of the Malawi Basement Complex of Precambrian to Lower Palaezoic age. The gneiss rocks are mainly biotite and biotite garnet gneiss, biotite sillimanite gneiss and cal-silicate gneiss (Eliyasi, 2015).The area has a number of hot springs occurring along the line of the E-W fault which forms the southern boundary of the Chiweta beds (Eliyasi, 2015). Some of the hot springs are clearly visible while others discharge beneath a stream called Mphizi. Reconnaissance studies done so far through surface temperature and chemistry of geothermal water, have indicated that Chiweta hosts the hottest geothermal hot springs recorded in Malawi, with a maximum surface temperature of 79°C and Na-K geothermometer subsurface temperature of 249°C (GDC, 2010).

The chemistry of water from Chiweta hot spring indicates rich chloride content and promising the highest input of geothermal fluid. The area has a strong sulphur smell and there are visible sulphur deposits around the spring (Figure 6).

The presence of sulphur deposits is a strong indication that the area has a good geothermal resource. When remote sensing and geological data integration techniques were used to assess the potential of

geothermal resource in northern Malawi, Chiweta provided very promising results for the country (Eliyasi, 2015). However, more studies need to be done for Chiweta to ascertain the extent of field's hydrological system in terms of recharge zones, reservoir and related size subsurface characteristics.

FIGURE 6: A hot spring in Chiweta with sulphur deposits, discharging into Mphizi stream. (Photo taken on 09/08/2015)

2.3 Geothermal utilization

Utilization of geothermal resource refers to the extraction of mass and heat from a geothermal resource to meet various energy demands. Geothermal resources are classified based on different aspects such as temperature, enthalpy and nature of their geological setting (Saemundsson et al., 2011).

The majority of the classification is based on the temperature of the system i.e. low temperature and high temperature systems. A lot of authors have provided different levels of temperature to classify geothermal systems but this study adopts the classification as low temperature, medium temperature and high temperature resource (Mburu, 2013). The low temperature systems are the ones with temperature of 150°C and below at 1 km depth and the high temperature systems are the ones with temperature of 200°C and above at 1 km (Saemundsson et al., 2011). The systems with temperature between 150 and 200°C are called medium temperature systems.

A summary of classification based on temperature, enthalpy and physical state of a system is presented in Table 1 below as summarized by Saemundsson et al. (2011).

TABLE 1: Categories of geothermal systems based on temperature, enthalpy and physical state (Saemundsson et al., 2011)

<table>
<tr><td>Low-temperature (LT) systems with reservoir temperature at 1 km depth below 150°C. Often characterized by hot or boiling springs.</td><td rowspan="2">Low-enthalpy geothermal systems with reservoir fluid enthalpies less than 800 kJ/kg, corresponding to temperatures less than about 190ºC.</td><td rowspan="2">Liquid-dominated geothermal reservoirs with the water temperature at, or below, the boiling point at the prevailing pressure and the water phase controls the pressure in the reservoir. Some steam may be present.</td></tr>
<tr><td>Medium-temperature (MT) systems with reservoir temperature at 1 km depth between 150- 200°C.</td></tr>
<tr><td rowspan="2">High-temperature (HT) systems with reservoir temperature at 1 km depth above 200°C. Characterized by fumaroles, steam vents, mud pools and highly altered ground.</td><td rowspan="2">High-enthalpy geothermal systems with reservoir fluid enthalpies greater than 800 kJ/kg.</td><td>Two-phase geothermal reservoirs where steam and water co-exist and the temperature and pressure follow the boiling point curve.</td></tr>
<tr><td>Vapour-dominated reservoirs where temperature is at, or above, boiling at the prevailing pressure and the steam phase controls the pressure in the reservoir. Some liquid water may be present.</td></tr>
</table>

In terms of geological setting, Saemundsson et al., (2011) classifies geothermal resources further as volcanic, convective fracture controlled, sedimentary geo-pressured, hot dry rock also known as enhanced/engineered geothermal system (EGS), and shallow resources. Of these classifications, the most commonly encountered geothermal systems are the volcanic systems, convective and the sedimentary systems and these are defined as follows:

a. Volcanic geothermal system is associated with volcanic activity and the system's heat source is hot intrusion or magma. Most of these systems are located at plate boundaries and some in hot spot areas and the system's water flow is controlled by permeable fractures and fault zones.
b. Convective systems have the hot crust at depth as a heat source in tectonically active areas. In this system, water travel at a considerable depth (> 1 km) through vertical fractures to mine the heat from the rock.
c. Sedimentary geothermal system have permeable sedimentary layers at depth (> 1 km) with a geothermal gradient of more than 30°C/km and they are mostly conductive in nature even though some may be convective.

In terms of geological setting, Saemundsson et al., (2011) classifies geothermal resources further as volcanic, convective fracture controlled, sedimentary geo-pressured, hot dry rock also known as enhanced/engineered geothermal system (EGS), and shallow resources. Of these classifications, the most commonly encountered geothermal systems are the volcanic systems, convective and the sedimentary systems and these are defined as follows:

a. Volcanic geothermal system is associated with volcanic activity and the system's heat source is hot intrusion or magma. Most of these systems are located at plate boundaries and some in hot spot areas and the system's water flow is controlled by permeable fractures and fault zones.
b. Convective systems have the hot crust at depth as a heat source in tectonically active areas. In this system, water travel at a considerable depth (> 1 km) through vertical fractures to mine the heat from the rock.
c. Sedimentary geothermal system have permeable sedimentary layers at depth (> 1 km) with a geothermal gradient of more than 30°C/km and they are mostly conductive in nature even though some may be convective.

Most of the high-temperature geothermal systems are associated with the volcanic geological setting while most medium- to low-temperature systems are associated with convective and sedimentary geological setting (Saemundsson et al., 2011).

With the studies done so far, there is not much indication of volcanism for the Malawi system which may determine the system as a high-temperature system. As such Malawi is therefore considered as having a medium- to low-temperature geothermal system associated with convective or sedimentary system as evidenced by the presence of limestone and sandstone in its geological setting. This plays a role in guiding what kind of utilization for the resource would be. However, more studies on the resource may reveal the real identification of the system.

For many centuries around the world, geothermal water has been used for bathing, cooking and heating. Studies and more experience on geothermal resources of various temperature over the years have contributed to utilizing the resources in meeting various energy needs as proposed in the Lindal diagram (Figure 7). Lindal's diagram proposes use of resources with temperature above 120°C for electricity generation. Outside the proposed

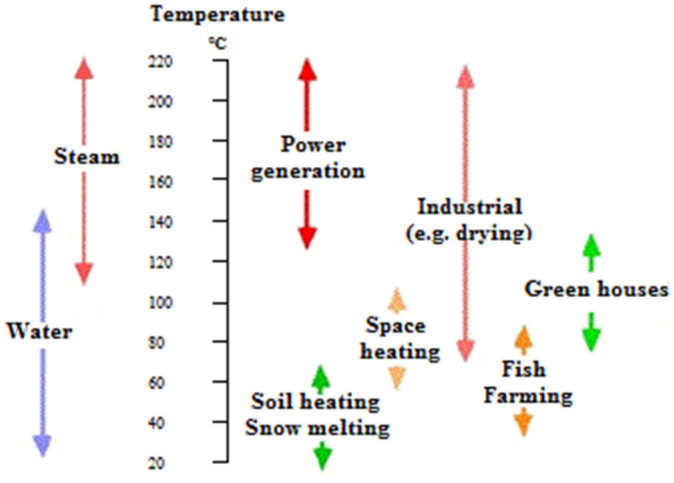

FIGURE 7: Lindal's geothermal utilization diagram. Source: modified from (Ragnarsson, 2006)

temperature ranges, utilization for electricity may be applicable but not economical.

Utilization of geothermal, which is influenced by the temperature of the resource, may be broadly categorized into electricity production, direct utilization and other applications. Electricity production from geothermal energy is the main use of geothermal resource in areas where the resource has adequate temperature. Generation of electricity using geothermal energy normally utilizes a resource that gives a fluid temperature of around 120°C and above, according to Lindal's diagram. The electricity generation is through binary technology and steam-flash technology. It has been studied that generation of electricity in this temperature range is commercially viable even though with advancement in technology lower temperatures are also being explored for binary power plants (Bertani, 2010).

Under direct utilization, energy in the geothermal water is used without any conversion for such things as; bathing and spas, district heating, aquaculture, greenhouses and various industrial processes.

Malawi belongs to the convective or sedimentary system and hence subsurface temperatures expected to be not more than 200°C. Utilization of such resource is therefore more realistic to use binary technology for electricity production, and many direct utilization applications.

2.4 Electricity supply in Malawi

The national population of Malawi was at 13 million people according to population census of 2008 and is estimated to be at 16.4 million people in 2014 (NSO, 2010). Of this population, only around 10% have access to the national grid electricity (Taulo et al., 2015). A large portion of the population that is not connected to the grid electricity, rely on other alternative sources of energy such as biomass for their daily needs.

According to the department of energy affairs, Malawi energy mix is predominantly dependent on biomass in the form of firewood and charcoal (DoE, 2003). The current status of energy mix pause a big challenge over the natural vegetation of Malawi as trees are wantonly cut to meet the energy demand without regard on their sustainability. The Malawi government came up with the National Energy Policy of 2003 which among others focused on improving efficiency and effectiveness in energy supply industries and improving security and reliability of energy supply systems as well as mitigating environmental impacts of energy production and utilization. The policy wanted to reduce over-dependence of biomass as energy source by increasing energy supply from other alternative sources (DoE, 2003). Despite having the policy in place, Malawi has stagnated in developing its alternative sources of energy in general and the electricity sector in particular, to meet the growing demand.

Malawi has a vertically integrated system of electricity supply industry and the major player of the industry is the Electricity Supply Corporation of Malawi (ESCOM), a government owned company. ESCOM owns the hydro power plants in Malawi, transmission lines and distribution system. The current installed electricity generation capacity for Malawi which is connected to the national grid is 351 MW (MCC-Malawi, 2015) and this is predominantly generated from hydro, making over 95% of the total capacity. There are some small scale off grid generators that are not included in this figure. All the major power stations are located in the southern part of Malawi along a single river Shire, which runs out of Lake Malawi. The projected maximum demand for electricity in the year 2014 was at 447 MW (MCC-Malawi, 2015). There has been no additional electricity generation into the grid this far despite continual connection of new customers onto the grid in a quest to boost the national access to electricity rate. This means that the electricity industry is affected by insufficient generation capacity that is failing to satisfy the current increasing demand. Apart from insufficient generation, poor service quality that comes with transmission and distribution losses emanating from long transmission distances, ageing equipment as well as environmental effects, affect the operations of the hydro power plants to the effect of reducing power production capacity further affecting the delivery of electricity. Because of these problems, customers are subjected to power rationing where load-shedding programmes are the order of the day as the utility company manages the electricity supply. This kind of electricity supply negatively affects the economic activities in the country.

With the erratic supply of electricity that the country experiences coupled with will development of electricity supply projects, the country's dependence on biomass may be higher than the currently projected as presented in Table 2.

TABLE 2: Energy Mix Projections 2000 – 2050. Source: adapted from DoE (2003)

Energy source	2000	2010	2020	2050
Biomass	93%	75%	50%	30%
Liquid Fuels	3.5%	5.5%	7%	10%
Electricity (hydro)	2.3%	10%	30%	40%
Coal	1%	4%	6%	6%
Renewables	0.2%	5.5%	7%	10%
Nuclear	0%	0%	0%	4%
TOTAL	**100%**	**100%**	**100%**	**100%**

Malawi has one of the lowest electricity consumption per capita in the world which stands around 93kWh (Taulo et al., 2015). With this fact, the country stands below the recommended sub-Saharan electricity consumption per capita rate of 432kWh, let alone the world's recommended average per capita rate of 2167kWh (Taulo et al., 2015). This means the country needs more energy projects to improve on its per capita consumption, which in a way assists in improving the living standards of the people.

With the electricity challenges being faced by the country and the desire to provide affordable and clean energy for the populace, it has become imperative for the country to review and assess the role of alternative sources of energy for the country to boost its energy capacity. The Department of Energy Affairs has embarked on a process of reviewing the energy policy in order to have a policy that is responsive to the prevailing energy ills. The reviewed policy is expected to incorporate various potential alternative energy sources in Malawi that would in one way or the other provide lasting solutions to the energy problems. Amongst the potential candidates, geothermal power technology is being considered for development that would assist in meeting the growing energy demand of the country. Being in the western branch of the EARS, this study therefore focuses on designing a binary cycle for Malawi's Chiweta geothermal resource that the country may adopt for development.

3. GEOTHERMAL POWER PLANT TECHNOLOGIES

Geothermal power plants are divided into two main categories: the steam cycle power plants and binary cycle power plants (Valdimarsson, 2010). Steam power plants convert thermal energy from geothermal fluid to electricity by letting the fluid boil (flashing), or using dry steam directly from the resource where the resource has the capacity to produce steam. Binary cycle power plants generally utilize the geothermal fluid in liquid form, without flashing, to produce electricity. Some binary plants are coupled to a steam-flash cycle (hybrid) to use the exhaust heat from the flash plant thereby improving cycle thermal efficiency of the entire system. Binary plants use two cycles with different fluids, the geothermal fluid in one cycle as a source of heat, and an organic fluid in the other cycle.

The two categories of power plants are further divided into various sub-types of power plants. For steam cycle plants, these include: Single-flash steam plants, double-flash steam plant, and cascaded-flash plants. For binary or Organic Rankine Cycle (ORC), there is the ordinary binary plant and the Kalina cycle. There is also a combination of flash plant with an ORC plant which sometimes is called hybrid plant. Application of a type of power plant technology mostly depends on specific characteristics of a given geothermal field in terms of resource temperature vis-à-vis enthalpy, and whether the field is steam dominated or liquid dominated. The power plant categories are discussed further below.

3.1 Steam-flash power plants

In steam-flash plant it is assumed that the geothermal fluid is a compressed liquid from the reservoir. The common assumption is based on the fact that generally dry steam reservoirs are very rare (DiPippo, 1999). Where vapour dominated reservoirs exist, direct-steam plants are used, and otherwise the assumption holds.

In a single-flash power plant, with reference to Figure 8, the geothermal fluid travels towards the surface and it experiences a flashing process along the way due to drop in pressure from the reservoir pressure. The fluid is directed to the power plant's separation station from wells in pipelines passing through the wellhead unit. The wellhead unit has a valve that is responsible for adjusting pressure of the fluid by throttling, causing the fluid to boil further thereby creating a mixture with more steam fraction than in the well.

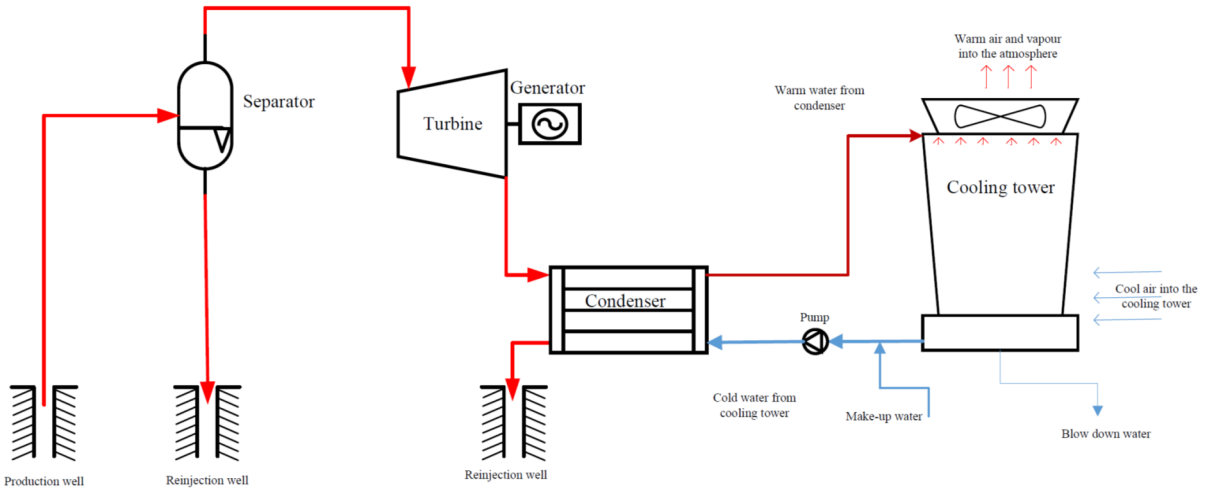

FIGURE 8: Process flow diagram of a single-flash power plant

The steam is expanded through the turbine thereby providing a mechanical force that drives the turbine. The turbine is coupled to a generator that eventually generates electricity as the steam is being expanded through the turbine.

After passing through the turbine, the steam is either released into the environment in a case of a back-pressure power plant, or it is sent to a cooling system through a hot well in a case of a condensing steam power plant. The condensate is then either directed to reinjection wells or may be used as make up water in the power plant's cooling system.

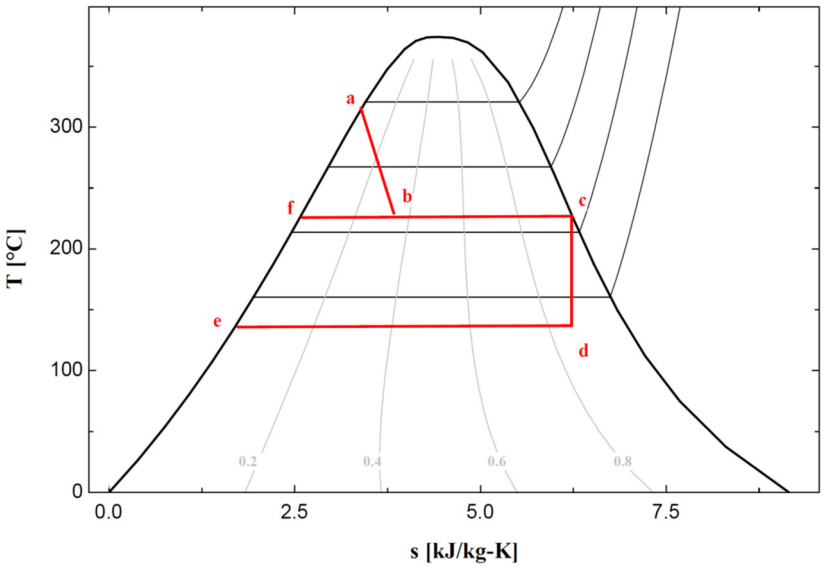

FIGURE 9: Typical T-s diagram for a single-flash power plant

The brine from the separator, which is not required to flash further, is directed to reinjection wells or directed for other utilization such as district heating where the chemistry allows. A typical thermodynamic process for a single-flash cycle follows a T-s diagram as shown in Figure 9.

In Figure 9, point [a] is the state of the fluid in the reservoir and is being flashed along the way as it goes to the surface, reaches the separation station at [b]. From point [b], steam is directed to the turbine at [c] while brine is directed to reinjection at [f]. The steam at [c] is expanded through the turbine through isentropic process and reaches the condenser at [d] where it is condensed at [e], sent to reinjection or as make-up water to the cooling system.

In some instances where the enthalpy of the fluid allows, the brine from the separator may be throttled down to a lower pressure and then passed through a low pressure separator thereby collecting low pressure steam. The low pressure steam thereof is directed to low pressure stages of the turbine or to a low pressure turbine, making the cycle a double-flash power plant. Double-flash power plants are normally associated with high enthalpy geothermal fields with temperatures in excess of 240°C. The process flow diagram for a double-flash cycle is as shown in Figure 10. Figure 11 shows a typical T-s diagram for a double-flash power plant. Point [a] is the state of the fluid in the reservoir and is being flashed along the way as it goes to the surface, reaches the high pressure separation station at [b]. From point [b], steam is directed to the high pressure stage of the turbine at [c] (or in some cases a high pressure turbine) while brine is directed towards low pressure separator at [f]. The steam at [c] is expanded through the turbine through isentropic process and reaches the condenser at [d] where it is

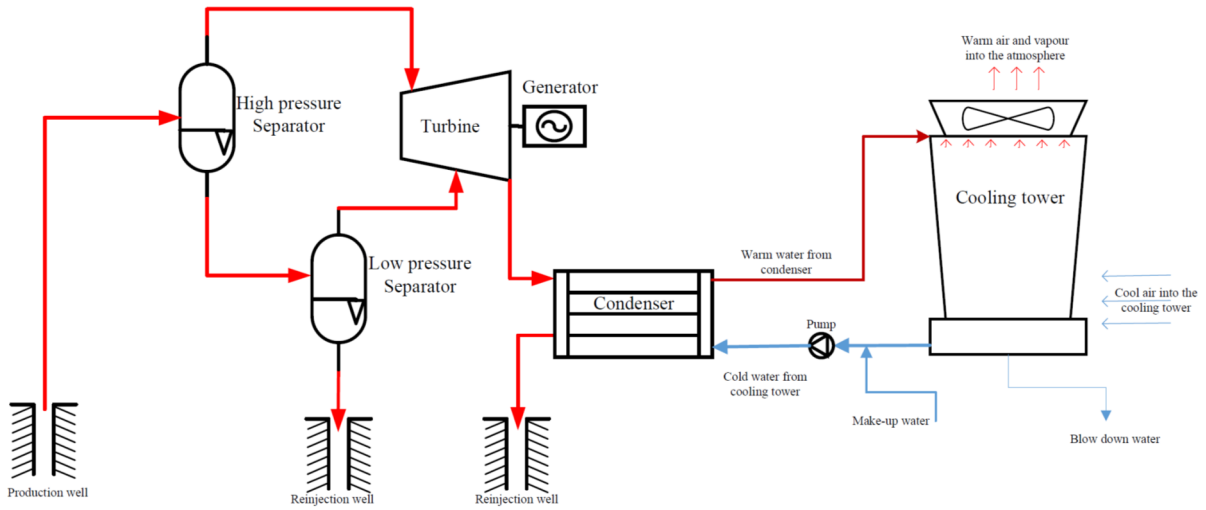

FIGURE 10: Process flow diagram for a double-flash power plant

condensed at [e], sent to reinjection or as make-up water to the cooling system. Brine from [f] is directed to the low pressure separator at [g]. The steam from the low pressure separator is directed to the low pressure stage of the turbine at [h] (or in some cases a low pressure turbine), while brine is directed to reinjection at [j]. The low pressure steam is expanded through the turbine and reaches the condenser at point [i]. The steam is then condensed to reach point [e] just as in high pressure steam and the condensate is either reinjected or used as make-up water in the cooling system. The process is presented in T-s diagram in Figure 11.

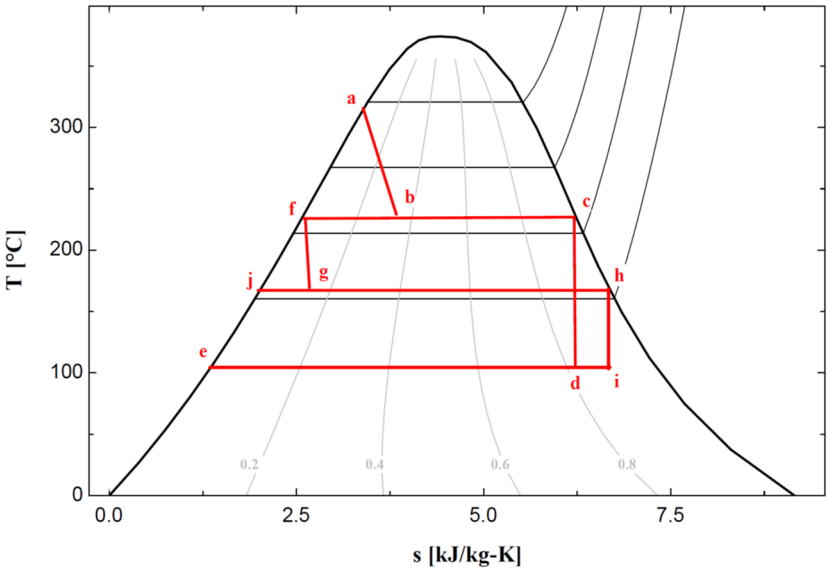

FIGURE 11: Typical T-s diagram for a double-flash power plant

Even though experimental machines are trying to use two-phase fluid to eliminate the separator for turbine running, the general approach is mostly separating the two phases for the conventional power plants (DiPippo, 1999). However, other studies are trying to implement steam-flash power plants on medium- to low-temperature resources at temperature levels of 120°C with an aim of lowering the power plant's costs, lower than binary power plants of similar capacity (Pritchett, 1996). Such applications are currently limited to smaller generation capacities normally in the order of a few kW to 1 MW.

3.2 Binary cycle power plant

Binary cycle plants or Organic Rankine Cycle (ORC) as they are also known, are used to generate electricity from medium- to low-temperature geothermal resources (Valdimarsson, 2010) and they help to increase efficiency of geothermal fluid through recovery of heat from waste fluid of steam-flash power plants. Binary power plants use a secondary working fluid, which is organic, to produce electricity. The secondary working fluid has a low boiling point and a high vapour pressure at low temperatures when compared to water (Maghiar and Antal, 2001).

The optimal temperature range for utilizing binary power plants varies from author to author. Some have given a temperature range of 80 - 170°C (Maghiar and Antal, 2001), others a range of 120 - 190°C (Elíasson et al., 2008) while yet others a range of 100- 220°C (Hettiarachchi et al., 2007). This work therefore considers that an optimal temperature range for binary application is 85 - 220°C. When a binary cycle is applied for a field with temperature above the upper temperature limit, there are issues of thermal stability with the organic fluids (Maghiar and Antal, 2001). On the other side, applying the binary cycle in the lower temperature limit becomes impractical and uneconomical. At low temperature, the heat exchanger size for a given capacity becomes impractical and the parasitic loads requires a large percentage of the power generated.

The medium- to low-temperature geothermal resources are in abundance worldwide and this makes the use of binary power plants to be popular in electricity generation applications for geothermal utilization.

In a binary plant, the thermal energy of the geothermal fluid in the primary cycle is transferred to the secondary working fluid by means of heat exchangers. The working fluid is first preheated in the preheater and then changed to steam (vaporized) in the vaporizer. The vaporized working fluid is directed to the turbine where it is expanded as it drives the turbine. The turbine is coupled to a generator,

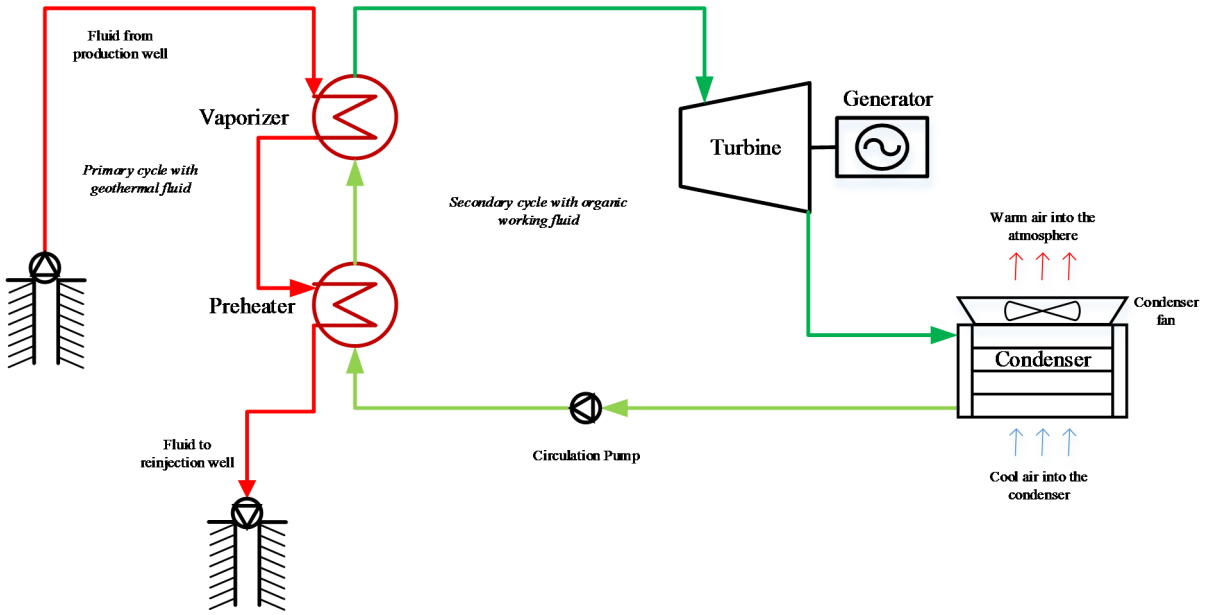

FIGURE 12: Process flow diagram of a dry cooled Binary cycle power plant

therefore as the turbine is being driven by the vaporized working fluid, it is also driving the generator thereby generating electricity. The vapour is then condensed in the condenser and returned to the heat exchanger in a closed loop by means of a circulating pump and the process continues in the cycle. The diagram of the binary process is depicted in Figure 12.

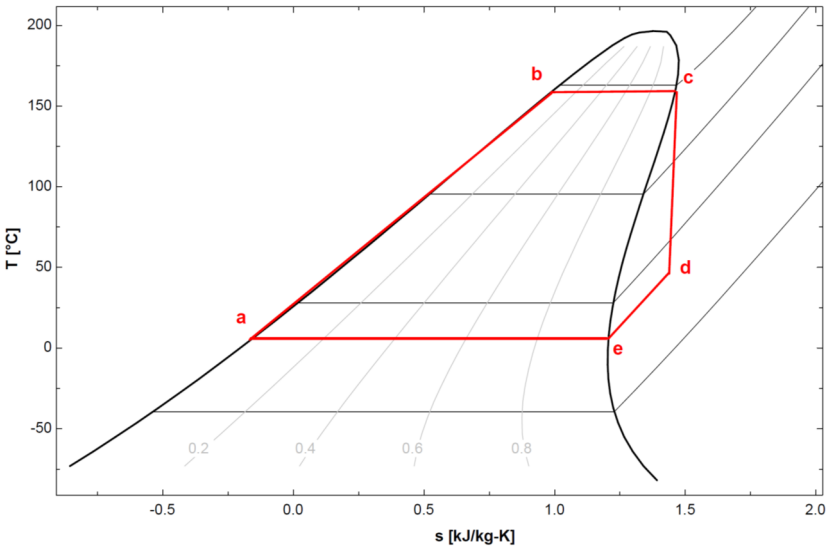

FIGURE 13: A typical T-s diagram for a binary cycle using dry fluid

A typical thermodynamic process for a binary cycle follows a T-s diagram as shown in Figure 13. There point [a] is after the circulation pump where working fluid pressure is raised. The working fluid is pushed through preheater to point [b] and then changed into vapour at point [c] through a vaporiser. The vaporized fluid is then expanded through a turbine in an isentropic process while it generates turbine work until it reaches a condenser at point [d]. The vapour is then cooled to condenser temperature and then condensed in the condenser to saturated liquid at point [a] which is the circulation pump. The process then repeats and continues to repeat at steady state conditions.

Work of improving the binary cycle has seen the coming in of a Kalina power plant. The Kalina cycle utilizes ammonia and water mixture as its working fluid and the geothermal fluid in its primary cycle just like the basic binary power plant (Valdimarsson, 2010). The cycle does not go into superheated condition, as such the working fluid is not entirely boiled as it leaves the vaporizer. The flow process of a Kalina cycle is explained according to Valdimarsson (2010). The working fluid from the vaporizer passes through a separator which separates liquid fluid and vapour. Thereafter, the vapour is expanded through the turbine, producing electricity in the process. As the vapour exits the turbine towards the condenser, it is mixed with the fluid coming from the high temperature regenerator. The mixture pre-

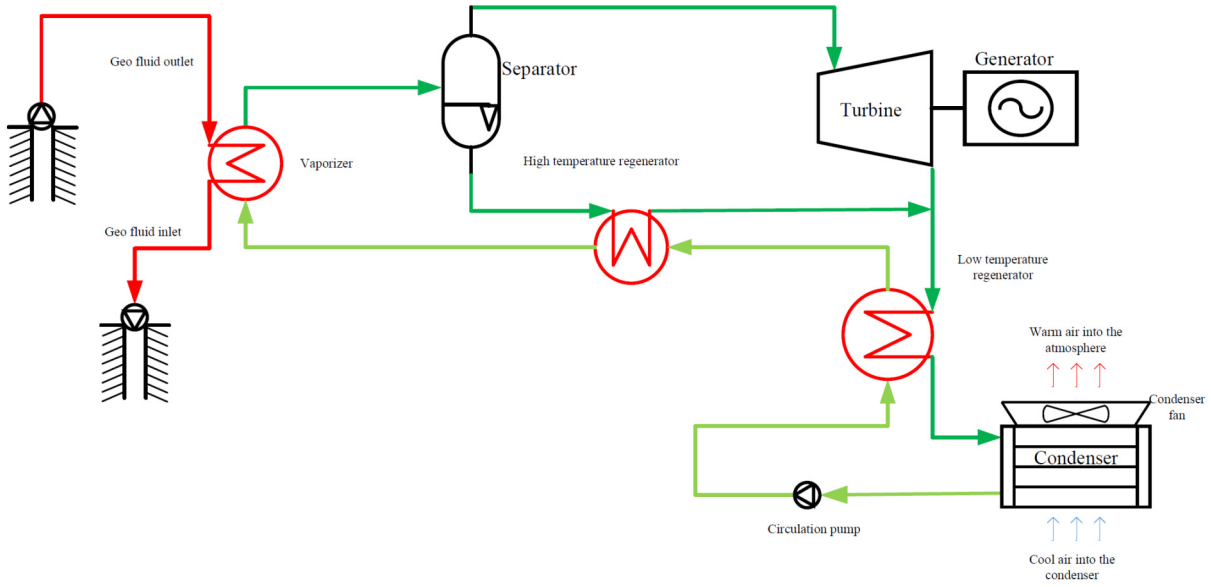

FIGURE 14: Schematic diagram of a Kalina cycle power plant.
Source: Adapted from Valdimarsson (2010)

heats the working fluid in a low temperature regenerator before being condensed in the condenser. From the condenser the fluid is pressurised for high pressure side by a circulation pump, then passes through the low temperature regenerator for the first pre-heating and then to the high temperature regenerator for a second pre-heating before being sent to the vaporizer. The fluid in the high temperature regenerator is heated by the fluid that comes from the separator which is of higher enthalpy. The schematic diagram for the Kalina process is as shown in the Figure 14.

With such levels of regeneration, a Kalina cycle has the advantage in that it allows a higher heat exchange effectiveness to be achieved over and above the traditional binary plant. It is estimated that Kalina power plants are up to 50% more efficient as compared to the traditional binary power plants (Mlcak, 2002) even though they are not yet as popular as the traditional binary plants. The Kalina power plant can be deemed as still under prototype studies and that their development may not be that economical.

Binary power plants are mostly considered to be viable energy conversion systems technically and environmentally when compared with the other types of geothermal energy conversions technologies because of the assurance of reinjecting almost all the fluid that is extracted from the reservoir. There is no flashing of the fluid in the binary application and hence no release of non-condensable gases into the environment.

With the advancement in technology and the demand for cleaner energy that geothermal offers, binary power plants, or ORC, are becoming popular in areas where the reservoir is of low enthalpy characteristic. Binary plants are as well being implemented for further utilization of geothermal brine from flash power plants where temperature allows and thereby improving the overall power plant's efficiency.

3.3 Combined cycle power plant

A combined cycle or hybrid power plant is a combination of steam-flash and binary cycles. A binary cycle is combined with single flash or a double flash depending on the levels of field enthalpy. The binary cycle may be used as a bottoming power plant where primary source of heat for the binary plant is either the steam from a back-pressure single-flash plant or the brine from the separator station. Using this fluid which would otherwise be lost into the environment, the binary plant assists in producing more megawatts to the power plant. As such, the binary cycle helps to improve the overall efficiency of the

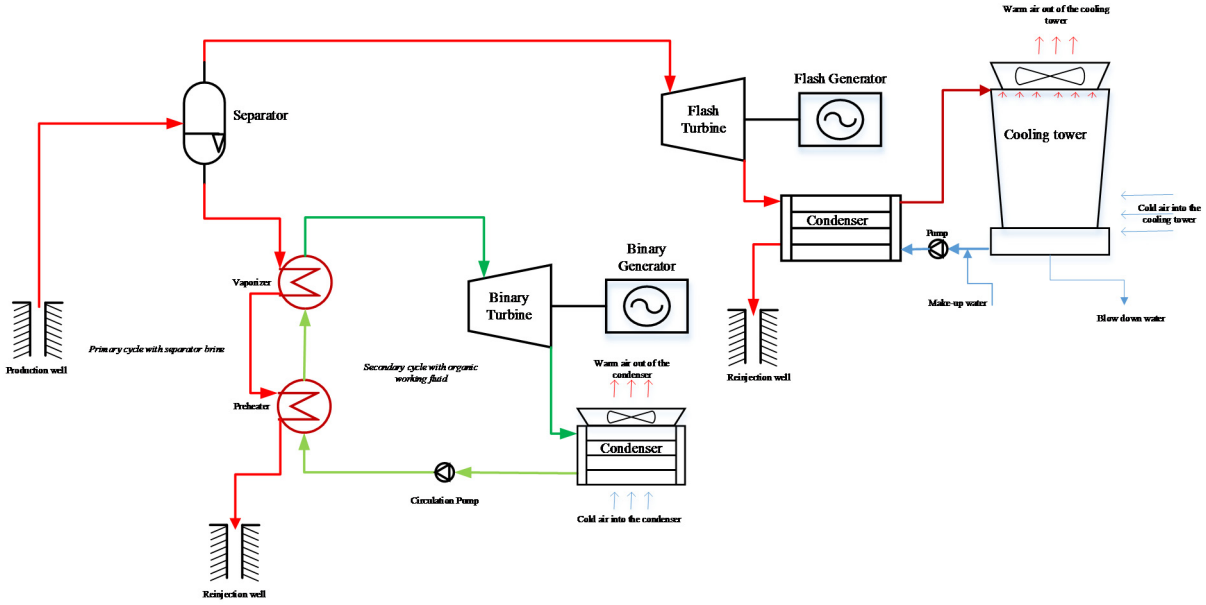

FIGURE 15: Combined single-flash and binary power plant

system. The rest of the cycles are as explained earlier. A schematic diagram of a combined single-flash and a binary plant that utilized the separator brine from the separation station is as shown in Figure 15.

A suitable power plant design for any field is supposed to match with the field's parameters in terms of enthalpy, mass flow and chemistry, at the same time it is supposed to be reliable and environmentally friendly while being economically viable. Previous studies based on the geochemistry data available for Malawi, indicated that Malawi may develop its geothermal resource through single-flash power plant, binary power plant or hybrid of single-flash and binary cycle power plant with an emphasis on the combined cycle (Mwagomba, 2013). However, with limited data available, it is extremely difficult to be certain that Malawi would develop a single-flash plant. Howbeit, basing on the knowledge of power plants and the little information on Malawi coupled with the facts of the western branch of the EARS where Malawi belongs, it can be proposed that Malawi would develop a modular binary power plant as the most suitable power plant for the Chiweta field. As the power plant is developed and being utilized, more information about the field will be gathered and adjustments to the model of the power plant would be effected along the way thereby providing a probability of scaling the production capacity of the field.

The analysis of the proposed cycles is presented in the following sections regarding the assessments in terms of both technical and economic feasibility.

4. TECHNICAL ANALYSIS OF THE TECHNOLOGY APPLICABLE FOR CHIWETA SYSTEM

The geothermal resources in Malawi are currently only used for direct applications, mainly for bathing. Hot springs in Nkhotakota, with surface temperature of around 72°C (GDC, 2010), were once used for district heating at a local hospital during winter periods showing that direct utilization of geothermal in Malawi is possible. This study, however, focuses on electricity generation.

There are a number of factors that are considered for extraction of energy from a geothermal resource some of which are the reservoir capacity, temperature of the resource, mass flow of the fluid and the chemistry of the fluid. Not much study has been done on Malawi's geothermal to ascertain reservoir parameters. Malawi needs to do detailed assessment of its geothermal resource to the point of drilling exploration wells in order to be certain of the said parameters.

This study therefore uses the surface data available and educated estimates wherever necessary, to give the resource parameters for modelling and improve the certainty of implementation. The proposed binary plant would be modular with provision for further capacity upgrade. Modular development of binary power plants is cost effective and facilitates short manufacturing and installation times and can be upgraded to as much as 50 MW (Maghiar and Antal, 2001).

As the binary power plant will be operated, more data of the field will be obtained to fine tune initial reservoir parameters which will guide further exploration and developments. The temperature of the resource is as guided by the various studies done in the area.

4.1 Thermodynamic analysis

The binary power plant will have two fluid circulation systems for generation of electricity i.e. the primary and the secondary systems. The primary circulating system, which is the heat source for the cycle, will use the hot geothermal water which is the energy source. The secondary system is a closed loop using working fluid with low boiling point and high vapour pressure as compared to water at a common given temperature. The working fluid will get its heat from the hot geothermal fluid from the primary system by means of heat exchangers. The cycle is cooled by a cooling system that is coupled to the cycle's condenser. The primary cycle is designated with a subscript (s) in all parameters concerned. The secondary cycle and the cooling cycle are designated with subscripts (wf) and (c) respectively.

The thermodynamic analysis of the binary power plant is based on the schematic diagram in Figure 12. Hot geothermal water comes from production well and is directed to heat exchangers. The heat from the geothermal water is transferred to a secondary working fluid through the heat exchangers in the preheater and vaporizer after which the geothermal water is sent back into the reservoir through a reinjection well.

The geothermal fluid enters the primary cycle at point s_1, vaporizes the working fluid and superheats the fluid at point s_2 in the vaporizer. The geothermal fluid then leaves the vaporizer and enters the pre-heater through point s_3. The geothermal fluid heats the working fluid in the pre-heater and leaves the pre-heater through point s_4 for reinjection (Figure 16).

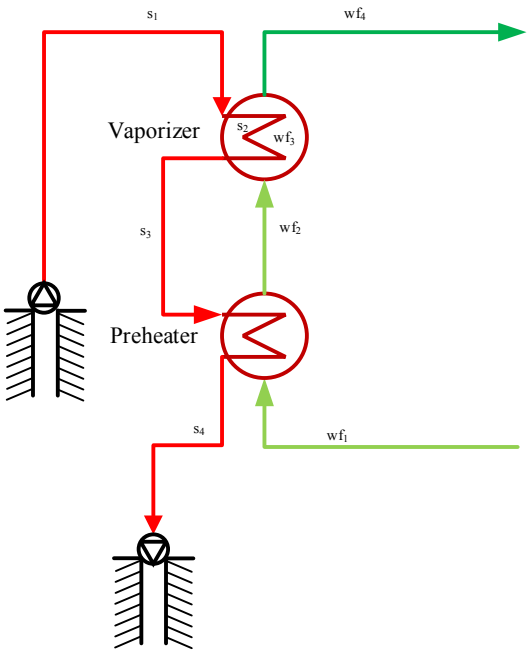

FIGURE 16: Vaporizer and preheater section of the binary cycle

For the working fluid in the secondary cycle, the working fluid enters the pre-heater through point wf_1 and is heated by the geothermal fluid. The working fluid leaves the pre-heater and enters the vaporizer through point wf_2. In the vaporizer the fluid is changed to vapour and then superheated at point wf_3. The working fluid leaves the vaporizer through point wf_4 as superheated vapour where it is directed towards the turbine (Figure 16).

The process of vaporizer and preheater heat exchange is in such a way that the heat rejected by the geothermal fluid is received by the working fluid. The thermodynamic assessment is therefore as follows:

$$\dot{Q}_s = \dot{Q}_{wf} \quad \textit{(kJ/s)} \tag{1}$$

where $\dot{Q}_s$ is the total heat rejected by geothermal fluid;
$\dot{Q}_{wf}$ is the total heat received by the working fluid.

Total heat rejected by the geothermal fluid is the sum of heat rejected by the geothermal fluid in both the vaporizer and the pre-heater and is given by the equation as follows:

$$\dot{Q}_s = \dot{m}_s * (h_{s1} - h_{s4}) \quad \textit{(kJ/s)} \tag{2}$$

where $\dot{m}_s$ is the geothermal fluid mass flow *(kg/s);*
h_{sx} is the source enthalpy at point *x (kJ/kg).*

If temperatures and heat capacity are used instead of enthalpy, Equation 2 becomes:

$$\dot{Q}_s = \dot{m}_s * c_{p\_s} * (T_{s1} - T_{s4}) \quad \textit{(kJ/s)} \tag{3}$$

where c_{p_s} is the geo fluid specific heat capacity *(kJ/kg-°C);*
T_{sx} is the source temperature at point *x (°C).*

Since all the heat rejected by the geothermal fluid is received by the working fluid, the mass balance across the primary and secondary cycle in the vaporizer and preheater then becomes:

$$\dot{m}_s * c_{p\_s} * (T_{s1} - T_{s4}) = \dot{m}_{wf} * (h_{wf4} - h_{wf1}) \tag{4}$$

where $\dot{m}_{wf}$ is the working fluid mass flow *(kg/s).*

For the mass balance across each component, i.e. the pre-heater and the vaporizer, it follows that:

Pre-heater: $$\dot{m}_s * c_{p\_s} * (T_{s3} - T_{s4}) = \dot{m}_{wf} * (h_{wf2} - h_{wf1}); \tag{5}$$
Vaporizer: $$\dot{m}_s * c_{p\_s} * (T_{s1} - T_{s3}) = \dot{m}_{wf} * (h_{wf4} - h_{wf2}). \tag{6}$$

Temperatures at point wf_2 and s_3 recognise the effect of pinch point in the preheater and vaporizer heat exchangers. The pinch temperature is the smallest difference in temperature that can be reached between the primary fluid temperature and the secondary fluid temperature (Valdimarsson, 2010) and is usually provided by the manufacturer of the heat exchanger.

The relationship of temperatures at these two points is therefore given in respect of the pinch as follows:

$$T_{s3} = T_{wf2} + T_{pinch\_HE} \tag{7}$$

where T_{pinch_HE} is the heat exchanger pinch temperature difference *(°C).*

The pinch temperature difference is usually provided by manufacturers and determines the size of the heat exchanger such that, for smaller pinch temperature difference heat exchanger size is smaller and vice versa.

After passing through the vaporizer, the working fluid is in vapour phase and directed towards the turbine entry at point wf_5. Normally at this point, the vapour may experience some loss in pressure which

is designated as ΔP. This pressure loss may be due to vapour transportation in the pipeline connecting the vaporizer and the turbine. The pressure loss may be considered negligible for purposes of this work.

From wf_5, the vapour is expanded through a turbine to point wf_6, in the process producing mechanical power that is used in turning the turbine coupled to an electricity generator thereby generating electricity. The work done by vapour in turning the turbine, causes drop in enthalpy at point wf_6 (Figure 17). It is ideally perceived that the process of expansion of vapour in the turbine is isentropic i.e. entropy at the output of the turbine is the same as entropy at the turbine inlet. However, in real application the process is not isentropic since the expansion is irreversible and the process increases the fluid entropy. Both the isentropic enthalpy h_{s_wf6} and the real enthalpy h_{wf6} are assessed at point wf_6.

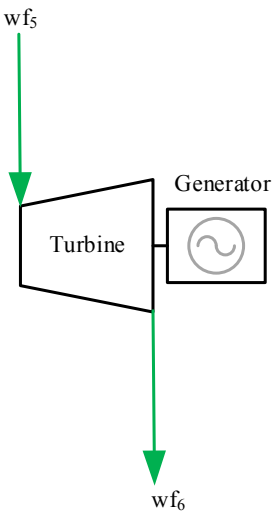

FIGURE 17: Binary turbine

The relationship between enthalpy and isentropic turbine efficiency is given by the Equation 8 below:

$$\eta_{tur} = \frac{h_{wf5} - h_{wf6}}{h_{wf5} - h_{s\_wf6}} \tag{8}$$

where η_{tur} is the turbine isentropic efficiency;
h_{s_wf6} is the isentropic enthalpy at point wf_6 *(kJ/kg)*.

The efficiency of a turbine is generally provided by the turbine manufacturer and it is common practice that this efficiency is 85% (Valdimarsson, 2010).

Work done by the vapour which is the mechanical power output from the turbine is given by turbine efficiency, mass flow rate of the fluid passing through the turbine and the enthalpy drop across the turbine and presented in the Equation 9 below:

$$\dot{W}_{tur} = \eta_{tur} * \dot{m}_{wf} * \left(h_{wf5} - h_{s\_wf6}\right) \tag{9}$$

where $\dot{W}_{tur}$ is the mechanical power output of the turbine.

From the turbine, the vapour is led to a condenser inlet (for cycle without recuperation) at point wf_6 where pressure is kept as low as possible with an aim of extracting more energy from the turbine process. The condenser is coupled to either a water cooling system or an air cooling system which performs 3 tasks: de-superheating, condensing and sub-cooling the working fluid. Two types of water cooled condensers are commonly used in geothermal power plants and these are the direct contact condenser and the surface condenser. The direct contact condensers mixes vapour from the turbine with cooling water by means of spraying in the condenser to form condensate. The direct contact condenser is applicable in flash plants but not appropriate for binary plants otherwise the closed loop secondary fluid would get in contact with water which may result into environmental hazards. The surface condenser, which is mostly a shell and tube type, works in such a way that two separate fluids exchange heat without directly getting in contact with each other. The operation of surface condenser is ideal for binary power plant application where secondary fluid need not to get in contact with cooling water.

The air cooled system uses electrically driven fans to cool the working fluid and is dependent on the prevailing environmental temperatures for its efficiency.

The condensing temperature is determined by the inlet temperature, the dew point temperature and the temperature range of the cooling medium. There is usually a small temperature difference between the dew point temperature of the cooling medium and its exit temperature, and this temperature difference is the de-superheating temperature. Based on Figure 18, the condensing temperature (T_{cond}) is therefore given by the Equation 10 below:

$$T_{cond} = T_{c2} + T_{pinch\_cond} \quad (°C) \tag{10}$$

where T_{cond} is the condenser temperature;
T_{c2} is the cooling medium's dew point temperature;
T_{pinch_cond} is the condenser pinch temperature difference.

In the condenser, heat ($\dot{Q}_{wf\_c}$) is rejected from the working fluid between stations wf_6 and wf_8, to the cooling medium in the condenser. Station wf_7 is the dew state where the working fluid is fully de-superheated and is saturated vapour at condensing temperature. The cooling medium accepts the heat from the working fluid as $\dot{Q}_{c\_c}$ across the stations c_1 and c_3 as shown in Figure 18.

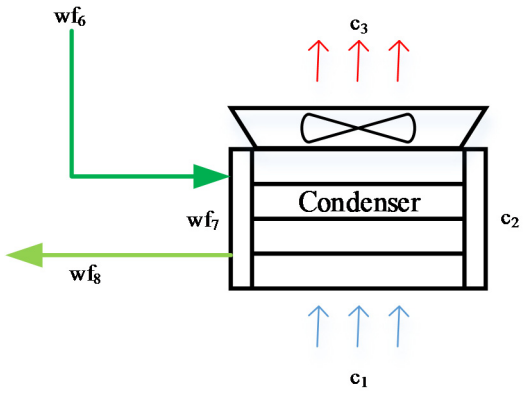

FIGURE 18: Power plant condensing unit

It is assumed that all the rejected heat from the working fluid is accepted by the cooling medium just like in the pre-heater and the vaporizer, hence rejected heat from the working fluid being equal to heat accepted by the cooling medium as in Equation 11:

$$\dot{Q}_{wf\_c} = \dot{Q}_{c\_c} \quad (kJ/s) \tag{11}$$

where $\dot{Q}_{wf\_c}$ is heat from working fluid in condenser;
$\dot{Q}_{c\_c}$ is heat to cooling medium in condenser.

The rejected heat from the working fluid is found by the mass flow rate of the fluid and the change in enthalpy across the condenser stations wf_6 and wf_8. Point wf_7 is the condensing point inside the condenser. The relationship is presented in the Equation 12 below:

$$\dot{Q}_{wf\_c} = \dot{m}_{wf} * \left(h_{\mathrm{wf6}} - h_{wf8}\right) \quad (kJ/s) \tag{12}$$

$\dot{Q}_{cw}$ is found by multiplying the cooling fluid mass flow rate and the change in enthalpy in the cooling water across the condenser as given in the Equation 13 below:

$$\dot{Q}_{c\_c} = \dot{m}_c * (h_{c3} - h_{c1}) \quad (kJ/s) \tag{13}$$

where h_{cx} is cooling fluid enthalpy at point x;
$\dot{m}_c$ is the cooling fluid mass flow.

When temperatures at stations c_1 and c_3 are used, the equation becomes:

$$\dot{Q}_{cw} = \dot{m}_c * C_{p_c} * (T_{c3} - T_{c1}) \quad (kJ/s) \tag{14}$$

where C_{p_c} is the specific heat capacity for cooling fluid;
T_{cx} is the cooling fluid temperature at point x.

After being condensed, the working fluid is directed to a fluid circulation pump at point wf_8 where pressure is added to the fluid after which it is sent to the preheater entry at wf_1 (Figure 19) and the cycle then repeats itself and continues.

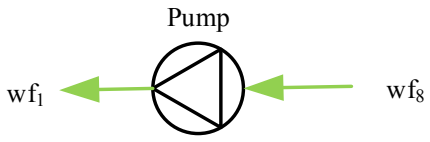

FIGURE 19: Fluid circulation pump

All things being equal, an ideal binary power plant is considered to have no emissions to the atmosphere hence being environmentally friendly. However the secondary fluid used in binary plants is mostly flammable and hazardous to the environment such that if not handled properly in terms of leakages, emissions into the atmosphere

becomes significant. The geothermal fluid in binary plants is never in contact with the turbine and is fully re-injected after heat extraction. By not letting the geothermal fluid get in contact with the turbine, it provides the turbine and the associated equipment a corrosion free operation hence guaranteeing longer life span. Such practice also makes the binary power plants avoid release of greenhouse gasses and related toxic elements such as CO_2 and H_2S which are common in flash power plants.

4.2 Power plant cooling system

Cooling systems in geothermal power plants are used as part of condensation of the vapour coming from the turbine in the condenser. Cooling systems help to improve the thermodynamic efficiency of the cycle and as such, choice of an appropriate system for a given geothermal power plant project is important to the resource's utilization. The main purpose of a cooling system is to remove some heat from the working fluid in the condenser while the condenser is changing the working fluid from vapour to liquid.

Mendrinos et al. (2006) categorises the cooling systems for binary plants into three: surface water system, wet cooling system and dry cooling system.

4.2.1 Surface water system

The surface water system which is also known as once-through cooling system, removes heat from the condenser by using water, passing the water through the condenser and releasing the water into the environment thereafter. This type of cooling system is able to yield the lowest condensing temperature thereby improving the significantly the thermodynamic efficiency of the cycle as compared to the other cooling systems (Mendrinos et al., 2006). The technology does not require cooling towers as in the case of the two systems to be discussed below, because the water used in cooling system are discharged into the environment once they have been used in the condenser. The analysis of the cooling system is basically the heat exchange in the condenser using Equation 14. The heat in the working fluid is rejected to the cooling water as the cooling water passes through the condenser. Mass balance and enthalpies are calculated based on Equations 12 and 14 to ascertain the quantity of water required for the system at the ambient water temperature and the desired condenser temperature. The system requires a considerably large and steady source of water body for its satisfactory operation and the water requirements in this system are almost 30 times as much as those required in a wet cooling system. Despite its standing on thermal efficiency improvement, the technology is not popular due to the large volume of water that are required in light of other water demands, water rights, and related water issues. The system results in increase in the water body's temperature thereby affecting the ecosystem in the water body. However, where water is not an issue and the quality of water is studied with an aim of preserving the condenser, implementation of surface water cooling system is recommended. This study however will not consider the surface water cooling system in its further analyses that follow.

4.2.2 Wet cooling system

Wet cooling system uses both water and air with a cooling tower that may be configured as cross flow or counter flow depending on the direction of air entering the cooling tower. The water from the cooling system is let to pass through the condenser where it removes heat from the working fluid. This water then directed to the top of the cooling tower where the heat is rejected into the environment by action of air. The water is collected at the bottom of the tower to remove the heat again from the working fluid in the condenser. The system requires considerably large amounts of water but not as much as in the surface water cooling system. Some of the cooling water may be lost in the process at the cooling tower presenting a requirement of a steady and abundant supply of fresh water to be used as make-up water for the system. A schematic diagram for a wet cooling system is as shown in Figure 20.

The wet cooling system involves the heat exchange between the working fluid and the cooling water in the condenser and the heat transfer between the cooling water and air in the cooling towers. Cooling tower considerations look at determining the tower dimensions such as tower height, tower base area

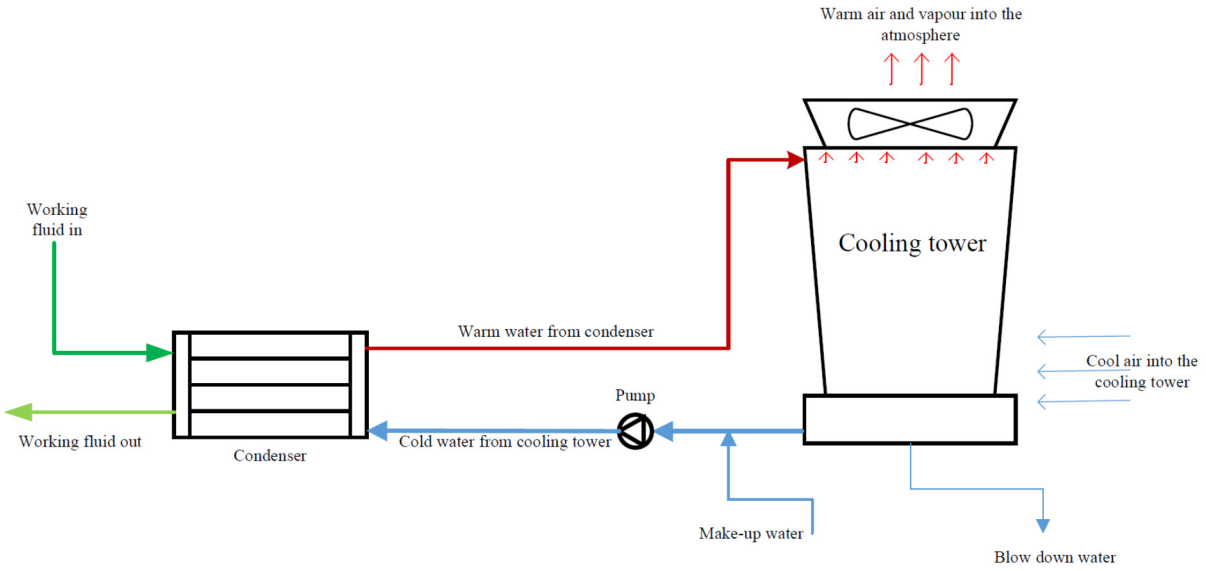

FIGURE 20: Schematic diagram of a wet cooling system

and the volume of water fill (Leeper, 1981). This includes the air flow in the cooling tower, water consumption and power requirements for the tower pump and tower fans.

The analysis of the wet cooling system according to Leeper (1981) is done by considering the mass balance around the cooling system based on Equation 14. Heat rejected by the working fluid is accepted by the cooling medium in the condenser. At this point the mass flow of the cooling medium is known according to the equation therefore linking the analysis to cooling tower calculations as follows:

$$\dot{m}_{air} * \Delta h_{air} = \dot{m}_{water} * Cp_{water} * \Delta T_{water} \quad (15)$$

where Δh_{air} is the enthalpy difference of air across the tower;
Cp_{water} is the cooling water specific heat capacity *(kJ/kg K);*
ΔT_{water} is the water temperature difference across the tower;
$\dot{m}_{air}$ is the air mass across the tower *(kg/s);*
$\dot{m}_{water}$ is the water mass across the tower *(kg/s)*.

The change in enthalpy of air considers change in relative humidity at the tower air inlet and air outlet such that the outlet air at the top of the tower has higher relative humidity than the inlet air due to evaporation.

Leeper (1981) suggests an estimate for calculating the optimal outlet air temperature which becomes the basis of estimating the enthalpy difference of air. The air exit temperature for the cooling tower is therefore provided in Equation 16:

$$t_{air,out} = \frac{\left[T_{water,in} + T_{water,out}\right]}{2} \quad (16)$$

where $t_{air,out}$ is the tower air outlet temperature *(°C);*
$T_{water,in}$ is the entry temperature of cooling water *(°C);*
$T_{water,in}$ is the exit temperature of cooling water *(°C)*.

However, given a temperature range as to how far the water can be cooled or how much the air can be warmed up, the temperature for air at the exit of the tower becomes:

$$t_{air,out} = t_{air,in} + t_{range} \ \ (°C) \quad (17)$$

With Equations 15 and 17, further parameters for the cooling tower such as the tower height and base area, may be determined. For pump calculations, Leeper (1981) suggest that the head for the cooling tower pump $H_{CoolingT}$ as Equation 18.

$$H_{Cooling,T} = Z_{dot} + 10 \quad (18)$$

where $H_{Cooling,T}$ is the head of the cooling tower;
Z_{dot} is the tower height *(m)*.

The cooling tower pump calculation is therefore given in Equation 19:

$$P_{cw} = 0.0981 * H_{Cooling,T} * SG_{water} \quad (19)$$

where P_{cw} is the pump power for the cooling tower;
SG_{water} is the specific gravity for water.

The wet cooling system is deemed not to be as efficient as the surface water system, but is more efficient than the dry cooling system which is discussed below. The chemistry of the water for cooling must be studied and the water treated to avoid growth of algae or fungi in the cooling tower (VERKÍS Consulting Engineers, 2014).

4.2.3 Dry cooling system

The dry cooling system uses air to condense the vapour coming from the turbine. The condenser is built as a cooling tower with fans that draw air across the condensers. To make the air cooling effective, the condensing area is spread as wide as possible thereby requiring large area for heat exchange surface. As a result, the cooling system calls for more use of fans that at times lead to double as much the power requirement for the fans as compared to wet cooling system (Mendrinos et al., 2006). The demand of more fan power increases the parasitic load for the power plant. Since the system depends on the ambient air, the system is sensitive and subjected to prevailing ambient temperature variations, both seasonal and hourly variations thereby affecting the system's efficiency. A schematic diagram of the dry cooling system is shown in Figure 21.

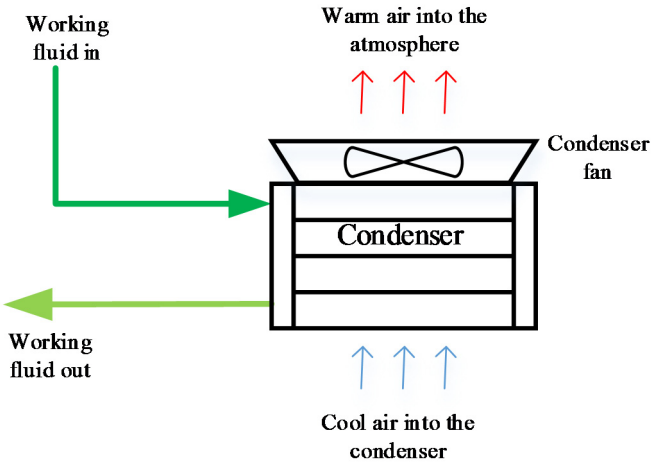

FIGURE 21: Schematic diagram of the dry cooling system

The cooling system is a condenser mounted on a tower and the assumption of heat in the working fluid being totally transferred to the cooling medium holds. The mass balance for this system is based on Equation 14 and given in the Equation 20 below:

$$\dot{m}_{wf} * \Delta h_{wf_c} = \dot{m}_{c_{air}} * C_{p_{air}} * \Delta t_{c\_air} \quad (20)$$

where Δh_{wf_c} is the enthalpy difference across the condenser;
C_{p_air} is the specific heat capacity for air *(kJ/kg-K);*
Δt_{c_air} is the air temperature difference across the condenser;
$\dot{m}_{c\_air}$ is the air mass across the condenser.

The work that is done by the fans to move the air in the cooling system is found by the Equation 21 below:

$$\dot{W}_{fan} = \frac{\dot{V}_{c\_air} * \Delta P_{c\_air}}{(\eta_{fan} * \eta_{motor})} \quad (21)$$

where $\dot{W}_{fan}$ is the work of the fan;

ΔP_{c_air} is the pressure difference across the fan;
η_{fan} is the fan efficiency;
η_{motor} is the efficiency of fan's motor;
$\dot{V}_{c\_air}$ is volume of air *(m^3)* which can be found by Equation 22.

$$\dot{V}_{c\_air} = \frac{m_{c\_air}}{(\rho_{air,out})} \tag{22}$$

where $\rho_{air,out}$ is density of air *(kg/m^3)*.

Dry cooling system is best suitable for areas where there is water stress or where strict water regulations prevail. However, it is observed that dry cooling system has fewer equipment installed when compared with the wet cooling system. This makes the dry system much easier to maintain.

Dry cooled binary plants highly depend on local ambient temperature hence subjected to efficiency fluctuations as the temperature changes both daily and seasonal. On a hot summer day, production can drop up to 50% because of insufficient cooling (VERKÍS Consulting Engineers, 2014). When this type of cooling system is preferred, the fluctuations in ambient temperature need to be considered.

Malawi is not a water stressed country and the environmental act currently in force only requires any energy undertaking to conduct a proper environmental impact assessment (EIA) as well as putting up a robust environmental management plan for the impacts of the undertaking on the environment. Chiweta being close to water bodies, 1.5 km from Lake Malawi and 500 m from North Rumphi River, may not pause very significant environmental impact by using water within its reach. With the abundance of water coupled with favourable climatic conditions of good average temperature all year round, Chiweta may implement an air cooled or water cooled system. Both systems will be subjected to analysis in the next sections.

4.3 Consideration of scaling potential

When the geothermal water is in the reservoir, it interacts with the host rock and in the process dissolves some constituents from the rocks until they reach a chemical equilibrium at reservoir conditions. This depends on a number of factors such as the geology of the resource, temperature, pressure as well as the source of the water. Different fields will therefore have geothermal fluid with different chemical compositions depending on these factors. As the geothermal water is being transferred from the reservoir for various utilization undertakings, the physical and chemical conditions of the water changes and some of the dissolved constituents may no longer remain soluble in the water thereby forming depositions along the way. Some of the minerals exhibit higher solubility in water where the temperature of water increases and when the water temperature starts to decrease, the dissolved minerals become less soluble thereby precipitating from the solution (DiPippo, 2012). Other minerals will precipitate where the fluid is being flashed and a portion of the fluid turns into steam (Nugroho, 2011). Such deposition and precipitation of minerals occurs on the surface of power plant equipment or in the wells and is experienced in many geothermal power plants. Problems such as equipment damage and failure, brine leaks and spills, well and line plugging, reduced brine flow and power production losses are some of the experiences associated with scaling. Dealing with scaling in production wells or power plant equipment proves to be normally expensive since they introduce cleaning expenses over and above reduced production. As such prevention is serving as a better option (Brown, 2013). The major scaling threats in geothermal power plants are calcite and silica scaling.

Calcite scaling occurs near the flash point in the production wells due to a decrease in calcite solubility as some fluid turns to vapour. Calcium solubility varies with the pressure of carbon dioxide (CO_2) and temperature of the fluid (Yanagisawa, 2015). Prevention of calcite scaling in wells is mostly by using various chemical inhibitors such as sodium polyacrylate. A capillary tube is inserted into a production well to the depth of flashing point where the chemical inhibitor is directly injected for scaling prevention (Yanagisawa, 2015). With calcite scaling, there is little that can be done at design stage for its prevention.

One of the ways of prevention is by preventing flashing in the production well by keeping well head pressures sufficiently high thereby maintaining the fluid in liquid phase.

Silica exists in different forms such as quartz, tridymite, cristobalite, amorphous silica and many others (Brown, 2013). Of all these forms, amorphous silica and quartz are much associated with geothermal scaling problems (DiPippo, 1985). As such, silica scaling is analysed using the amorphous silica and quartz concentration in the fluid. When the geothermal water is in the reservoir, the solubility of silica is controlled by quartz but as the water is cooling down, silica solubility is controlled by amorphous silica (DiPippo, 2012). Amorphous silica is more soluble than quartz and this provides a window of opportunity to utilize the geothermal fluid between the quartz solubility curve and the amorphous silica solubility curve without experiencing silica scaling (Brown, 2013) as the fluid tends to precipitate the silica through flashing and lowering temperature. Beyond the amorphous silica solubility curve, scaling is inevitable.

Since the chemistry of Chiweta field which is under study is not fully known at the moment, a general considerations for scaling potential is therefore made to account for a reasonable reinjection temperature that considers potential of scaling. It is anticipated that the fluid in the Chiweta field may have a higher value of pH (GDC, 2010) and therefore there may be more precipitation of some minerals since mineral precipitation is also affected by the pH value of the fluid (DiPippo, 1985).

To achieve maximum utilization of a geothermal resource, the geothermal fluid must be cooled to the lowest temperatures possible. However, as the cooling is taking place, the geothermal fluid becomes supersaturated with minerals such as silica and precipitation begins. As a result, a temperature that allows geothermal exploitation without the possibility of silica scaling needs to be assessed. This temperature, the silica saturation temperature (SST), is the temperature of the geothermal fluid at the exit of the heat exchanger before the fluid reaches saturation with respect to the amorphous silica (Brown, 2013). When in the reservoir, silica concentration is controlled by quartz while in the surface equipment the concentration is mostly controlled by amorphous silica.

In the absence of data, analysis of amorphous silica solubility is done using the Equation 23 below with respect to temperature. This gives the SST for a given resource temperature. The equation is true for temperature range of 0° – 250°C (Utami et al., 2014):

$$\log C = \left(-\frac{731}{T} + 4.52\right) \tag{23}$$

where C is the amorphous silica concentration *(mg/L)*;
T is the absolute temperature *(°K)*.

According to DiPippo (2012), the quartz solubility estimate with respect to temperature is given by Equation 24 below:

$$\mathrm{Q}(t) = 41.598 + 0.23932t - 0.011172t^2 + 1.1713 * 10^{-4}t^3 - 1.9708 * 10^{-7}t^4 \tag{24}$$

where Q is the silica concentration *(mg/kg)*;
t is the reservoir temperature *(°C)*.

Fournier and Rowe (1977) made some experiments regarding the solubility of silica in water and came up with the plots in Figure 22. The window of opportunity is between the quartz plot and the amorphous silica plot.

4.4 Choice of working fluid in binary plant

The choice of working fluid to be used in a binary power plant requires consideration of a number of factors. All the factors may be grouped in two: environmental safety and health, and performance.

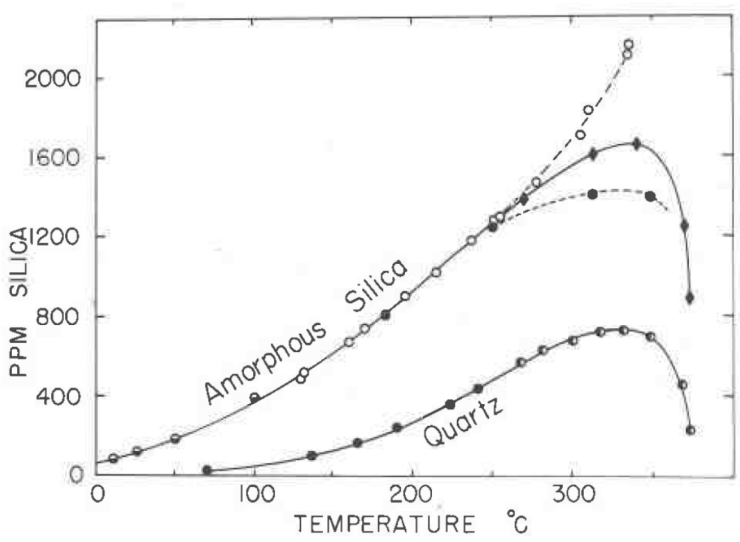

FIGURE 22: Silica solubility curve. Source: (Fournier and Rowe, 1977)

The environmental safety and health of the fluid considers such things as flammability, toxicity and environmental impact as a result of the fluid interacting with the environment. The goal in choice of working fluid is to have a working fluid with a lower level of catching fire at the same time safe to work with, in the event of some percentage of its volume being found in the air.

Over and above the safety of the fluid, the choices are also based on performance in terms of good thermal efficiency, utilizing the most of the heat available in the resource (Saleh et al., 2007). Performance of the fluid considers the thermodynamic properties of the working fluid that in the end affect the overall performance of the plant and hence impact the overall cost of the power plant. Some of the factors that need to be considered in choice of working fluid include: the critical temperature of the fluid, critical pressure and the cycle's thermal efficiency.

There are a lot of working fluids that are applicable in binary power plants. DiPippo (2012) compiles and compares some working fluids that are commonly used and most likely candidates for a binary power plant application according to their critical temperature, critical pressure, toxicity, flammability, Ozone Depletion Potential (ODP) and Global Warming Potential (GWP). The GWP is considered to be relative to the amount of heat that can be trapped by similar mass of carbon dioxide as the working fluid being analysed (DiPippo, 2012). The comparison of the fluids is summarized in Table 3.

TABLE 3: Properties of binary plant working fluids. Source: modified from DiPippo, (2012)

Fluid	Formula	Critical Temp (°C)	Critical Pressure (bar)	Toxicity	Flammability	ODP	GWP
R-12	CCl_2F_2	-	-	Non-toxic	Non-flammable	1	4500
R-114	$C_2Cl_2F_4$	-	-	Non-toxic	Non-flammable	0.7	5850
Propane	C_3H_8	96.95	42.36	low	very high	0	3
i-Butane	i-C_4H_{10}	135.92	36.85	low	very high	0	3
n-Butane	C_4H_{10}	150.8	37.18	low	very high	0	3
i-Pentane	i-C_5H_{12}	187.8	34.09	low	very high	0	3
n-Pentane	C_5H_{12}	193.9	32.4	low	very high	0	3
Ammonia	NH_3	133.65	116.27	low	lower	0	0
Water	H_2O	374.14	220.89	Non-toxic	Non-flammable	0	-

From Table 3, the fluids exhibit lower values of critical temperature and pressure as compared to water. This helps to reduce thermodynamic losses in the heat exchangers hence making the fluids ideal for use in binary power plant application (DiPippo, 2012). Almost all the fluids as presented by DiPippo have a low toxicity as well as low ODP and global warming potential with reference to their release of carbon dioxide into the atmosphere. Despite not being toxic and flammable, R-12 and R-114 exhibit high ODP and GWP thereby pausing an environmental hazard. R-12 and R-114 have since been banned from use in binary plant application (DiPippo, 2012).

Further to the parameters compared by DiPippo (2012), the shape of the saturation vapour curve in the T-s diagram is also considered. Working fluids are divided into three types according to their saturation

vapour curves. Bao and Zhao (2013) gives the three types of working fluids as: the wet fluids, isentropic fluids and dry fluids. The dry fluids exhibit a positive slope of a saturation curve in a T-s diagram while the wet fluids have a negative slope just like water, and ammonia is an example of wet fluids (Bao and Zhao, 2013). The isentropic fluids exhibit a nearly infinitely large slope which is almost vertical. Examples of isentropic fluids include flourinal 85 and R-11. The isentropic fluids remain in a vapour saturated state as they expands through the turbine since the expansion occurs along the vertical line of the T-s diagram. This results in the fluid not condensing at the turbine outlet thereby the turbine not experiencing liquid droplets from the working fluid.

Wet fluids normally leave some level of saturated liquid at the turbine outlet due to their negative saturation vapour curve which may damage the turbine blades. To sustain operations with wet fluids in binary power plant, the fluid is normally superheated at the turbine inlet and the dryness fraction of fluid is kept at above 85% (Bao and Zhao, 2013) below which, damage to the turbine blades becomes severe. The isentropic and dry fluids generally do not need superheating and minimum dryness fraction since they are already in the vapour saturated phase at the turbine exit (DiPippo, 2012). This is the reason why in most binary applications, the dry fluids and the isentropic fluids are commonly used as they do not form condensate as they pass through the turbine. The dry fluids, sometimes known as retrograde fluids, that are commonly used in power plants are normal butane, isobutene, normal pentane and isopentane. Figure 23 depicts the T-s diagrams of different fluid types as discussed.

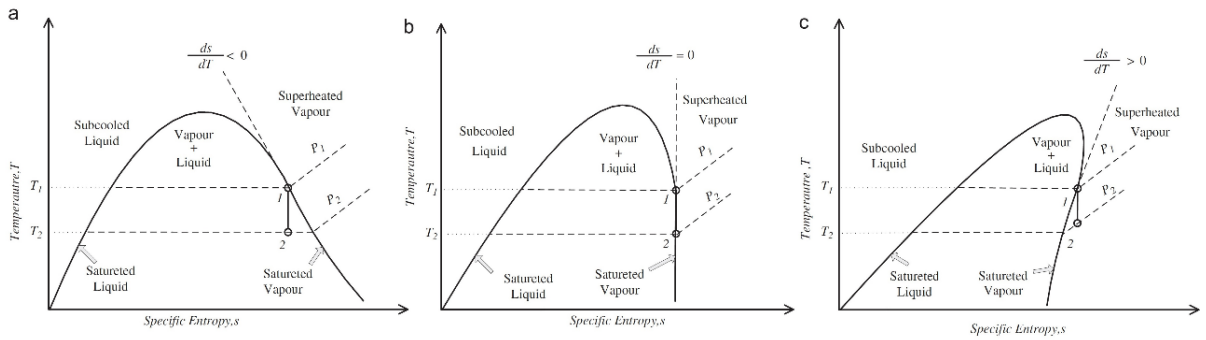

FIGURE 23: A T-s diagram for (a) wet fluid, (b) isentropic fluid and (c) dry fluid (Bao and Zao, 2013)

The fluids that are considered environmentally friendly according to DiPippo are then subjected to a thermal efficiency test in a simple binary cycle to see their performance under external source of heat. The purpose of this analysis is to show how the different fluids utilise the geothermal heat under some given set of cycle parameters. In the simple cycle, heat is added to the working fluid from the geothermal fluid through a heat exchanger and removed from the fluid through the condenser after the fluid has driven a turbine. The cycle considers some parasitic load required to drive a circulation pump and related equipment depending on the fluid's pressure requirements. The thermal efficiency is therefore determined using the Equation 25 below as presented by Marcuccilli and Thiolet (2010):

$$\eta_{th} = 1 - \frac{\Delta h_{wf\_c}}{\Delta h_{s\_HE}} \tag{25}$$

where η_{th} is the cycle's thermal efficiency;
Δh_{wf_c} is the enthalpy difference in condenser;
Δh_{s_HE} is the enthalpy difference across the preheater and vaporizer.

For purposes of this study, four working fluids are considered i.e. n-butane, n-pentane, isobutane and isopentane. Though not a retrograde, ammonia is incorporated for comparison sake. The fluid that presents better results is recommended for use in the study.

5. MODELLING OF THE BINARY POWER PLANT

Modelling of the power plant is done using the Engineering Equation Solver (EES) Program. EES program provides solutions of set algebraic equations, differential equations and do various optimizations and analyses while generating plots to the analyses. EES program has a library of mathematical and thermophysical properties of vast number of fluids that are associated with geothermal plant cycles. These built-in functions of steam tables facilitate thermodynamic modelling of geothermal power plants. Modelling of the power plant assumes that the cycle reaches a steady state and that pressure drops in pipes and heat exchangers as well as heat losses to the environment in the turbine and all the heat exchangers in the cycle are negligible unless stated otherwise in the process wherever necessary.

5.1 Boundary conditions

Boundary conditions provide input parameters to the model based on data at hand. Where data is not available, some reasonable assumptions based on literature review are made as reasonable as possible. The boundary conditions for this work include geothermal fluid mass flow, working fluid for the cycle, equipment efficiency, pressures and temperatures and are discussed further in the next sections below.

5.1.1 Fluid gathering system

Even though the GDC - Kenya report (2010) proposes a subsurface of 249°C in Chiweta, this study considers a lower temperature to be in tandem with the generally experienced geothermal gradient of the western branch of the EARS (Kraml et al., 2010). The proposed subsurface temperature indicates that Chiweta has a good geothermal resource, however being within the western branch, this study proposes a temperature of 180°C and this is used in the modelling. It is generally expected that at such temperatures, the production well would be artesian and that fluid may start boiling at some point and producing steam along the way. This study bears in mind that such expectations are site specific and that there is need to have field characteristics to incorporate such behaviour in power plant modelling. With only temperature at hand and without necessary field characteristics, it is better to assume that production wells are non-artesian as such pumping is required. In this aspect, the pumping assures of geothermal fluid that is kept in liquid phase and thereby acting as a preventive measure in calcite scaling. The pumping parasitic load is accounted for in the total parasitic load of a given power plant. Further work is recommended to validate the reservoir temperature and characteristics of the field.

Fluid gathering system requires field characteristics such as borehole pressure and well discharge from production wells. Chiweta has little information regarding the field characteristics and therefore fluid gathering system may be speculated at this time. Since the model considers calcite prevention in a way of maintaining the geothermal fluid in liquid phase, the geo-fluid pressure is kept at slightly above the saturation pressure of the reservoir temperature. The saturation reservoir pressure at 180°C temperature is 10.03 bars. Considering that the fluid may lose some pressure along its path through the system to the reinjection well, consideration is made to keep the fluid from boiling even as it loses pressure in the system. As such 1 bar is added to the saturation pressure of the geo-fluid, hence the considered pressure for geo-fluid in this work is 11.03 bars.

Mass flow of a geothermal field is more dependent on the permeability of the reservoir. Generally, wells drilled in medium to low temperature geothermal field may have the capacity of delivering geothermal liquid of 20 – 60 kg/s (Mannvit Eng., 2012). It is therefore likely that a geothermal well in low to medium temperature may deliver 40 kg/s which is also in agreement with what is considered to be generally acceptable discharge for a well (VERKÍS Consulting Engineers, 2014). This study proposes to design a 10 MW binary power plant. Depending on the model characteristics, required mass flow from the geothermal fluid that delivers the 10 MW is calculated for each model. The calculated geothermal mass flow is divided by the estimated mass flow of a well (40 kg/s) that gives the number of wells to deliver the 10 MW. For every 2 production wells, 1 reinjection well is required (Mannvit - Geoelec, 2012).

5.1.2 Scaling consideration

Calculations for scaling consideration are made to provide a limiting reinjection temperature. In flashing plant, the silica concentration in the fluid increases with the increase of steam fraction as the fluid is being flashed. In a binary system, since the fluid is maintained in liquid phase, silica concentration remains constant as the fluid is being cooled in the process of extracting heat from the fluid (Nugroho, 2011). However, as the liquid cools down, the amorphous in the fluid begins to precipitate. Using the Equations 23 and 24, silica solubility curves are plotted for amorphous silica and quartz. With a working temperature assumption of 180°C for the geothermal fluid reservoir, a precipitation curve (a,b,c) is plotted in Figure 24 for the fluid assuming a constant concentration. In Figure 24, for a 180°C geothermal water, amorphous silica saturation in the water is reached at point (c) with temperature of around 60°C, below which precipitation of silica is prone to scaling. Maintaining geothermal fluid temperature above this solubility level of amorphous silica helps in reducing the silica scaling rate (Thórhallsson, 2005). Out of experience, Thórhallsson (2005) proposes a rule of thumb to the effect that geothermal water be cooled 100°C below its initial temperature without potential of silica scaling for any given geothermal water temperature (Thórhallsson, 2005). This study therefore considers reinjection temperature of 80°C in line with both Thórhallsson's recommend-dation as well as not to be too close to the minimum limit of the scaling potential temperature as presented in Figure 24.

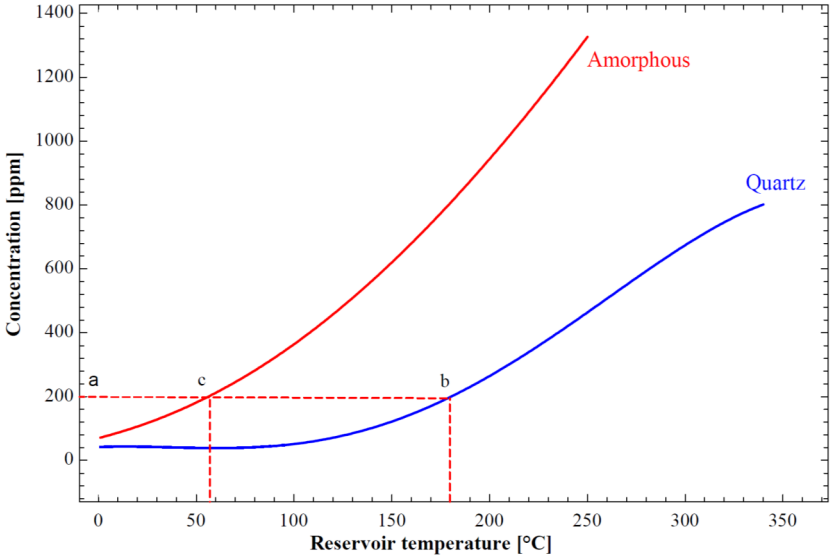

FIGURE 24: Calculated silica concentration in geothermal fluid

The two plots of quartz and amorphous silica are as presented in Figure 24.

5.1.3 Choice of working fluid

The four working fluids i.e. n-butane, n-pentane, isobutane and isopentane, are subjected to vaporizer temperature tests according to their capability. The T-s diagrams for the fluids are shown in Figure 25 below with ammonia, which is not a retrograde fluid, as a distinguishing fluid from the selected candidates.

Figure 25 shows that isopentane and n-pentane have better thermodynamic properties when operating at higher temperatures than butane and ammonia. Isopentane and n-pentane can operate in temperatures between 150 and 200°C while the rest can only operate at temperatures approximately below 150°C. The fluids are further subjected to vaporizer pressure test (turbine inlet pressure) in a working basic binary at resource temperature of 180°C and geothermal fluid mass flow of 100 kg/s. Condenser pressure for this analysis is saturated pressure at condenser temperature of 40°C. The vaporizer pressure is varied up to 40 bars and turbine work output is observed with the varying pressure. Results for response to varying vaporizer pressure of the fluids are presented in the Figure 26 below. The figure shows that n-butane and isobutane provides highest turbine output at higher pressures than n-pentane and isopentane. As the vaporizer pressure approaches the critical point for the fluids, the model fails to determine the turbine output of the two fluids. The turbine output of n-pentane and isopentane gives a clear trend of the turbine work output. These two fluids have an increase in turbine work with increase in vaporizer pressure and a peak is reached, which is the optimal pressure. Beyond the peak, any increase in vaporizer pressure decreases the turbine work output. Isopentane has a higher work output at slightly higher pressure than n-pentane. Basing on Figure 26 analysis, isobutene gives the highest turbine work

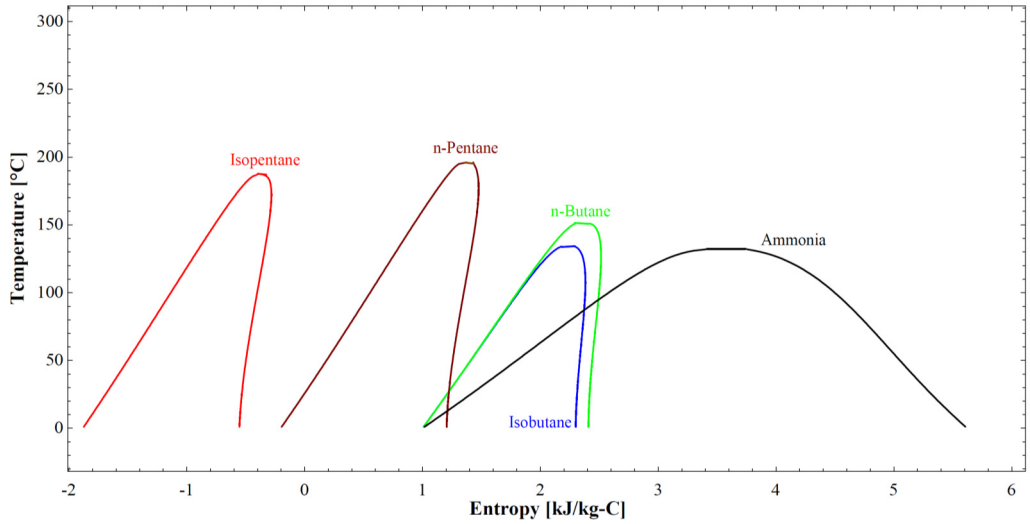

FIGURE 25: T-s diagram for various working fluids

output at pressures between 25 and 30 bars when compared with the other fluids. The second best performer is n-butane followed by isopentane and the least is n-pentane.

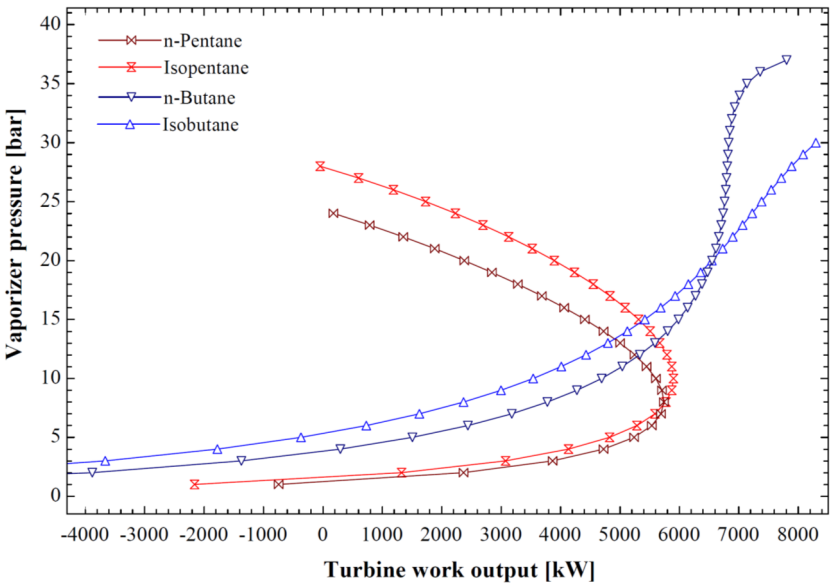

FIGURE 26: Vaporizer pressure and turbine work output of working fluids

The working fluids are then subjected to a reinjection temperature restriction test according to scaling consideration. The analysis seeks to obtain the best turbine work output that the fluids deliver at the given reinjection temperature of 80°C. The geo fluid temperature is 180°C and the analysis assumes a guess selected 140 kg/s mass flow of the geothermal fluid. Reinjection temperature is varied from condenser temperature until the geothermal fluid source temperature. By this the analysis assumes that the working fluid cannot cool the geothermal fluid below the condenser temperature. Observations are made for turbine work output at reinjection temperatures not less than the suggested silica scaling prevention level. A plot of turbine work output and the reinjection temperature for the fluids is presented in Figure 27. The figure shows that for reinjection temperatures below 80°C, all the working fluids are able to give their maximum power output from the model. At reinjection temperature of 80°C, n-pentane and isopentane gives some good output of turbine work with isopentane leading n-pentane. Isobutane delivers all its turbine work output below the 80°C while n-butane has uncertain turbine work output at 80°C reinjection temperature. For reinjection temperatures between 80 and 100°C, isopentane provides a higher turbine work output than n-pentane and for reinjection temperatures above 100°C the turbine work output for isopentane and n-pentane is the same.

Looking at the performance of the fluids as discussed above, the best candidate is selected for operating at reasonably higher temperature while offering a better work output when subjected to vaporizer pressure and delivers at the set reinjection temperature. Isopentane meets the criteria and is the working fluid used in this study.

Isopentane has been used in a number of binary power plant applications. Some of the power plants that are using isopentane for working fluid include: Svartsengi in Iceland, Tuzla in Turkey, Aluto Langano in Ethiopia, Olkaria (OrPower) in Kenya and Berlin in El Salvador. This gives an assurance of the use of isopentane as an appropriate working fluid.

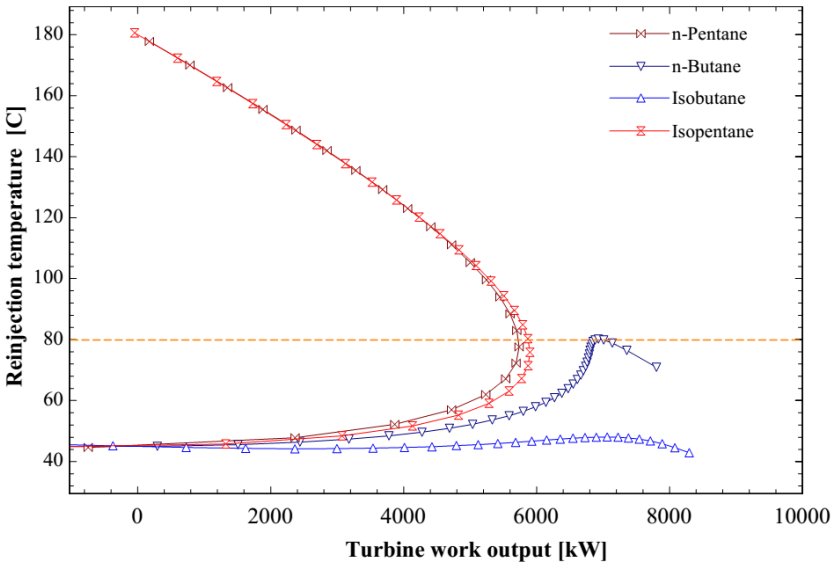

FIGURE 27: Reinjection temperature and turbine work output of working fluids

5.1.4 Vaporizer pressure optimization

The vaporizer pressure is optimized for the selected working fluid, which is isopentane, considering the properties of working fluid. The purpose of the vaporizer pressure optimization is to have a pressure that delivers the highest turbine work output or generates more power at the given restricted reinjection temperature of 80°C.

The basic binary model is given isopentane as working fluid, and is set to calculate the reinjection temperature and the generated power output as the vaporizer pressure is being varied. A plot of generator work output and vaporizer pressure is presented in Figure 28. The figure shows that the cycle has its maximum turbine output at a pressure of around 10 bars and it provides a maximum generated power output of about 4400 kW. When considering the generator power output under varying vaporizer pressure, the reinjection temperature is assessed and a contour plot of reinjection temperature on vaporizer pressure and turbine work is presented in Figure 29 below.

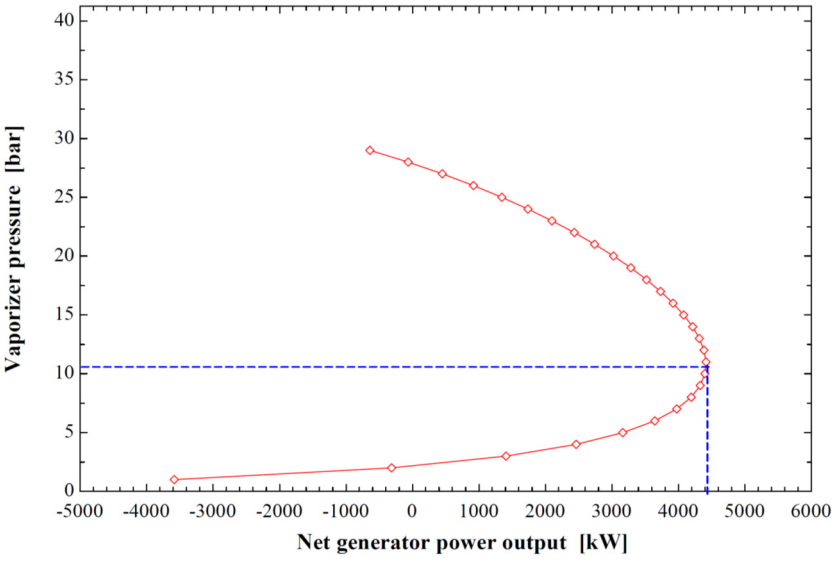

FIGURE 28: Optimal vaporizer pressure for isopentane in dry cooled basic model

Figure 29 reveals that the pressure of 10 bars which is giving the maximum power output falls in the reinjection temperature of close to 72.16°C, which is less than the desired 80°C. This means that an optimal pressure for the reinjection temperature is between 10 and 15 bars which is shown in the plot of reinjection temperature and vaporizer pressure in Figure 30 below.

From Figure 30, at reinjection temperature of 80°C, the optimal vaporizer pressure is about 11.5 bars. This means that any vaporizer pressure less than 11.5 bars results in higher generator power output but at a lower reinjection temperature than 80°C. It also follows that any pressure above 11.5 bars results in lower generator power output at a higher reinjection temperature than 80°C. Based on this understanding, this study therefore uses 12 bars as optimal vaporizer pressure, for the basic binary model which assures of reinjection temperature of not less than

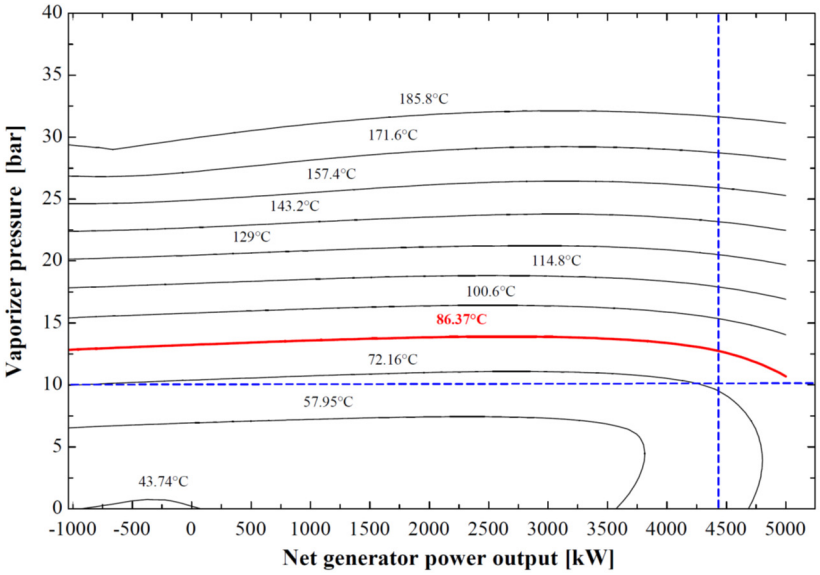

FIGURE 29: Reinjection temperature considering generator output and vaporizer pressure

80°C. The same procedure is performed for the wet cooled basic model, dry and wet cooled recuperative models (Appendices 1 – 3) and the optimal vaporizer pressure for all these models is 11 bars.

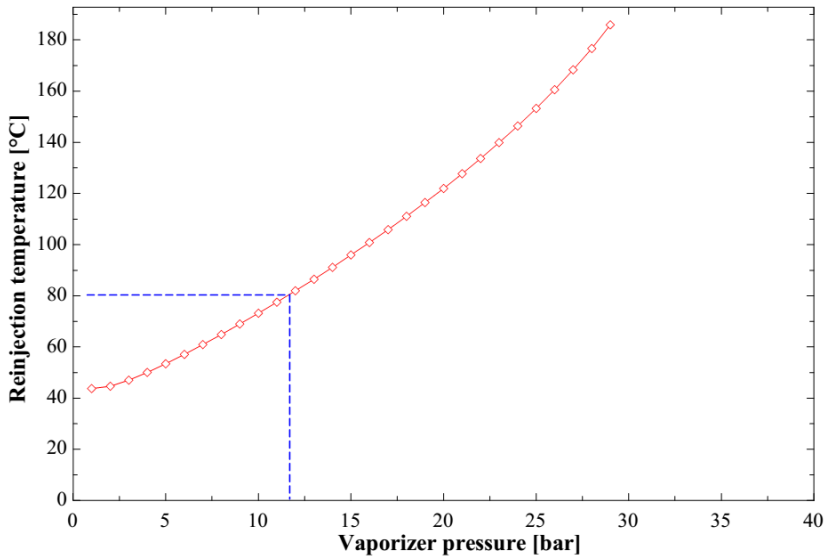

FIGURE 30: Optimal vaporizer pressure for dry cooled basic binary

5.1.5 Efficiencies of equipment and associated parameters

Typically, the efficiency of turbines are in the range of 81-85% (Dickson and Fanell, 2003) and this study uses turbine work efficiency of 85% as it looks forward to having the best performing turbine implemented for such a project. The fan efficiency for the cooling system used in this work is 70% and the pump efficiency used for all pump requirements is 80% (Frick et al., 2015). The motor efficiency for all the motors used in pumps and fans is 95%. The generator efficiency assumes 95% (Mendrinos et al., 2006). The overall heat transfer coefficients for heat exchangers in this study are based on Ahangar (2012) where preheater has 1000 W/m^2°C, vaporizer has 1600 W/m^2°C, recuperator has 400 W/m^2°C and condenser has 800 W/m^2°C.

The pinch temperature used for all the heat exchangers in this work is 5°C (Marcuccilli and Thiolet, 2010). Usually the choice of a pinch temperature is an optimization issue of efficiency and cost of the heat exchangers. However, the final pinch selection is usually based on the vendor's available pinch (VERKÍS Consulting Engineers, 2014). The air-side pressure drop for both air cooled condenser and

the cooling tower fans (ΔP_{Acc}) is 175 Pa (Ashwood and Bharathan, 2011). The wet cooling system assumes a cooling tower height of 4.645 m (Ura and Saitou, 2000).

The condensing temperature used in this study is calculated as ambient temperature. The condensing temperature may be optimized by considering the efficiency of the cycle and the cost of the condenser. However, this work has chosen a fixed condensing temperature since choice by optimal condenser cost may be subjective and requires a number of guessing and iterations which may be beyond the scope of this work.

5.1.6 Local ambient conditions

Atmospheric pressure varies with altitude in metres above sea level (m a.s.l.). The higher you go from the sea level, the lower the atmospheric pressure. The altitude of Chiweta is 500 m a.s.l. and therefore the atmospheric pressure for the area is found by the Equation 26 below:

$$P_{air,alt} = \frac{P_{atm,zero} - \rho_{air} * g * altitude}{100{,}000} \text{ (bars)} \quad (26)$$

where $P_{air,alt}$ is the atmospheric pressure at altitude;
$P_{atm,zero}$ is the atmospheric pressure at sea level;
ρ_{air} is the density of air;
$altitude$ is the site elevation above sea level.

This gives the atmospheric pressure of Chiweta as 0.9495 bars and this is used in this work.

The average ambient temperature used in the model is 24°C (Climate Data, 2015); the relative humidity is 70% (ClimaTemps.com, 2015) and the Lake Malawi water surface temperature is 23°C (Programme U, 2015). With the given air and water temperatures, a condensing temperature of 40°C is selected for calculating condenser parameters. This is used to find the temperature range of the condenser and subsequently determining the condenser size. A summary of the boundary conditions is presented in Table 4 below.

TABLE 4: Common boundary conditions for the models

Parameter	Value	Unit
Working fluid	Isopentane	
Geothermal fluid source pressure	11.03	bar
Atmospheric pressure	0.9495	bar
Vaporizer pressure (basic and recuperative)	12 and 11	bar
Condenser pressure	1.513	bar
Pressure change in fan (ΔP_{Acc})	175	Pa
Geothermal fluid source temperature	180	°C
Condenser temperature	40	°C
Vaporizer-Preheater pinch temperature difference	5	°C
Condenser pinch temperature difference	5	°C
Surface water temperature	23	°C
Ambient temperature for Chiweta	24	°C
Relative humidity for Chiweta	70	%
Fan efficiency	70	%
Feed pump efficiency	80	%
Turbine efficiency	85	%
Generator efficiency	95	%
Motor efficiency (for pump and fan)	95	%
Preheater heat transfer coefficient	1000	W/m^2°C
Vaporizer heat transfer coefficient	1600	W/m^2°C
Recuperator heat transfer coefficient	400	W/m^2°C
Condenser heat transfer coefficient	800	W/m^2°C

5.2 Modelling of scenarios and results

The modelling is based on four scenarios which are: basic binary plant with dry cooling system, basic binary plant with wet cooling system, regenerative binary with dry cooling system and regenerative

plant with wet cooling system. The boundary conditions discussed in the previous section are applied to the binary system in an EES model.

The performance of the models are as follows:

5.2.1 Basic binary with dry and wet cooling system

The vaporizer pressure of 12 bars is used in the dry cooled basic binary models, 11 bars for the wet cooled model and the models are set to calculate the required geothermal fluid mass flow for producing a net generator power output of 10 MW. A plot of required geothermal fluid mass flow and generator power output for the dry cooled basic model is presented in Figure 31. The figure is a direct proportionality plot and the cycle requires geothermal fluid of 230.2 kg/s to produce a net generator work output of 10 MW.

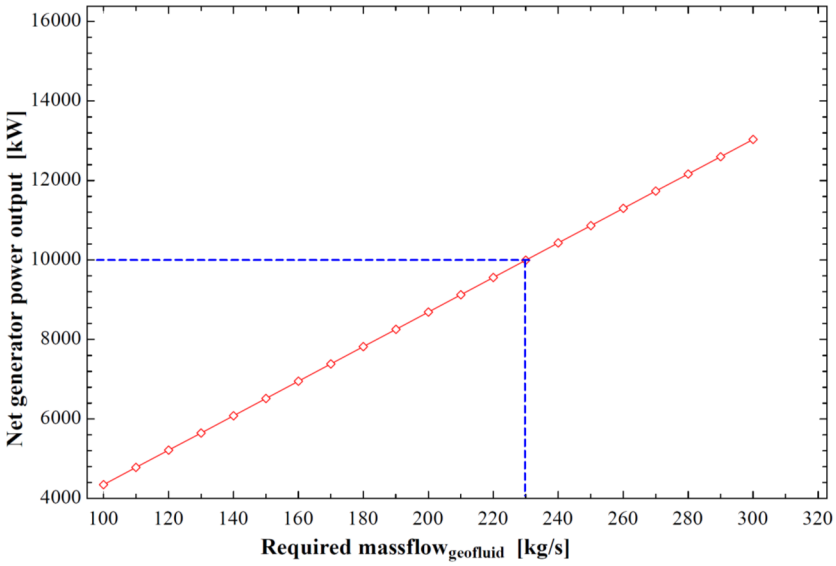

FIGURE 31: Required geothermal fluid mass flow for dry cooled basic binary model

For the wet cooled basic binary to produce 10 MW, it requires geothermal fluid mass flow of 209.8 kg/s. The plot of required geothermal fluid mass flow for wet cooled basic binary is presented in Appendix 1c.

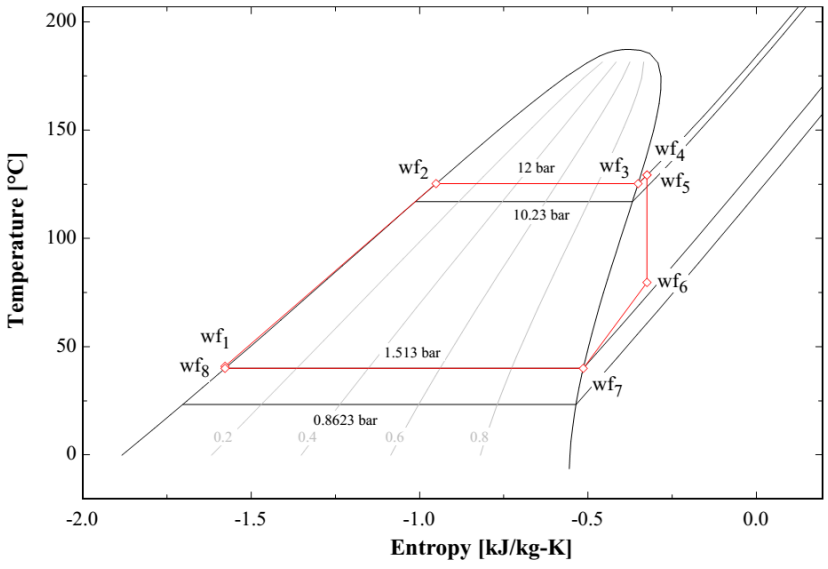

FIGURE 32: T-s diagram for the dry cooled basic binary cycle

The Process Flow Diagrams (PFD) for the dry and wet cooled basic binary models with parameters around the cycles, are presented in Appendices 4 and 5. The working fluid in the cycles has both its Temperature – Entropy (T-s) and Temperature – Enthalpy (T-h) diagrams trending in the normal way of a binary cycle. The T-s diagram for the dry cooled cycle with isopentane as a working fluid is presented in Figure 32 and the T-h diagram for the dry cooled cycle is presented in Figure 33. With reference to Appendix 5, the working fluid at point wf_8 is immediately after the condenser and at the circulation pump entry. Pressure is added to the fluid by means of the circulation pump from a pressure of 1.513 bar at point wf_8 to a pressure of 12 bar at point wf_1. At point wf_1, the fluid gains in pressure at the same time slightly gaining in temperature (hence slight gain in enthalpy in Figure 33). The fluid enters the preheater at station wf_1, changes in entropy and gains enthalpy as it is being heated in the preheater until point wf_2. At point wf_2, which is the bubble

(boiling) point, the fluid is saturated liquid and it changes to saturated vapour at point wf_3 by action of vaporizer. In order to eliminate any potential moisture in the vapour that may have detrimental consequences to the turbine as the vapour is being expanded through the turbine, the vapour is superheated at point wf_4, to 5°C more than the vaporizer temperature.

The vapour is then expanded through the turbine between stations wf_5 and wf_6.

As the vapour is expanded through the turbine, it moves from region of high pressure at point wf_5 (12 bar), to region of lower pressure at point wf_6 (1.513 bar) which is the condensing pressure. Stations in the cycle that are at the high pressure level include wf_1, wf_2, wf_3, wf_4 and wf_5. Stations in the cycle that are at the low pressure level include wf_6, wf_7 and wf_8 as shown in Figure 34 which is the P-h diagram for the cycle.

The T-s, T-h and P-h diagrams for wet cooled binary cycle are presented in the Appendix 6. All the stages of the cycle are similar to the dry cooled basic binary cycle, with vaporizer pressure of 11 bars.

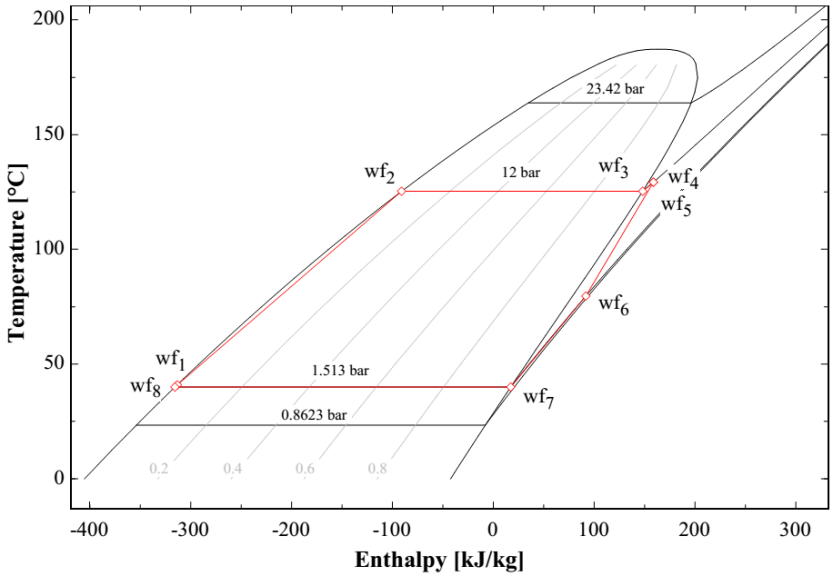

FIGURE 33: T-h diagram for the dry cooled basic binary cycle

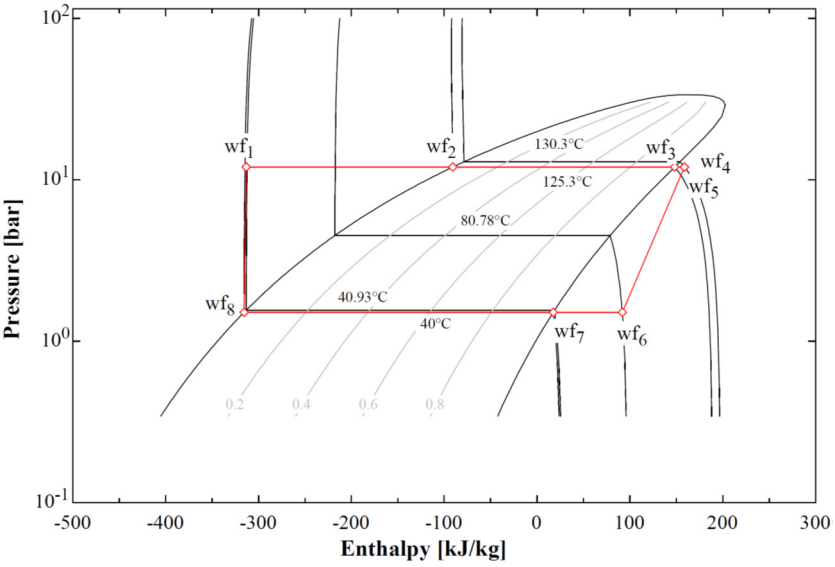

FIGURE 34: P-h diagram for the dry cooled basic binary cycle

The performance of the heat exchangers and the condensers of the models are presented below. The heat exchanger i.e. the preheater and the vaporizer for the dry cooled basic binary, has the geothermal fluid entering the vaporizer at station s_1 at temperature 180°C superheating the working fluid with 5°C between stations s_1 and s_2, vaporizing the working fluid at constant temperature between stations s_2 and s_3 and preheating the working fluid between stations s_3 and s_4 after which it exits the preheater for reinjection. The working fluid coming from the circulation pump at temperature 40°C, enters the preheater at station wf_1 where it is heated to a liquid saturation temperature at the pressure of 12 bars between stations wf_1 and wf_2. The fluid gains a temperature of 125.3°C at station wf_2, is then vaporized between stations wf_2 and wf_3 until it becomes saturated vapour at station wf_3. Between stations wf_3 and wf_4, the working fluid is superheated by 5°C and it exits the vaporizer as superheated vapour at a temperature of 130.3°C. The heat exchanger process is similar in dry cooled and wet cooled basic binary but operating at 11 bar vaporizer pressure. The process of heat transfer in the preheater and vaporizer is presented in the Figure 35.

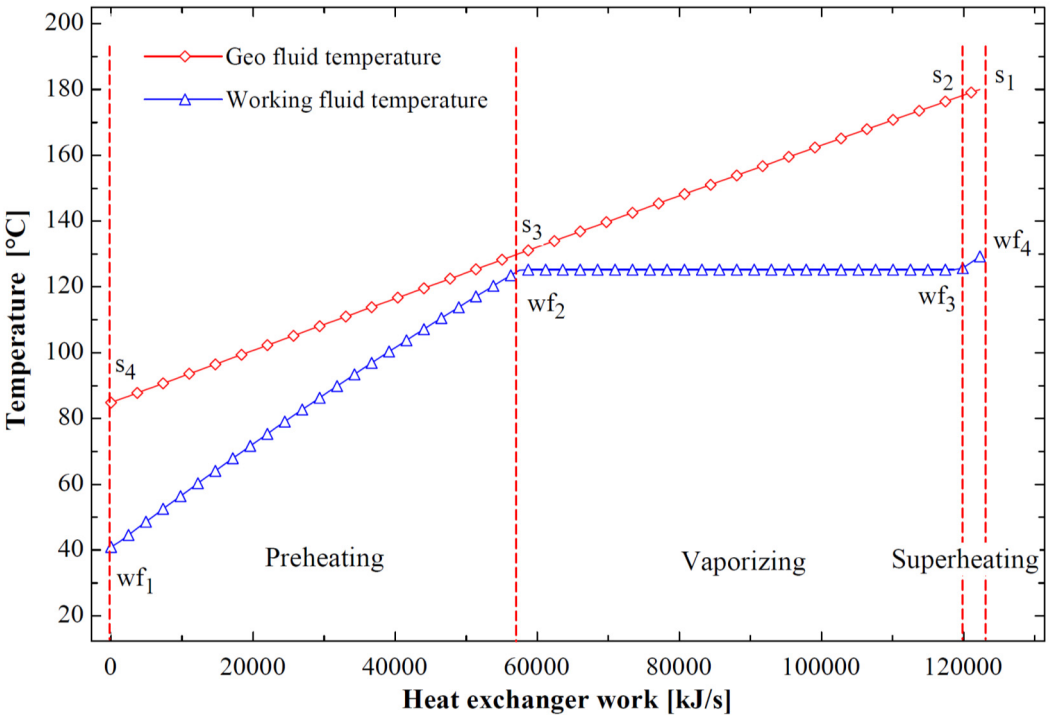

FIGURE 35: Heat transfer process in the preheater
and vaporizer for the basic binary model

In the condenser, the working fluid comes from the turbine exit at station wf_6 and enters the condenser as superheated vapour at 80.78°C in the case of dry cooled basic model. The fluid is de-superheated between stations wf_6 and wf_7 in the condenser until it reaches condensing temperature of 40°C. The fluid is saturated vapour at point wf_7 and passes through a process of condensation between stations wf_7 and wf_8 until it is saturated liquid at station wf_8 after which the fluid exits the condenser at condenser temperature. The heat transfer process in the condenser is presented in the Figure 36.

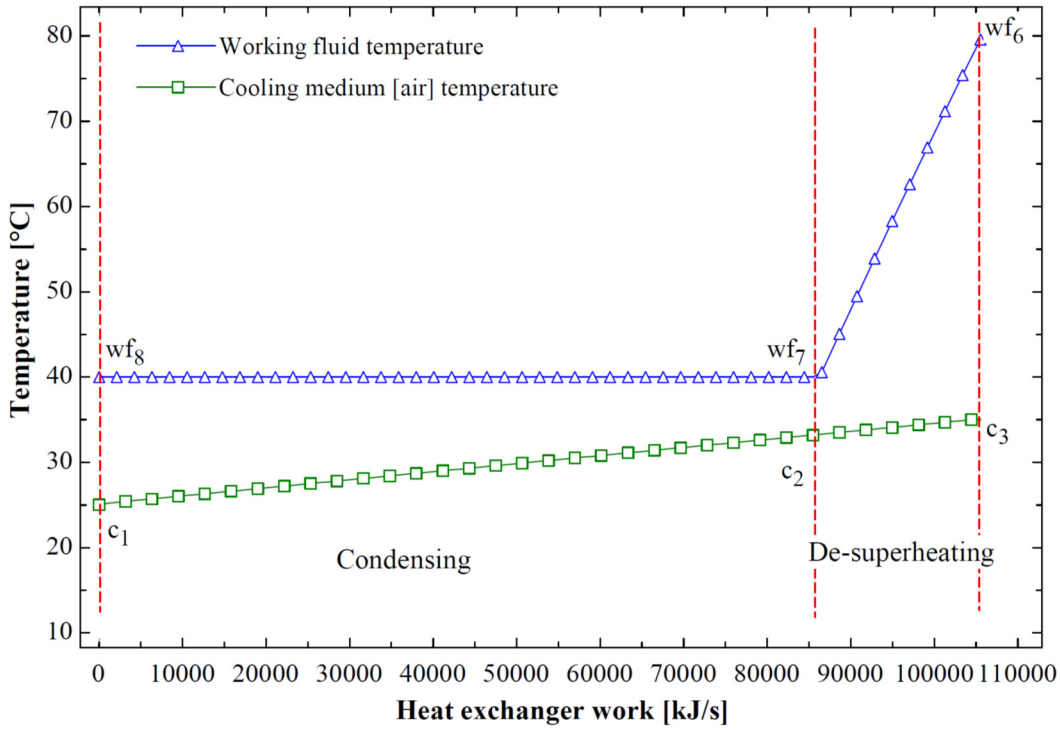

FIGURE 36: Heat transfer process in the condenser for the basic binary model

Results of the dry and wet cooled basic binary modelling with the given boundary conditions are presented in Table 5. With the given boundary conditions at vaporizer pressure of 12 bars and geothermal fluid mass flow of 230.2 kg/s, the dry cooled basic binary model produces 10.002 MW of net generator power output at a parasitic load ratio of 20.55% and the cycle efficiency is 13.72%. At vaporizer pressure of 11 bar and geothermal fluid mass flow of 209.8 kg/s, the wet cooled basic binary model produces 10.002 MW of net generator power output at a parasitic load ratio of 14.06% and the cycle efficiency is 13.32%. With the given geothermal fluid mass flow, the models require 6 production wells.

TABLE 5: Results of the dry and wet cooled basic binary plant

Parameters	Values for basic model		Units
	Dry	Wet	
Gross power	13.252	12.25	MW
Parasitic load	2.724	1.722	MW
Parasitic load proportion to gross power	20.55	14.06	%
Net power	10.002	10.002	MW
Cycle efficiency	13.72	13.32	%
Preheater area	2426	2371	m^2
Vaporizer area	1509	1416	m^2
Recuperator area	n/a	n/a	m^2
Condenser area	5062	4918	m^2
Fan power	1640	346.7	kW
Pump power	1083	1375	kW
Required geothermal fluid mass flow	230.2	209.8	kg/s
Estimated number of production wells	6	6	Wells
Working fluid mass flow	196.7	190.6	kg/s

5.2.2 Recuperative binary with dry and wet cooling system

The optimal vaporizer pressure for recuperative models is 11 bar as presented in Appendices 2 (a and b) and 3 (a and b). Dry cooled recuperative binary model requires a geothermal mass flow of 224.9 kg/s while the wet cooled recuperative model requires a geothermal mass flow 208.8 kg/s to produce 10 MW (Appendices 2c and 3c).

The Process Flow Diagrams (PFD) for the dry and wet cooled recuperative binary models with parameters around the cycles, are presented in Appendices 7 and 8. The T-s, T-h and P-h diagrams for the cycles exhibits the expected way of a recuperative binary cycle. The T-s diagram for the cycle is presented in Figure 37 and the T-h diagram for the dry cooled cycle is presented in Figure 38. The working fluid at station wf_{10} is immediately after the condenser and at the circulation pump entry. The fluid increases in pressure as it passes through the pump across station wf_{10} and wf_1. At

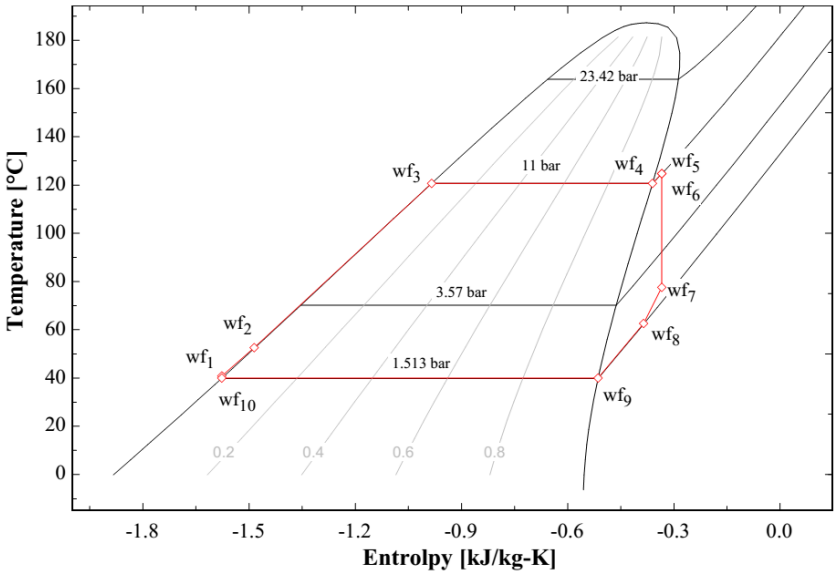

FIGURE 37: T-s diagram for the dry cooled recuperative binary cycle

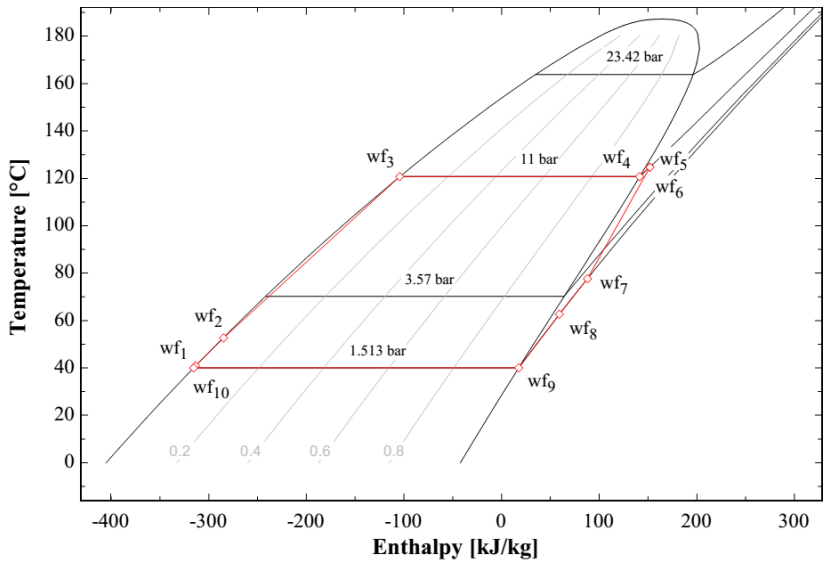

FIGURE 38: T-h diagram for the dry cooled recuperative binary cycle

station wf_1, the fluid gains in pressure as well as slight gain in temperature (hence slight gain in enthalpy). The working fluid changes in entropy and gains in enthalpy at station wf_2 by means of waste heat recovery in a recuperator as shown in Figures 37 and 38. The fluid changes more in entropy as well as gaining in enthalpy as it passes through the preheater until station wf_3 where it attains a saturation temperature of 120.7°C. At wf_3, the fluid is saturated liquid and changes to saturated vapour at station wf_4 by going through the vaporizer at constant temperature. In order to eliminate any potential moisture as explained in the basic binary, the vapour is superheated at station wf_5, to 5°C more than the vaporizing temperature hence reaching a temperature of 125.7°C. The vapour is then expanded through the turbine between stations wf_6 and wf_7. In a process of waste heat recovery, the working fluid from the turbine rejects some of its heat to the working fluid coming from the condenser across the recuperator (stations wf_7 and wf_8). This design considers that 40% of heat required for condenser de-superheating, is rejected in the recuperator (expert opinion). The 40% de-superheating duty provides a temperature drop of 15.92°C across the recuperator for the working fluid coming from the turbine which is at temperature of 78.76°C. The fluid from the turbine exits the recuperator at a temperature of 62.84°C and is sent to the condenser inlet at station wf_8. The working fluid is de-superheated in the condenser from 62.84°C until it reaches saturated vapour state at station wf_9 and thereafter condensed to saturated liquid at condensing temperature of 40°C. By using the recuperator, the work of the condenser is reduced, and so is the size of the condenser. The fluid is saturated at station wf_{10} and the process repeats. The same process and stages are done in the wet cooled recuperative binary model.

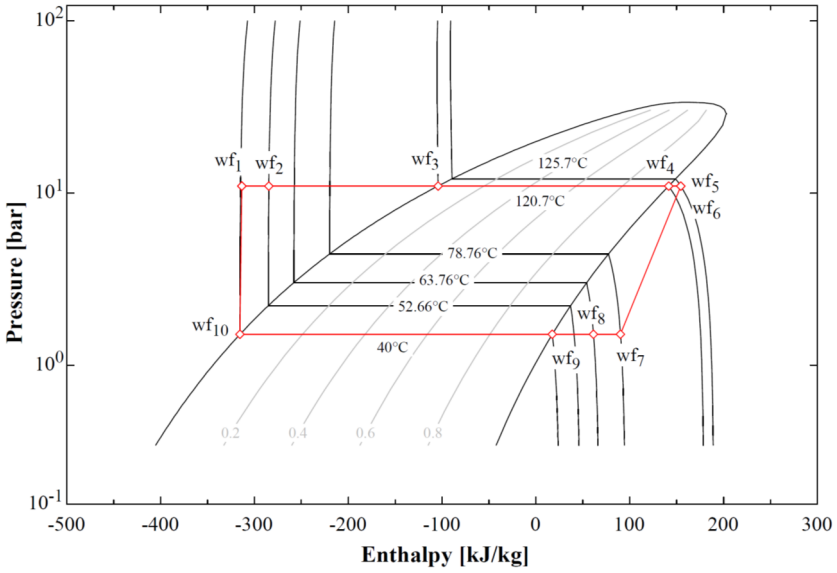

FIGURE 39: P-h diagram for the dry cooled recuperative binary cycle

As the vapour is expanded through the turbine, it moves from region of high pressure at point wf_6, to region of lower pressure at point wf_7 which is the condensing pressure. Just like the basic binary, the recuperative cycle has two pressure levels, the high pressure level and the low pressure level. Stations in the cycle that are at the high pressure level include stations wf_1, wf_2, wf_3, wf_4, wf_5 and wf_6. Stations in the cycle that are at the low pressure level include points wf_7, wf_8, wf_9 and wf_{10} as shown in Figure 39 which is the P-h diagram for the cycle.

The T-s, T-h and P-h diagrams for wet cooled recuperative binary cycle are presented in the Appendix 9(a – c). All the stages of the cycle are the same as in the dry cooled recuperative binary cycle, only differing in the cooling system.

Results of the dry and wet cooled recuperative binary models according to the boundary conditions are presented in Table 6. At vaporizer pressure of 11 bars and geothermal fluid mass flow of 224.9 kg/s, the dry cooled recuperative binary model produces 10.002 MW of net generator power output at a parasitic load ratio of 19.82% and the cycle efficiency is 14.24%. At vaporizer pressure of 11 bar and geothermal fluid mass flow of 208.8 kg/s, the wet cooled recuperative binary model produces 10.003 MW of net generator power output at a parasitic load ratio of 13.62% and the cycle efficiency is 14.19%. With the given geothermal fluid mass flow, the well requirement is 6 production wells, like in the basic model.

TABLE 6: Results of dry cooled and wet cooled recuperative binary plant

Parameters	Values for recuperative model		Units
	Dry	Wet	
Gross power	13.13	12.19	MW
Parasitic load	2.602	1.661	MW
Parasitic load proportion to gross power	19.82	13.62	%
Net power	10.002	10.003	MW
Cycle efficiency	14.24	14.19	%
Preheater area	2607	2409	m^2
Vaporizer area	1518	1410	m^2
Recuperator area	659.3	565.8	m^2
Condenser area	4570	4079	m^2
Fan power	1560	320.4	kW
Pump power	1042	1340	kW
Required geothermal fluid mass flow	224.9	208.8	kg/s
Estimated number of production wells	6	6	Wells
Working fluid mass flow	204.3	189.7	kg/s

A summary of results for the technical performance of the four cycles, i.e. dry and wet cooled basic binary and dry and wet cooled recuperative binary are presented in Figure 40. The models have been presented to deliver the same net generator power output of 10 MW. From the figure presented, the dry cooled models are generating the net generator power at a higher gross turbine output than the wet cooled models. Much of the power generated is being used by the parasitic load mainly in terms of condenser fan and this leave the models with lower net power generated. With the restriction of reinjection and maintain cycle parameters, it is observed that recuperative models are more efficient than basic models due to the waste heat recovery system implemented.

The wet recuperative cycle gives the best technical performance of the 4 models. The model produces 10 MW from the least gross turbine output of 12.19 MW with higher efficiency. The model has the lowest parasitic load of 13.62% produced from the least required geothermal fluid mass flow of 208.8 kg/s using the lowest working fluid mass flow of 189.7 kg/s. This eventually leads to general use of smaller equipment in the power plant.

The dry cooled basic binary is the lowest performers of the models having a highest gross turbine work output of 13.252 MW at very high parasitic load of 20.55%. The model requires 230.2 kg/s of geothermal fluid to produce 10 MW, which is the highest geothermal fluid requirement of all the models. As a result, the model increases in equipment surface area as which results in high parasitic load.

The second best model technically is the wet cooled basic binary model. The model produces the 10 MW net generator power output from 12.25 MW of turbine work output at 14.06% parasitic load consumption.

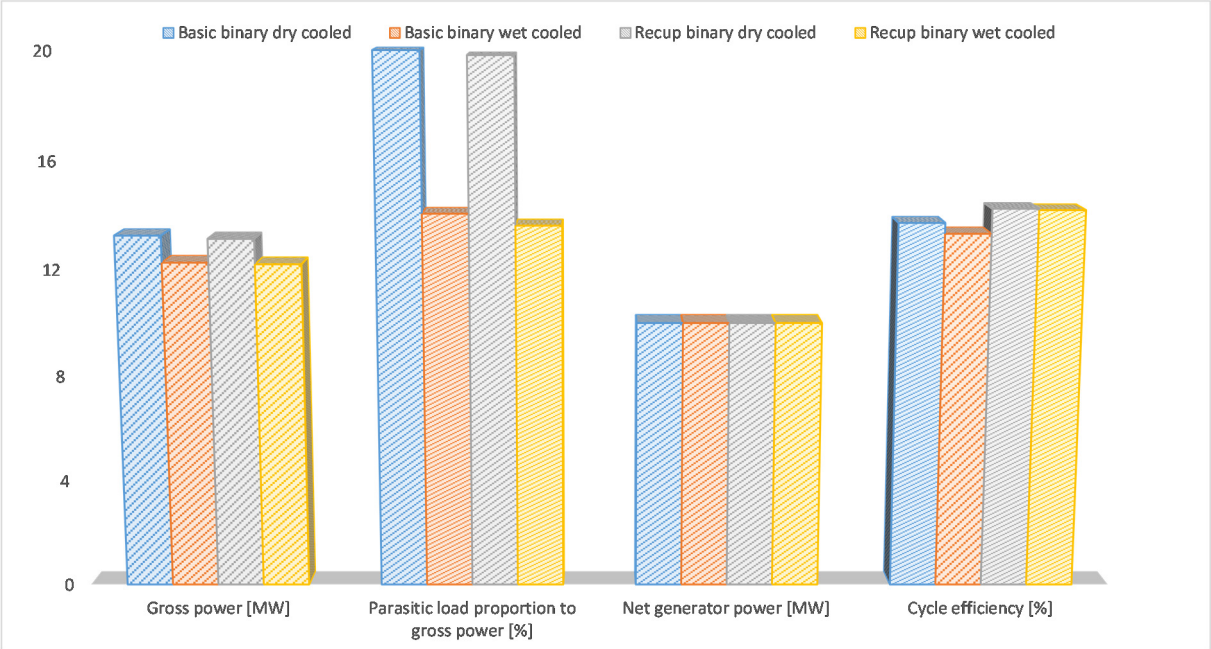

FIGURE 40: Summary of technical analysis of power for the binary models

Note: for each group of bars in Figure 40, first bar is for dry cooled basic binary, second bar is for wet cooled basic binary, third bar is dry cooled recuperative binary and fourth bar is for wet cooled recuperative binary.

The effect of introducing a recuperator is observed by changes in different parameters of the model's equipment. With the restricted net output models discussed, the impact of the recuperator is observed more in the efficiency of the cycles. The recuperative cycle is more efficient than the basic cycle with 4% and 7% more efficient in the dry cooled and wet cooled models respectively. This results in net reduction in size and capacity of various cycle equipment. The condenser reduces by 10 and 17% in wet and dry models respectively upon introducing the recuperator. These reductions are presented in Table 7 below where recuperator effect on dry cooled model and wet cooled model are presented as a percentage change.

TABLE 7: Recuperator effect on wet and dry cooled models

Parameters	**Recuperator effect**	
	Dry model	**Wet model**
Gross power	-1%	0%
Parasitic load	-4%	-4%
Parasitic load proportion to gross power	-4%	-3%
Net power	0%	0%
Cycle efficiency	4%	7%
Preheater area	7%	2%
Vaporizer area	1%	0%
Recuperator area	0%	0%
Condenser area	-10%	-17%
Fan power	-5%	-8%
Pump power	-4%	-3%
Required geothermal fluid mass flow	-2%	0%
Estimated number of production wells	0%	0%
Working fluid mass flow	4%	0%

The effect of cooling medium on the basic and recuperative models is presented in Appendix 10. The change in cooling system from dry cooling to wet cooling shows general reduction in parasitic load mainly in fan power which reduces by almost 79% and cause total parasitic load to reduce by 37% and

36% in basic and recuperative models. The heat exchanger areas are also reduced by implementing wet cooling over dry cooling, with 4% area reduction in both models. The change from dry cooling to wet cooling however, increases pump power by 27 and 29% in basic and recuperative models respectively. Figure 41 presents the change in equipment size and mass flow of geothermal fluid as well as working fluid.

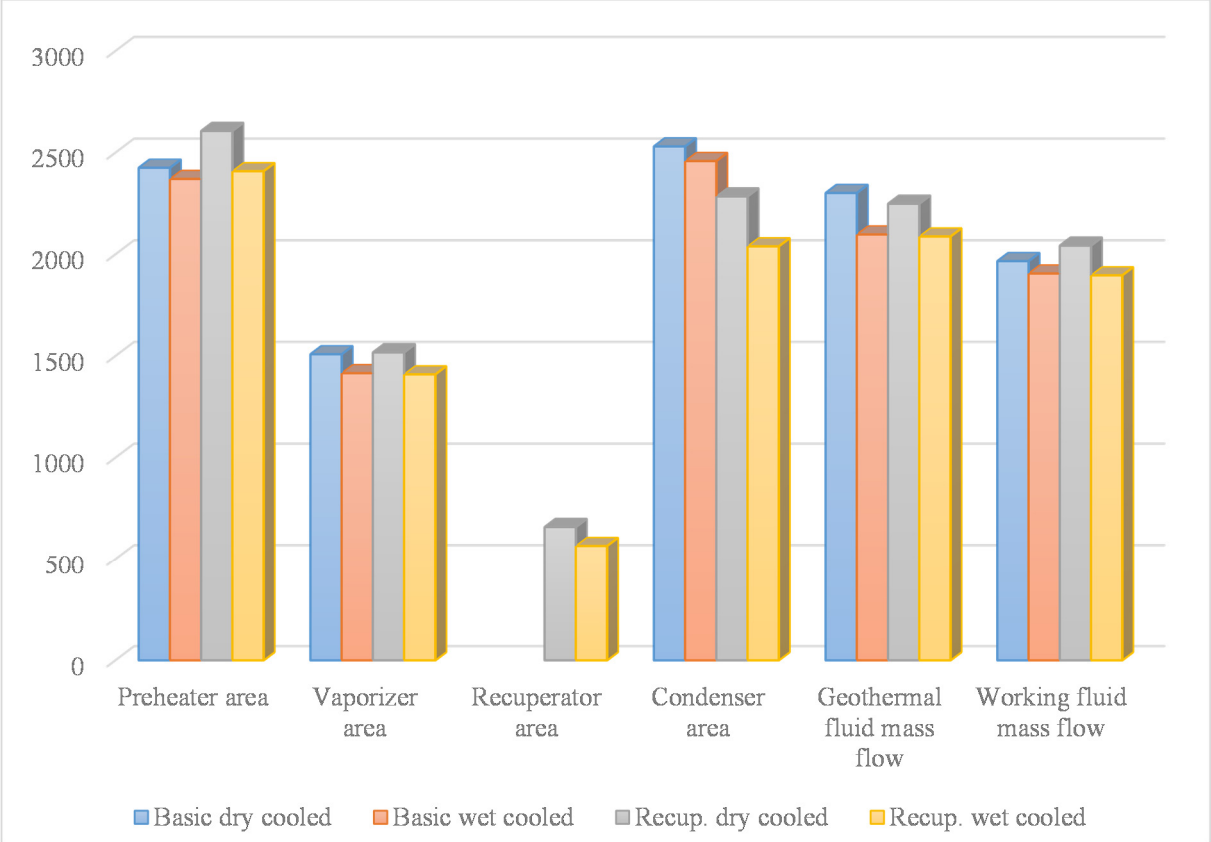

FIGURE 41: Comparison of equipment size and fluids for the binary models

6. ECONOMIC ANALYSIS OF THE APPLICABLE TECHNOLOGY

This section discusses the cost of developing the binary power plant for Chiweta in Malawi. Since Chiweta requires field exploration as well as well drilling, the study considers field development costs which covers mainly the cost of drilling required number of wells. This is done to provide a holistic perspective of developing the geothermal field for binary power plant.

The field lies within reach of the national grid transmission line, within 1 km distance from a 33 kV power lines that supply the surrounding areas. However, the next transmission substation is not within the reach of the area. This calls for considering a substation for the power station that will link the power station with the 33 kV transmission line passing through the area. Accessibility to the area is within 0.5 km from the main road, however an access road from the main road will be required. Cost of the access road to the plant as well as to wells is not included in the analysis for the sake of focusing on the things that matter to the power plant, however it is supposed to be put under consideration when developing the field. The economic analysis considers costs of various works and power plant equipment as discussed below.

6.1 Cost of field development

The study assumes that the exploration costs are excluded in this assessment. The study considers undertaking well drilling for both production and reinjection. There will be 6 production wells with 3 reinjection wells to cater for the geo-fluid requirement for each model in line with the geothermal fluid demand. For purposes of this study, success rate of drilling production wells is not considered, but it is acknowledged that drilling of a production well at a proper target sometimes may not be successful. According to communications with EFLA consulting firm, drilling a single geothermal well may cost between US $4 and US $6 million depending on the complexity of the environment that the well is being drilled. However, VERKÍS details that for European environment it cost around US $2.6 million to have a well at an average depth of 1400 m with complete installation of line shaft pump at a depth of 200 m (VERKÍS Consulting Engineers, 2014). With Chiweta being in tropical region in Africa and not in Europe as suggested by VERKÍS, this study considers the minimal suggested cost from EFLA which is US $4 million/well. With 6 production wells, the well cost is US $24 million.

Based on VERKÍS Consulting Engineers (2014), the cost of gathering system for a 40 l/s mass flow is estimated at US $80,000.00. Since this is equivalent to one production well, the total cost of gathering system for the models is US $480,000. The cost of reinjection wells is assumed to be half the cost of production wells and in this case it is US $2million. Cost of reinjection system is given to be US $40,000.00 and this is also based on the capacity proposed by VERKÍS. For the models, the reinjection system cost is therefore US $120,000. A summary of the field costs is given in the Table 8.

TABLE 8: Geothermal field cost estimates

Description	Cost (US $)
Cost of 6 production wells	24,000,000.00
Cost of 3 reinjection wells	6,000,000.00
Fluid gathering system	480,000.00
Reinjection system	120,000.00
Total dry cooled field cost	***30,600,000.00***

The study assumes that the production wells will deliver as desired throughout the project life. However, the reality is that production wells tend to decline in their fluid production as the reservoir responds to the extraction of fluid. Such reservoir response calls for drilling of make-up wells in order to maintain the production capacity of the power plant. Since reservoir characteristics are not known at the moment, the assumption of constant well production of geo-fluid holds.

6.2 Cost of power plant's major equipment

The major components in the power plant are given in Table 9 below. The costs of the major equipment are based on Ahangar (2012) and others where the unit costs of the equipment are given as follows:

Vaporizer unit cost (US$/m^2)	500
Preheater unit cost (US$/m^2)	450
Recuperator unit cost (US$/m^2)	600
Condenser unit cost (US$/m^2)	400
Turbine unit cost (US$/kW)	500
Fan unit cost (US$/kW)	400
Pump unit cost (US$/kW)	450

The cost of wet cooling tower estimated as proposed by Forsha and Nichol is 170/kW (Forsha and Nichols, 1992). When this cost is considered using inflation for the period 1992 – 2015, the inflation consideration is 69.5% (BLS, 2015), the cost of cooling towers become enormous, bearing in mind that improvements in technology have a bearing on costs. A model cooling tower is created in cooling tower depot website, considering the required cooling water flow in the cooling tower, based on model calculations, and the height of the tower. The cost of the modelled cooling tower that satisfy the cooling requirements of the models and is made of fibre glass, is US $936,138.00 (Cooling Tower Depot, 2015). This work rounds up the cooling tower cost to US $1million.

The costs proposed by Ahangar (2012) are subjected to the inflation factor and used to calculate indicative cost of major equipment according to their size and capacity and the cost of the equipment is presented in Table 9.

TABLE 9: Estimated costs of power plant major equipment

Parameters		***Values for basic model***		***Values for recuperative model***	
		Dry	***Wet***	***Dry***	***Wet***
Gross power	*(MW)*	13.25	12.25	13.13	12.19
Vaporizer	*Size (m^2)*	*1509*	*1416*	*1518*	*1410*
	Cost	796,752.00	747,648.00	801,504.00	744,480.00
Preheater	*Size (m^2)*	*2426*	*2371*	*2607*	*2409*
	Cost	1,152,835.20	1,126,699.20	1,238,846.40	1,144,756.80
Recuperator	*Size (m^2)*	*0*	*0*	*659.3*	*565.8*
	Cost	-	-	278,488.32	238,993.92
Condenser	*Size (m^2)*	*5062*	*4918*	*4570*	*4079*
	Cost	3,207,283.20	3,116,044.80	2,895,552.00	2,584,454.40
Turbine	*Size (kW)*	*13,252.00*	*12,250.00*	*13,130.00*	*12,190.00*
	Cost	5,597,644.80	5,174,400.00	5,546,112.00	5,149,056.00
Wet cooling tower	*Size (kg/s)*	-	*1,500.00*	-	*1,500.00*
	Cost	-	1,000,000.00	-	1,000,000.00
Fan	*Capacity (kW)*	*1,640.00*	*346.70*	*1,560.00*	*320.40*
	Cost	692,736.00	146,446.08	658,944.00	135,336.96
Pump	*Capacity (kW)*	*1,083.00*	*1,375.00*	*1,042.00*	*1,340.00*
	Cost	514,641.60	653,400.00	495,158.40	636,768.00
Total cost of equipment		***11,961,892.80***	***11,964,638.08***	***11,914,605.12***	***11,633,846.08***

Table 9 shows that there is insignificant change in cost of major equipment when using either wet cooling or dry cooling system in basic model. This comes as the gains in some equipment are lost to other equipment, for example there is reduction in fan power when moving from dry to wet cooling, but there is an increase in pump power. In recuperative model, there is an overall reduction of 2.4% in equipment cost when changing from dry to wet cooling system.

Table 9 also shows that introduction of a recuperator in the model increases the cost of major equipment by 2.8% in the wet cooled model and 0.4% change in equipment cost in dry cooling model. This comes as the effect of general equipment size as presented in Table 7 thereby having a net reduction in costs due to reduction of capacities of such equipment as cooling fans and condensing area for the 10 MW models.

6.3 Civil, electrical and controls cost

Cost of putting up civil structures and related electrical and control equipment, generally corresponds to the capacity of the power plant. The bigger the power plant, the higher the civil works and electrical and control equipment associated with it and hence the higher the costs.

According to report from DoE, the 2012 costs for civil works and electrical and control equipment for a 50 MW binary power plant are US $8,351,000.00 and US $18,335,000.00, respectively (US EIA, 2013). Using the average inflation rate of 1.4% and hence the cumulative inflation of 5.6%, the cost for civil works is US $176.37/kW and the cost of electrical and control equipment is US $387.24/kW. These per unit costs are used to calculate their related estimated costs for the models under analysis and these estimates are summarised in Table 10.

TABLE 10: Summary of civil works and electrical and control equipment costs

	From US EIA (2013)	Per kW cost Inflation Corrected
Inflation 2013 to 2015		**106%**
Capacity (kW)	50,000	
Civil works cost (US$)	8,351,000.00	176.37
Electrical & control equipment cost (US$)	18,335,000.00	387.24

Description	Values for basic model (US$)		Values for recuperative model (US$)	
	Dry	Wet	Dry	Wet
Civil works cost	2,337,296.59	2,160,570.72	2,315,779.07	2,149,988.33
Electrical & control equipment cost	5,131,640.87	4,743,631.20	5,084,398.18	4,720,397.09

6.4 Total costs of developing the models

All costs discussed are summarised in the Table 11 below. The table shows that wet cooled recuperative binary is the least cost model in this assessment costing US $49.1 million, while the dry cooled basic binary is the most expensive cycle in the analysis costing US $50 million. Wet cooled basic binary model and dry cooled recuperative binary model come second and third respectively as the least cost models with the wet cooled basic model being cheaper than the dry cooled recuperative model at US $49.47 million and US $49.91 million respectively. A graphical presentation of the total cost of the models is presented in the Figure 42.

TABLE 11: Total cost of developing the models

Description	Values for basic model (US$)		Values for recuperative model (US$)	
	Dry	Wet	Dry	Wet
Field development	30,600,000.00	30,600,000.00	30,600,000.00	30,600,000.00
Major equipment cost	11,961,892.80	11,964,638.08	11,914,605.12	11,633,846.08
Civil works cost	2,337,296.59	2,160,570.72	2,315,779.07	2,149,988.33
Electrical & control equipment cost	5,131,640.87	4,743,631.20	5,084,398.18	4,720,397.09
Total cost without field development	*19,430,830.26*	*18,868,840.00*	*19,314,782.36*	*18,504,231.50*
Grand total project cost	***$ 50,030,830.26***	***$ 49,468,840.00***	***$ 49,914,782.36***	***$ 49,104,231.50***

The cost of development without field development, i.e. drilling costs, is close to the cost of a 12 MW binary power plant of US $20 million as suggested by EFLA experts.

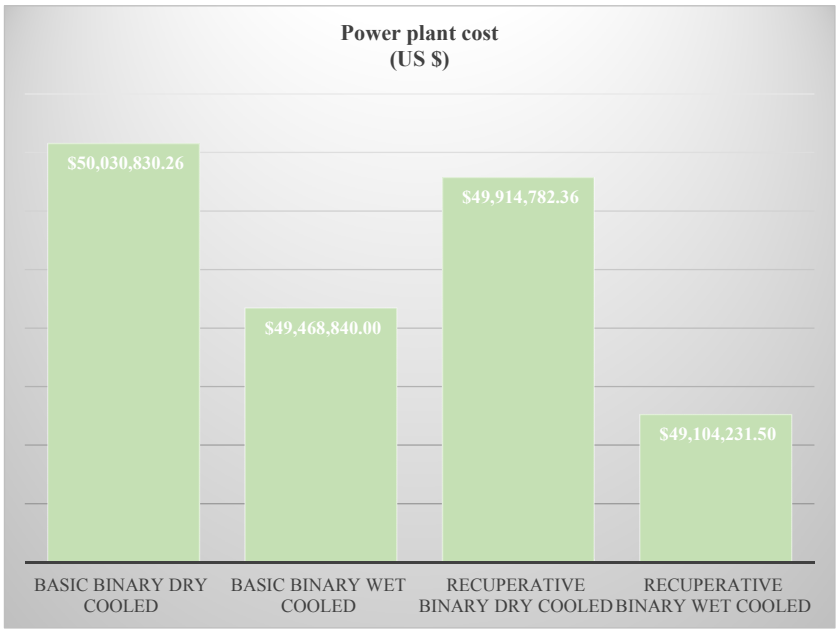

FIGURE 42: Total cost of models

The presentation in Figure 42 shows that the wet cooled models have a slight margin in cost making them relatively cheaper to develop with the given parameters when compared to the dry cooling models. Wet cooling models have a net reduction in power plant equipment size, which eventually cause the models to be cost efficient than the dry cooled models. However in this case, the margin is not much, a reason that can attributed to the proximity of average ambient air temperature and average water temperature used in the cooling medium.

From the summary of power plant model cost, the cost of generating a kW of electricity from the 10 MW models given their development cost is as follows:

Basic binary dry cooled model	US $5,002.08 /kW
Basic binary wet cooled model	US $4,945.89 /kW
Recuperative binary dry cooled model	US $4,990.48 /kW
Recuperative binary wet cooled model	US $4,908.95 /kW

A graphical presentation of the models' cost of generating a kW is presented in Figure 43. The figure is a reflection of the total cost of model as described in Figure 42. The figures from this analysis are out of the range of most authors. ESMAP proposes an average cost of binary plants as between US $2,500 and US $4,000 per kW (Energy Unit, 2012). Based on a number of authors, Hance (2005) puts a range of capital cost of geothermal binary power plants as US $1700 – 2700 /kW and he quotes Califonia Energy Commission's estimate of developing a 10 – 30 MW binary plant as between US $3000 – 3300 /kW. The out of range in this study's per kW cost is a result of uncertainty in field costs that uses pessimistic average values of well discharge, leading to low production from wells at high cost. Improvement in the field costs significantly improves the per kW cost of generating electricity for the models.

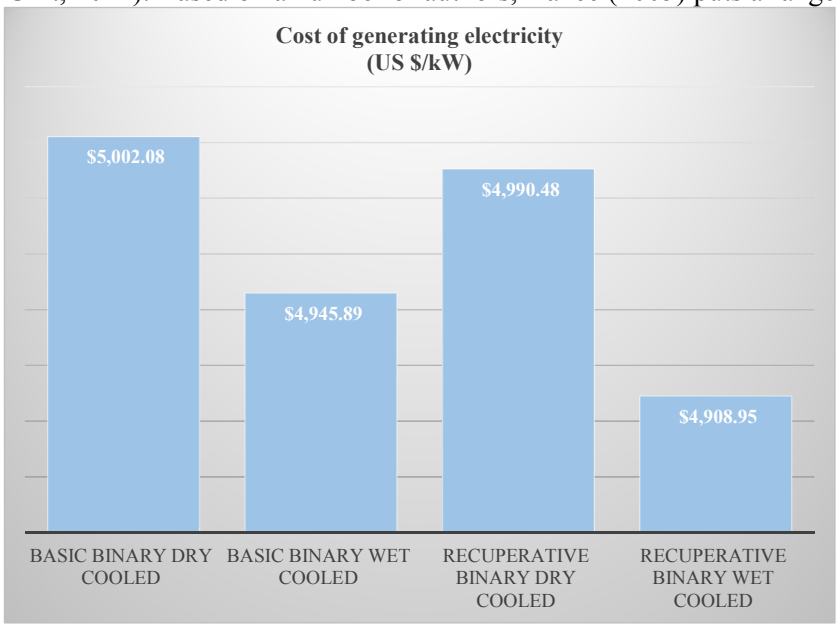

FIGURE 43: Cost of generating a kW for the models

6.5 Financial ratios analysis

The study assumes that the project will integrate into the already existing national grid with appropriate transmission and power purchase agreements with the prevailing electricity industry. The Weighted Average Cost of Capital (WACC) is normally used in financial analysis. WACC may be replaced with discount rate which is used in this work. The discount rate used for the NPV and IRR analysis in this work is 12% (ESMAP, 2012). For the sake of this work, changes in factors such as impact of inflation, electricity tariff changes, operation and maintenance cost over time are not taken into consideration. However, they are acknowledged that they may have an impact on the economics of the power plant.

6.5.1 Operations and maintenance costs

The annual operation and maintenance (O and M) cost as provided by US EIA is US$100/kW at a dollar rate of 2012 (US EIA, 2013). Using the cumulative inflation of 5.6% (The Federal Reserve, 2015), the maintenance cost would be US$ 105.6/kW. The O and M cost for the four models at turbine power output using the US EIA provision are presented in Table 12.

TABLE 12: O and M cost for the four models

Description	*Units*	*Values for basic model*		*Values for recuperative model*	
		Dry	*Wet*	*Dry*	*Wet*
Capacity	(MW)	13.25	12.25	13.13	12.19
O&M cost	US$	1,399,411.20	1,293,600.00	1,386,528.00	1,287,264.00

The values found in this annual O and M costs are not very different from VERKÍS' proposal which is about US $1.3 million for a 10 MW recuperative power plant (VERKÍS Consulting Engineers, 2014). Where cost is not certain, the rate of O and M for geothermal is usually pegged between 1.5 and 2.5% of the power plant cost (ESMAP, 2012).

6.5.2 Revenue estimates for the models

The Feed in tariff policy for Malawi has provided tariff for various renewable energy sources. For geothermal source, the policy has provided a tariff of US $0.105/kWh for bulk supply to the grid (MERA, 2012), and this is used in this study. Since market forces change over time, the tariff can be negotiated for revision with the regulator, depending on changes of the factors that affect the tariff and the operating environment. However, the study assumes no change in tariff for the life time of the project.

Revenue of a power plant is dependent on the capacity of the generator and the availability of the power plant to deliver the energy otherwise known as the capacity factor. Capacity factor of geothermal power plants vary between 60 and 95% (Mines et al., 2015), but the commonly applicable capacity factor is 90% (Sanyal, 2004) which this work uses. Using the tariff and the capacity factor given, the expected annual revenue of the power plants is calculated. The tariff is multiplied by generator's annual production capacity which is the model power production capacity multiplied by hours in a year and capacity factor. This is provided in Equation 27.

$$C_t = C_{geo} * W_{net.tur} * \eta_g * h_{annual} * \eta_{cf} \quad (27)$$

where C_t is the revenue of the model at year t;
C_{geo} is the tariff for geothermal;
$W_{net.tur}$ is the turbine net output;
η_g is the generator efficiency;
h_{annual} is hours in a year;
η_{cf} is the capacity factor of the plant.

Considering the operations and maintenance, the net annual net revenue of the models is found by subtracting the O and M cost from the C_t in Equation 27 which gives Equation 28 as follows:

$$C_{t\_net} = C_t - C_{Oand\,M} \quad (28)$$

where C_{t_net} is the net annual revenue of the model;
$C_{O\,and\,M}$ is the O and M cost of the model.

The estimated net annual revenue calculated using Equations 27 and 28 is presented in Table 13 below.

TABLE 13: Estimated annual revenue for the models

Model	Annual production capacity (GWh)	Annual revenue (US $)
Basic binary dry cooled	78.856	6,880,444.44
Basic binary wet cooled	78.856	6,986,255.64
Recuperative binary dry cooled	78.856	6,893,327.64
Recuperative binary wet cooled	78.864	6,993,419.46

Since the net generation capacity of the models is almost equal, the net revenues only differ with respect to the O and M cost of the respective models. The O and M cost is based on the gross turbine work output and hence the more the model produces at turbine, the more the O and M cost and the less the net revenue generated. Table 13 show that the wet cooled recuperative binary has a higher net annual revenue of US $6,993,419.46 per year while dry cooled basic binary has a lowest revenue of US $6,880,444.44 per year. The wet cooled basic binary and dry cooled recuperative binary are in second and third positions respectively with wet cooled basic binary having US $6,986,255.64 per year and dry cooled recuperative binary having US $6,893,327.64 per year. Considering the basic binary as a benchmark model, the revenue from the models show that a wet cooled basic binary model has 1.54% more revenue, dry cooled recuperative binary has 0.19% more and wet cooled recuperative binary model has 1.64% more revenue compared to basic binary model.

6.5.3 The Net Present Value assessment for the models

The Net Present Value (NPV) rule states that all projects that have a positive net present value should be accepted and the projects that have a negative NPV should be rejected (Copeland and Weston, 1986). Where a project gives a positive NPV, it signifies that the project would increase the value of the firm or owners. NPV is computed using the Equation 29 below:

$$NPV = -C_0 + \sum_{t=1}^{N} \frac{C_{t\_net}}{(1+r)^t} \quad (29)$$

where t is the annual time of the project;
N is the life time of the project;
$-C_0$ is the initial capital of the project;
r is the cost of capital (discount rate).

The life time of the project is set for 20 years at the discount rate of 12%. Using Equation 29 the NPV for the models are calculated and presented in Figure 44 below.

It is observed from Figure 44 that all the models have positive NPV for the 20 years life time of assessment. The model with the least NPV is the dry cooled basic binary with US $1.36 million and the model with the highest NPV is the wet cooled recuperative binary with US $3.13 million which is 130% more than the least NPV model. The wet cooled basic binary has an NPV of US $2.71 million which is 99.27% more as compared to the least NPV model, while the dry cooled recuperative binary has an NPV of US $1.57 million representing a 15.58% more than the least NPV model. For mutually exclusive projects, a decision is usually based on an investment with the higher NPV. In this case the wet cooled recuperative binary would be considered.

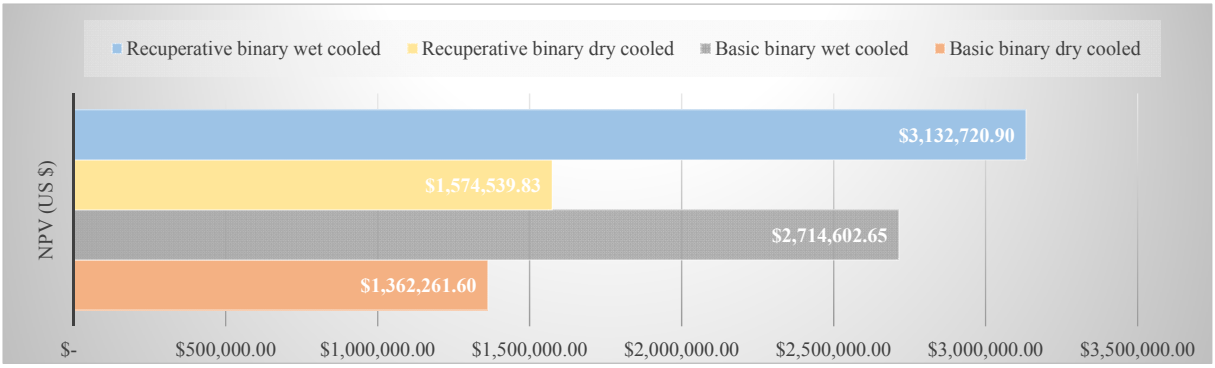

FIGURE 44: Net Present Value for the models

6.5.4 The Internal Rate of Return

The internal rate of return (IRR) is a discount rate of a project which equates the present value of the project's cash outflows and inflows or equates a project's investment in a certain time period with its cash inflows. In other words, IRR is the rate at which the project's NPV is zero (Copeland & Weston, 1986) i.e. where the project can break even. Hence this is the rate of return on invested capital that the project is returning to the firm. The IRR helps to assess profitability of the project and is found by using Equation 30 as shown below.

$$C_0 = +\sum_{t=1}^{N} \frac{C_{t\_net}}{(1+r_i)^t} \tag{30}$$

where r_i is the internal rate of return (*IRR*).

The initial guess rate for this analysis assumes the given discount rate for NPV analysis above. There is a relationship between the IRR and the opportunity cost of alternative capital investment project. IRR is associated with the expected rate of return from the project such that if the result of IRR is more than the expected return, the investment is acceptable. Otherwise the investment is rejected if the value of IRR is less than expected rate of return. It also goes that the higher the IRR for a project, the better the project is economically.

Using Equation 30 and the initial guess rate of 12 as in discount rate, the IRR for the 4 models is computed and the results are given in Table 14.

TABLE 14: Internal Rate of Return for the models

Model	IRR (%)
Basic binary dry cooled	12.43%
Basic binary wet cooled	12.87%
Recuperative binary dry cooled	12.50%
Recuperative binary wet cooled	13.01%

The results of IRR follow the NPV trend, with slim margins between the models. The wet cooled recuperative model has a highest IRR of 13.01%, dry cooled basic model has the lowest IRR of 12.43%. The wet cooled basic model has an IRR of 12.87% which is close to the highest, and dry cooled basic model has an IRR of 12.50%. With the rule of the bigger the better, the wet cooled recuperative model would also be considered in this analysis. The results of IRR are similar to the results from a hypothetical 50 MW geothermal power plant as presented by ESMAP (2012), which is 13.4% at a tariff of US $0.12 /kWh for 30 years.

6.5.5 Discounted payback period

In this analysis, the discounted annual revenue are used to give an indication of how soon the model can recover its investment i.e. estimating the years to recover the initial capital investment. The traditional payback period does not account for the time value for money thereby providing not so realistic estimate of investment recovery as the discounted method does. Discounted payback period incorporates time value for money by discounting all the future revenue of the project thereby providing a better estimate of how long the project would recover its initial investment.

The discount payback period is a sum of all discounted future revenues and the initial investment. The initial investment is a negative value while all revenues are positive values. The year that the sum of investment and revenue becomes a positive, is the payback period. The discount rate used in this analysis is the same as used in NPV. The discounted payback period is presented in Figure 45.

From Figure 45, wet cooled recuperative binary and wet cooled basic binary models have early discounted payback period in the 17th year. The two models are followed by dry cooled recuperative model in year 18 and lastly the dry cooled basic model in year 19. The discounted payback period is sensitive to the discount rate and the tariff of electricity in such a way that with higher discount rate, the payback period gets longer while with lower discount rates the models have a shorter payback period. In terms of tariff, the higher the tariff, the shorter the payback period and the lower the tariff, the longer the payback period.

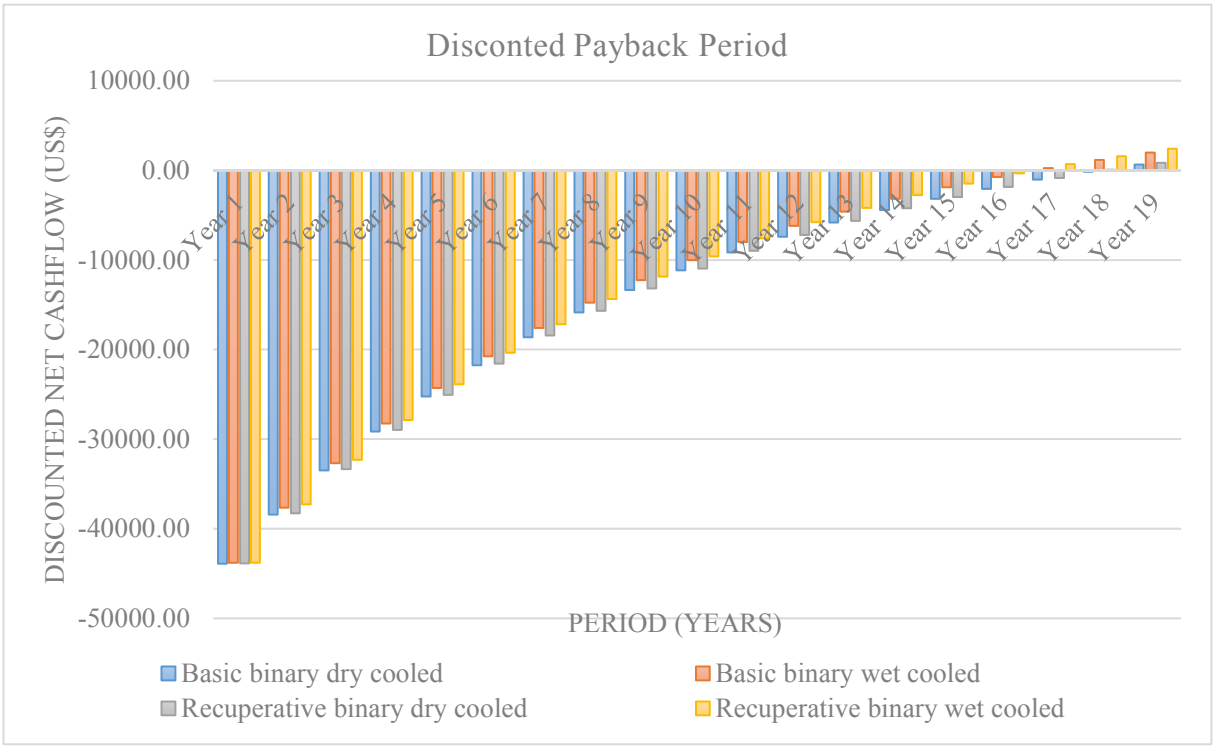

FIGURE 45: Discounted net cash flow for payback period

7. CONCLUSION

The East African Rift System is the major source of geothermal power in Africa. The system is divided into three branches, the eastern branch, western branch and the south eastern branch. The eastern branch is more active with volcanoes. Many studies have been done to understand the branch which has high temperature resource and hence more high temperature utilization projects have been developed. The western branch is paucity of volcanoes and is relatively cooler when compared to the eastern branch. Limited number of studies have been carried out and hence there is less understanding of this branch. With lower temperatures, mostly below 200°C, estimated along the western branch and considering the Lindal diagram of geothermal utilization, it is recommended that geothermal electricity production projects along the branch be of binary type unless substantial detailed studies prove otherwise. Malawi being within the western branch of the EARS and not showing surface manifestations of high temperature system, should consider developing its resource for electricity using binary power plant technology.

Four models of binary technology can be applicable for Chiweta geothermal field in Malawi, which are wet cooled basic binary, dry cooled basic binary, wet cooled recuperative binary and dry cooled recuperative binary. The four models have been subjected to technical and economic analysis using available data and literature based assumptions wherever necessary.

The differences in the technical performance of the models are attributed to use of either air or water as a cooling medium in the models' condensers as well as introducing a recuperator as a waste heat recovery system.

Wet cooled models are observed to operate much better than the dry cooled models in terms of equipment size at the same net power generation. The impact of the cooling medium on performance is such that air is less dense than water and therefore would require more volume of air to cool the same amount of working fluid at a given temperature range which less volume of water would do. The specific heat capacity for air is much less compared to the specific heat capacity of water making wet cooling systems more efficient that dry cooling systems. This then translates into more surface area for condensing in a dry cooling system than in wet cooling system. The models show a decrease in condenser area by 3% in basic models and by 11% in recuperative models due to cooling system. Due to the nature of air, more parasitic load is demanded by fans to push the volume of the cooling medium across the condenser in the dry cooling system thereby presenting less net power output than in wet cooling system. The models show a 37% and 36% reduction in parasitic load in basic and recuperative models respectively.

The introduction of recuperator in the models provides an improvement in efficiency of the cycle with reduction in parasitic load. The recuperative cycle is more efficient than the basic cycle with 4% and 7% more efficient in the dry cooled and wet cooled models respectively. This results in net reduction in size and capacity of various cycle equipment. The most noted change in size is the condenser that reduces by 10% in dry models and by 17% in wet models.

The differences in the economic performance of the models are attributed mainly to the size of equipment as demanded by the models. The technical analysis reveals that dry cooled models require larger cooling and parasitic load equipment to do a similar job that wet cooled model equipment would do thereby affecting the model's efficiency as well as demanding more geothermal fluid than the wet cooled models. This eventually leads to higher capital cost as well as lower revenue when compared to the wet cooling system with the same primary cycle conditions. The model with the lowest cost of power plant is the wet cooled recuperative binary costing US $49.1 million. The second lowest cost model is the wet cooled basic binary which is 0.7% more costly as compared to wet cooled recuperative model. The third least cost model is the dry cooled recuperative binary with 1.65% and the most expensive model of the dry cooled basic binary at 1.89% more than the wet cooled recuperative model.

All the models have a positive Net Present Value when analysed using a discount rate of 12%. The best NPV is from wet cooled recuperative binary with US $3.1 million followed by wet cooled basic binary

with US $2.7 million. All the models give a satisfactory Internal Rate of Return which is more than the discount rate used in the NPV. The wet cooled recuperative model gives the best IRR of 13% while the least IRR is 12.43% for dry cooled basic binary. Using discounted revenue, the earlies discounted payback period for the models is from wet cooled recuperative model and wet cooled basic model in 17th year followed by dry cooled recuperative model in year 18 and finally the dry cooled basic model in year 19.

The results of the analysis show that the best model for implementation is the wet cooled recuperative binary with respect to both technical and economic performance. With a gross power of 12.19 MW the wet cooled recuperative model produces 10 MW of net generator power output using parasitic load of 13.62% and at cycle efficiency of 14.19%. The model is 8% better in turbine work output and 39% better in parasitic load consumption when compared to the least technical performer.

With per capita consumption of 93kWh, generating 10MW from geothermal for Malawi would serve up to 900,000 people or 180,000 households assuming a household of 5 people. The country is still below the recommended sub-Saharan per-capita rate of 432kWh let alone the world's recommended average per capita rate of 2167kWh (Taulo et al., 2015), therefore any additional MW for the people matters for the country to improve on its per capita consumption.

8. RECOMMENDATIONS

The study has shown that a wet cooled recuperative binary is the best in both technical and economic analysis. The analysis has included challenges of silica scaling potential in geothermal fluid hence consideration minimum reinjection temperature to avoid silica scaling. Usually the purpose of including a recuperator in a cycle is to improve cycle efficiency where waste heat is recovered leading to less extraction of heat from the source fluid (Valdimarsson, 2010). In geothermal, this helps in case where source fluid presents high potential of silica scaling driven by fluid chemistry. The recuperator helps to improve the reinjection temperature. However, the inclusion of a recuperator which is another heat exchanger, introduces additional pressure loss at the turbine exit leading to reduction in power output as the turbine exit operates at higher pressure than in a case without a recuperator. Without considering pressure drops in heat exchangers, the determined reinjection temperature for this study shows that working with a wet cooled basic binary achieves almost the same results as the wet cooled recuperative model. This would mean that incorporating heat exchanger pressure losses in the models would introduces more pressure instabilities in the recuperative model than the basic model. This work therefore recommends implementation of a wet cooled basic binary model as the most ideal model for Chiweta geothermal field in Malawi. The recommended model comes second to the wet cooled recuperative model in both technical and economic analysis with small differences such as producing 10 MW at 14.06% parasitic load unlike 13.62% for the wet cooled recuperative. Per kW cost of production of wet cooled basic binary is 0.74% more than the wet cooled recuperative, meaning their cost is almost the same but would differ in terms of cycle stability in light of pressure drops in heat exchangers. The total cost of wet cooled basic binary is US $49.5 million which can be recovered in 17 years. Further studies that include pressure drops in the heat exchangers are recommended.

With emerging technologies, the fluid at temperature of 180°C, may be flashed and the flashed steam used for vaporizing the working fluid while the liquid used for preheating. Depending on the actual characteristics of the field this model may be further analysed if it can be applicable for Chiweta. The analysis may also dwell on incorporating a flash plant to use the steam and the binary in the event that Chiweta field proves to be much better for just a binary plant.

Binary cycle plants use flammable working fluids as discussed in the choice of working fluid section. This study has not included safety and mitigation of the working fluid in an emergency. Further studies are recommended to incorporate technical requirements for fire-fighting equipment and their cost implications to the model.

It is also recommended for more resource assessment studies to be done for the Chiweta field, especially sub surface studies, in order to obtain real data for a better model of a power plant to be implemented. This will assist in improving the models in such areas as restriction of reinjection temperature where more energy can be extracted from the resource for utilization.

The recommended model will use water from either Lake Malawi or the North Rumphi River. The proposed area of the model has settlements within the vicinity that would be affected by the development of the model. As such, it is recommended that a detailed Environmental Impact Assessment (EIA) for developing the model be considered prior to model development as required by the Environmental Act of Malawi. This will ensure that appropriate mitigation measures in the form of Environmental Management Plan be developed, addressing any impacts that may arise from developing the model in the area.

REFERENCES

Ahangar, F., 2012: Feasibilty study of developing a binary power plant in the low-temperature geothermal field in Puga, Jammu and Kashmir, India. Report 6 in: *Geothermal training in Iceland 2012*. UNU-GTP, Iceland, 1-24.

Ashwood, A., and Bharathan, D., 2011: *Hybrid cooling systems for low-temperature geothermal power production*. US DoE, NREL, Colorado, Technical Report NREL/TP-5500-48765, 74 pp.

Bao J. and Zhao L., 2013: A review of working fluid and expander selections for organic Rankine cycle. *Renewable and Sustainable Energy Reviews, 24,* 325-342.

Bertani, R., 2010: Geothermal power generation in the world, 2005–2010, update report*. Proceedings of the World Geothermal Congress 2010, Bali, Indonesia,* 41 pp.

BLS, 2015: *Databases, tables and calculators by subject*. Bureau of Labour Statistics. Department of Labour, USA, webpage: *www.bls.gov/data/inflation_calculator.htm* [Accessed 04 December 2015].

Brown, K., 2013: *Mineral scaling in geothermal power production*. UNU-GTP, Reykjavik, Iceland, report 39, 30 pp.

Chorowicz, J., 2005. The East African rift system. *J. African Earth Science, 43*, 379-410.

Climate Data, 2015*: Climate Chiweta.* Climate Data, webpage: *en.climate-data.org/location/207402/.*

ClimaTemps.com, 2015: *Karonga climatemp*, webpage: *www.karonga.climatemps.com/humidity.php.*

Cooling Tower Depot, 2015: *Cooling tower optimization.* Cooling Tower Depot, webpage: *www.coolingtowerdepot.com/content/depot/cooling-tower-optimization* [Accessed 10 12 2015].

Copeland, T., and Weston, J., 1986: *Financial theory and corporate policy*. Addison-Wesley Publ. Co., Reading, Massachusetts, 958 pp.

Dickson, M., and Fanelli, M., 2003: *Geothermal energy: utilization and technology*. UNESCO, Paris, France.

DiPippo, R., 1985: A simplified method for estimating the silica scaling potential in geothermal power plants. *Geothermal Resources Council, Bulletin, May 1985*, 3-9.

DiPippo, R., 1999: Small geothermal power plants: design, performance and economic. *Geo-Heat Center Bulletin, June 1999*, 1-8.

DiPippo, R., 2012: *Geothermal power plants: principles, applications, case studies and environmental impact* (3rd Ed.). Elsevier, Oxford, UK.

DoE, 2003: *National energy policy of Malawi*. Department of Energy Affairs, Zomba, Malawi, Government Printers, Malawi Government.

Dulanya, Z., Morales-Simfors, N. and Sivertun, A., 2010: A comparison between silica and cation geothermometry of the Malawi hot springs. P*roceedings of the World Geothermal Congress 2010, Bali, Indonesia,* 6 pp.

Elíasson, E., Thórhallsson, S. and Steingrímsson, B., 2008: Geothermal power plants. *Papers presented at "Short Course on Geothermal Project Management and Development", organized by UNU-GTP, KenGen and MEMD-DGSM, Entebbe, Uganda,* 15 pp.

Eliyasi, C., 2015: *Geothermal potential mapping of northern Malawi using remote sensing and geological data intergration*. University of Twente, MSc thesis, Enschede, Netherlands.

Energy Unit, 2012: *Drilling down on geothermal potential: an assessment for Central America*. ESMAP, World Bank.

ESMAP, 2012: *Geothermal handbook: planning and financing power generation*. World Bank Group, Washington DC, USA, 160 pp.

Forsha, M.D., and Nichols, K.E., 1992: Factors affecting the capital cost of binary power plants. *Geothermal Resources Council, Bulletin, August 1992*, 261-264.

Fournier, R., and Rowe, J., 1977: The solubility of amorphous silica in water at high temperatures and high pressures. *American Mineralogist, 62*, 1052-1056.

Frick, S., Kranz, S. and Saadat, A., 2015: Improving the annual net power output of geothermal binary power plants. *Proceedings of the World Geothermal Congress 2015, Melbourne, Australia*, 9 pp.

GDC, 2010: *Assessment of the geothermal potential of Malawi (unpublished)*. Geothermal Development Company – Kenya, report prepared for Geothermal Projects Ltd., Lilongwe, Malawi.

Gondwe, K., Allen, A., Georgsson, L.S., Loga, U., Tsokonombwe, G., 2012: Geothermal development in Malawi – a Country Update. *Proceedings of the 4th African Rift Geothermal Conference - Nairobi, Kenya.*

Hance, C., 2005: *Factors affecting costs of geothermal power development*. Geothermal Energy Association, Washington D.C.

Hardarson, B., 2014: Structural geology of the western branch of the East African Rift: tectonics, volcanology and geothermal activity. *Presented at Short Course IX on Exploration for Geothermal Resources", organized by UNU-GTP, GDC and KenGen, in Naivasha, Kenya, UNU-GTP SC-19,* 14 pp.

Hettiarachchi, H., Golubovic, M., Worek, W., and Ikegami, Y., 2007: Optimum design criteria for an Organic Rankine cycle using low-temperature geothermal heat sources. *Energy*, *32,* 1698-1706.

Kraml, M., Mnjokava, T., Mayalla, J. and Kabaka, K., 2010: Surface exploration of a viable geothermal resource in Mbeya Area, SW Tanzania. Part II: Geochemistry. *Proceedings of the World Geothermal Congress 2010, Bali, Indonesia,* 8 pp.

Leeper, S., 1981: *Wet cooling towers: 'Rule of thumb' design and simulation.* US Department of Energy, Idaho, USA.

Maghiar , T. and Antal, C., 2001: Power generation from low-enthalpy geothermal resources. *GeoHeat Center Bulletin, June 2001,* 35-37.

Mannvit Eng., 2012: *A Software to evaluate financial viability of geothermal projects*. Mannvit Engineering, Reykjavik, Iceland.

Marcuccilli, F. and Thiolet, D., 2010: *Optimizing binary cycles thanks to radial inflow turbines*. *Proceedings of the World Geothermal Congress 2010, Bali, Indonesia,* 9 pp.

Mburu, M., 2013: *Geothermal energy utilization*. *Presented at Short Course VIII on Exploration for Geothermal Resources", organized by UNU-GTP, GDC and KenGen, in Naivasha, Kenya*, UNU-GTP SC-17, 11 pp.

MCC-Malawi, 2015: *Investment outlook - business opportunities in the Malawi power sector*. Millenium Challenge Corp., Lilongwe, Malawi.

Mdala, H., 2015: *Determining Structural variations between the northern and southern provinces of the Malawi Rift by using automatic lineament extraction method*. University of Twente, MSc thesis, Enschede, Netherlands.

Mendrinos, D., Kontoleontos, E., and Karytsas, C., 2006: *Geothermal binary plants: water or air cooled?* ENGINE 2nd Workpackage Meeting, Strasbourg, France.

MERA, 2012: *Malawi feed-in tariff policy*, Malawi Energy Regulatory Authority, Lilongwe, Malawi.

Mines, G., Richard, C., Nathwani, J., Hanson, H., and Wood, R., 2015: Geothermal plant capacity factors. *Proceedings of the 40th Workshop on Geothermal Reservoir Engineering, Stanford University, Stanford, Ca, 8* pp.

Mlcak, H., 2002: Kalina cycle concepts for low temperature geothermal. *Geothermal Resource Council, Transactions, 26,* 707-713.

Mwagomba, T., 2013: Comparative Analysis of geothermal power plant designs suitable for Malawi's Chiweta geothermal field. Report 22 in: *Geothermal training in Iceland 2013*. UNU-GTP, Iceland, 501-530.

NSO, 2010: *Population projection Malawi*, National Statistical Office, Zomba, Malawi.

Nugroho, A., 2011: *Optimization of electrical power production from high temperature geothermal fields with respect to silica scaling problems*. University of Iceland, MSc thesis, UNU-GTP, Iceland, report 2, 49 pp.

Omenda, P., 2013: The geology and geothermal activity of the East African Rift. *Presented at Short Course VIII on Exploration for Geothermal Resources", organized by UNU-GTP, GDC and KenGen, in Naivasha, Kenya, UNU-GTP SC-17,* 18 pp.

Pritchett, J., 1996: A study of electrical generating capacities of self-discharging slim holes. *Proceedings of the 21st Workshop on Geothermal Reservoir Engineering, Stanford University, Stanford, Ca,* 55-66.

Programme U, 2015: *Encyclopaedia of Earth, Lake Malawi*. Website: *www.eoearth.org/view/article/154128*

Ragnarsson, A., 2006: *Geothermal utilization, direct use and power generation*. Paper presented at Geothermal Workshop Nicaragua.

Saemundsson, K., Axelsson, G., and Steingrimsson, B., 2011: Geothermal systems in global perspective. *Presented at „Short Course on Geothermal Drilling, Resource Development and Power Plants" organized by UNU-GTP and LaGeo, in Santa Tecla, El Salvador*, 13 pp.

Saleh, B., Koglbauer, G., Wendland, M. and Fischer, J., 2007: Working fluids for low-temperature organic Rankine cycles. *Energy, 32*, 1210-1221.

Sanyal, S., 2004: Cost of geothermal power and factors that affect it. *Proceedings of the 29th Workshop on Geothermal Reservoir Engineering, Stanford University, Stanford, Ca*, 12 pp.

Simiyu, S.M., 2010: Status of geothermal exploration in Kenya and future plans for its development. *Proceedings of the Word Geothermal Congress 2010, Bali, Indonesia,* 11 pp.

Taulo, J., Gondwe, K., and Sebitosi, A., 2015: Energy supply in Malawi: options and issues. *J. Energy in Southern Africa, 26*, 19-32.

The Federal Reserve, 2015: *Monetary policy.* Federal Reserve, webpage: *www.federalreserve.gov/monetarypolicy/files/fomcprojtabl20150318.pdf* [Accessed December 2015].

Thórhallsson, S., 2005: *Common problems faced in geothermal generation and how to deal with them. Paper presented at "Workshop for Decision Makers on Geothermal Projects and Management", organized by UNU-GTP and KengGen in Naivasha, Kenya,* 12 pp.

Ura, K., and Saitou, S., 2000: Geothermal binary power generation system. *Proceedings of the World Geothermal Congress 2000, Kyushu - Tohoku, Japan*.

US EIA, 2013: *Updated capital cost estimates for utility scale electricity generating plants.* US DoE, Washington, DC, 201 pp.

Utami, W., Herdianita, N. and Atmaja, R., 2014: The effect of temperature and pH on the formation of silica scaling of Dieng geothermal field, Central Java, Indonesia. *Proceedings of the 39th Workshop on Geothermal Reservoir Engineering. Stanford University, Stanford, Ca,*

Valdimarsson, P., 2010: Production of electricity from geothermal source. In: Popovski K. (ed.), *Geothermal energy*. MAGA, Macedonia 150-180.

VERKÍS Consulting Engineers, 2014: *Binary power plants: preliminary study of low temperature utilization, cost estimates and energy cost.* VERKÍS, Reykjavik, Iceland,

Yanagisawa, N., 2015: Case study of calcium carbonate scale at EGS and hot spring binary system. *Proceedings of the World Geothermal Congress 2015, Melbourne, Australia*, 10 pp.

APPENDIX 1: Wet cooled basic model's required vaporizer pressure and geo-fluid mass flow

a) Maximum net generator power output for wet cooled basic binary model

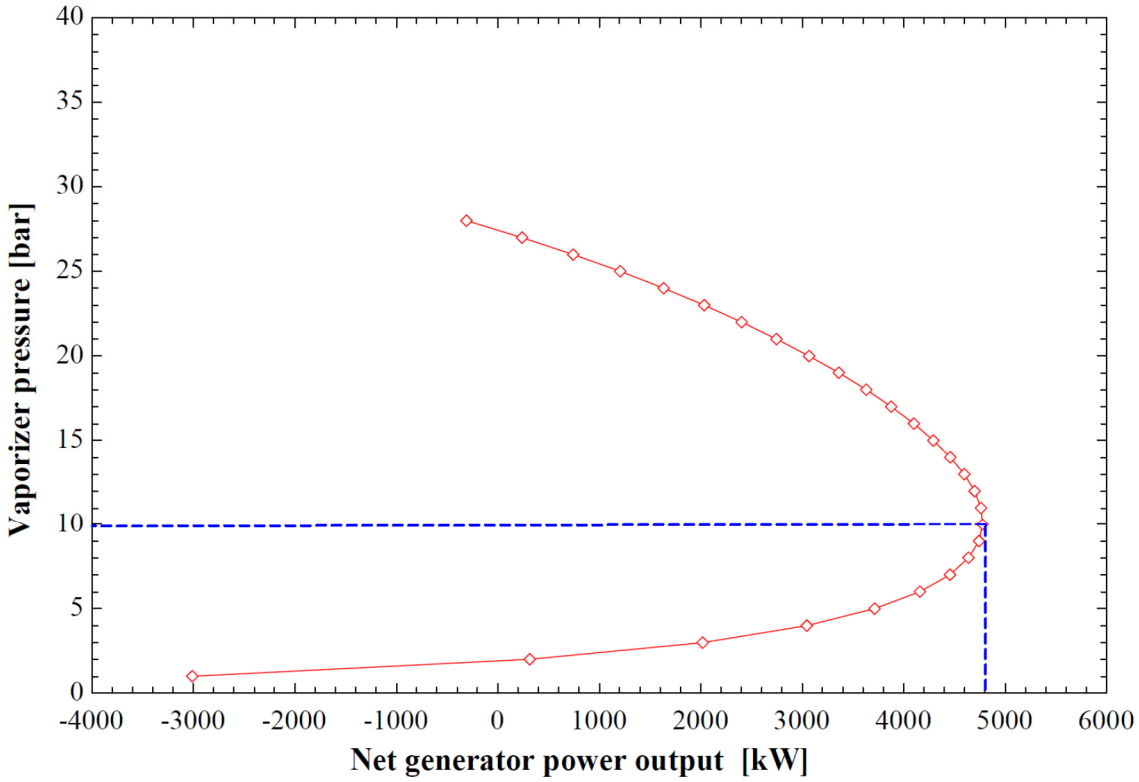

b) Optimal vaporizer pressure for wet cooled basic binary model

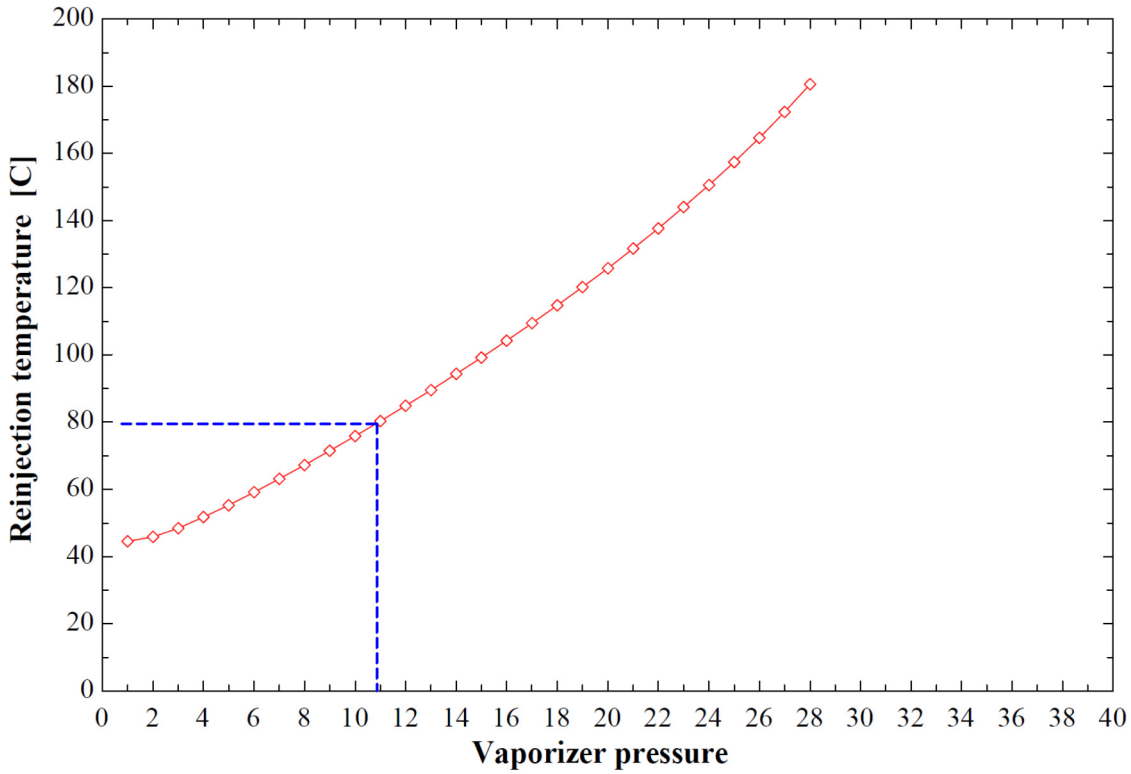

c) Required geo-fluid mass flow for wet cooled basic models

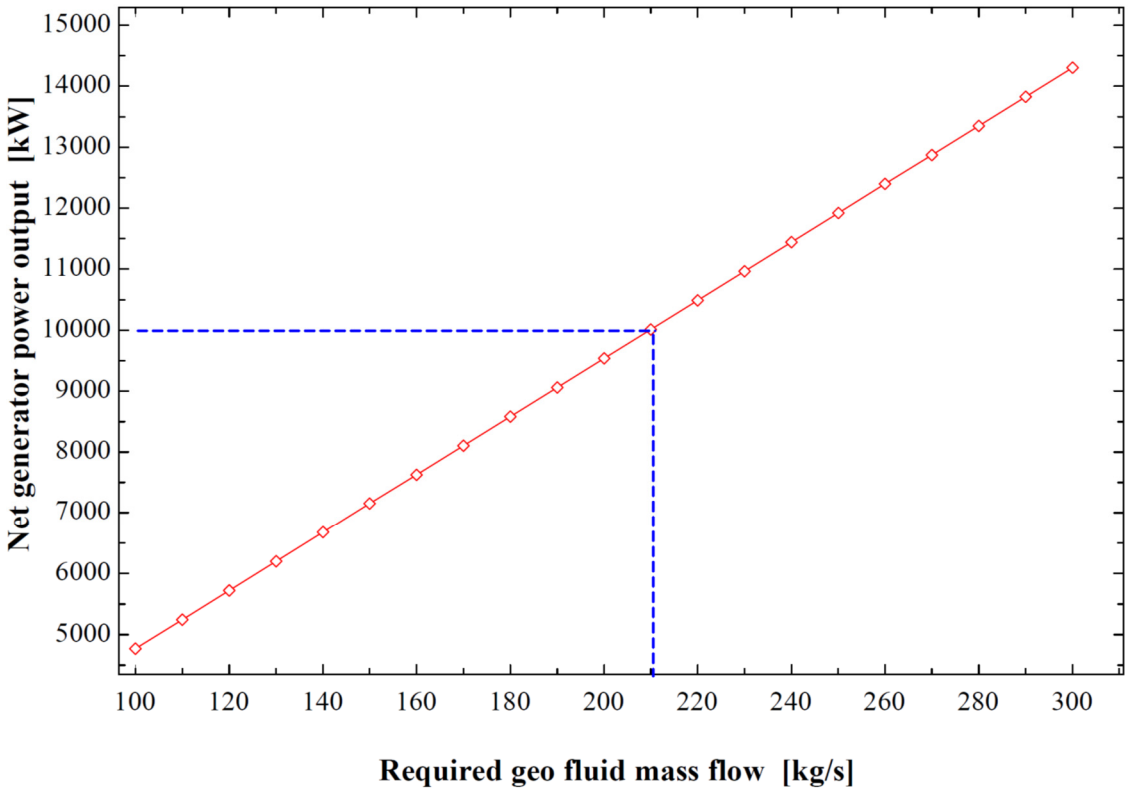

APPENDIX 2: Dry cooled recuperative model's required vaporizer pressure and geo-fluid mass flow

a) Maximum net generator power output for dry cooled recuperative binary model

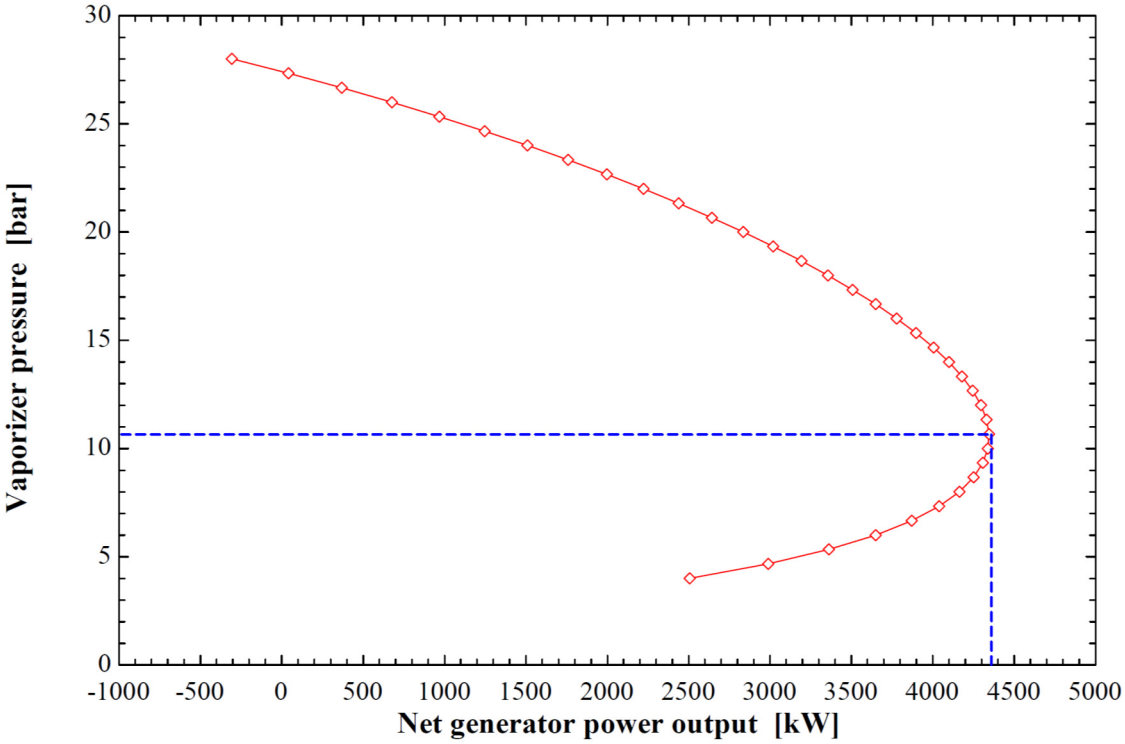

b) Optimal vaporizer pressure for dry cooled recuperative binary model

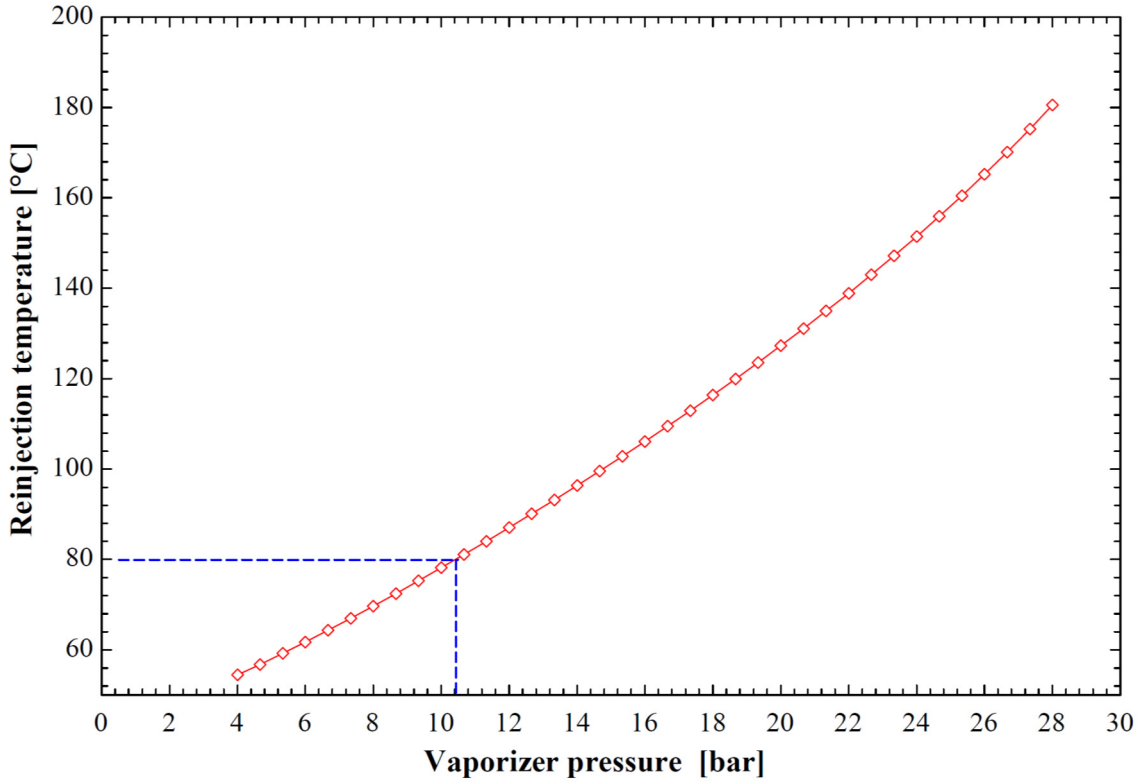

c) Required geo-fluid mass flow for dry cooled recuperative models

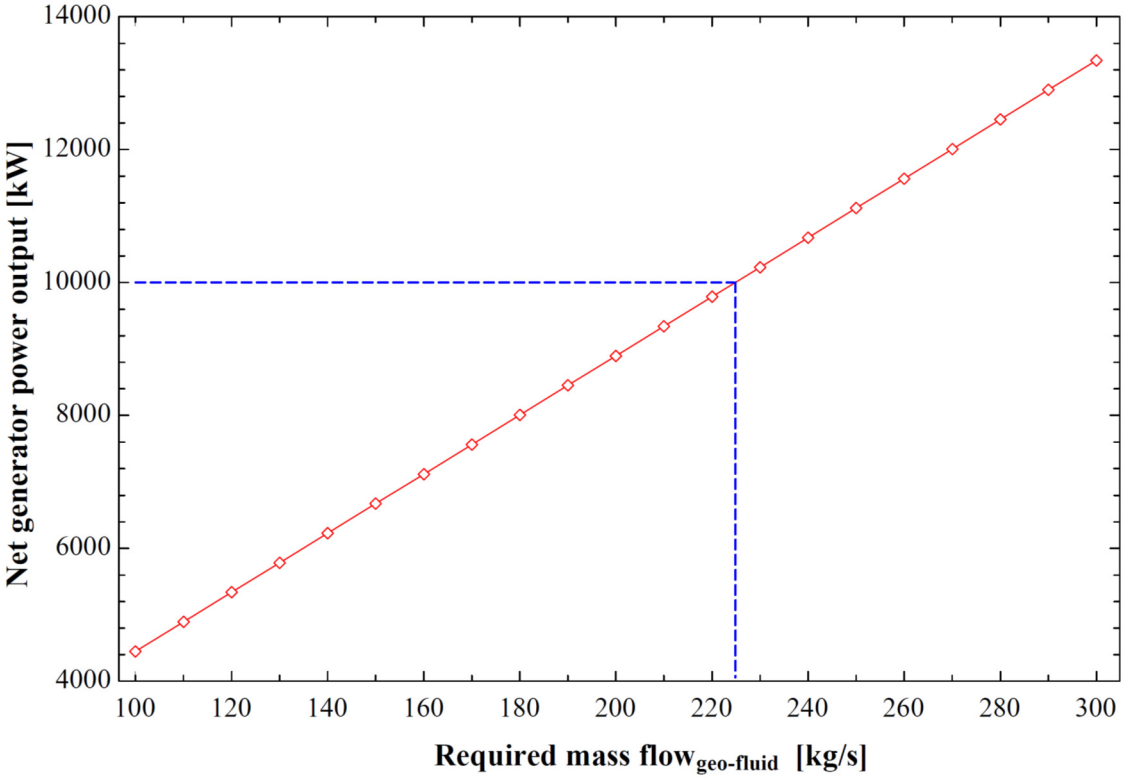

APPENDIX 3: Wet cooled recuperative model's required vaporizer pressure and geo-fluid mass flow

a) Maximum net generator power output for wet cooled recuperative binary model

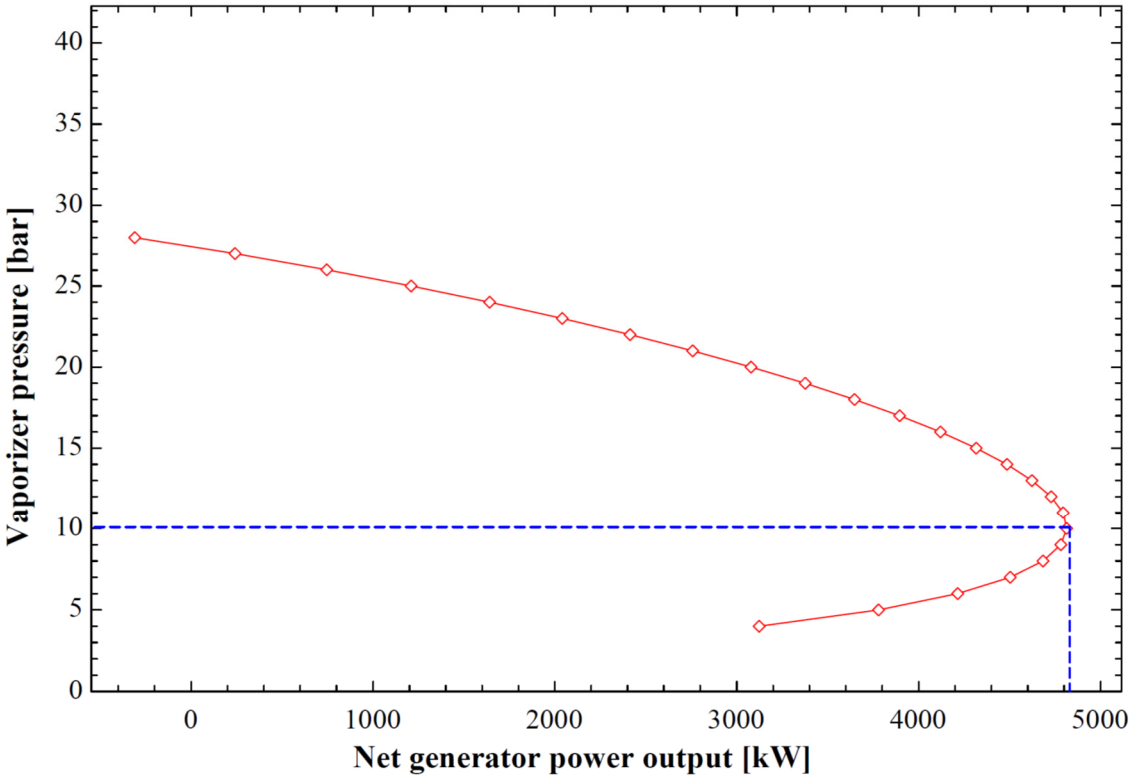

b) Optimal vaporizer pressure for wet cooled recuperative binary model

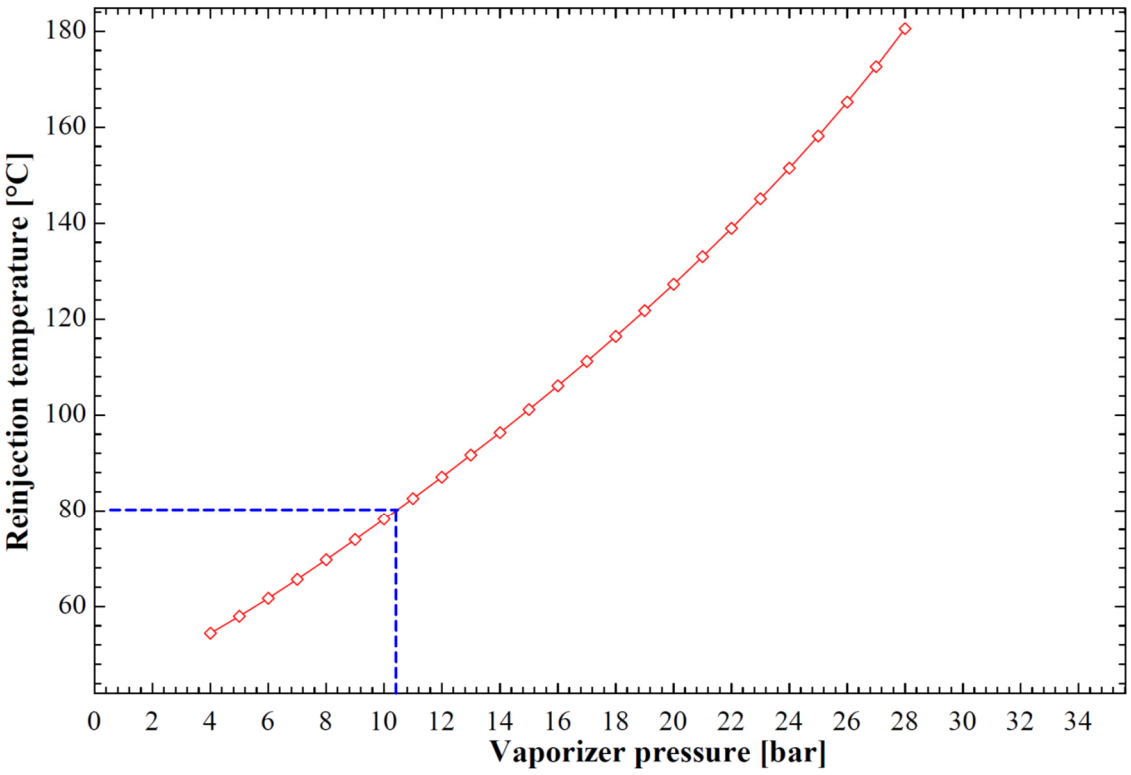

c) Required geo-fluid mass flow for wet cooled recuperative models

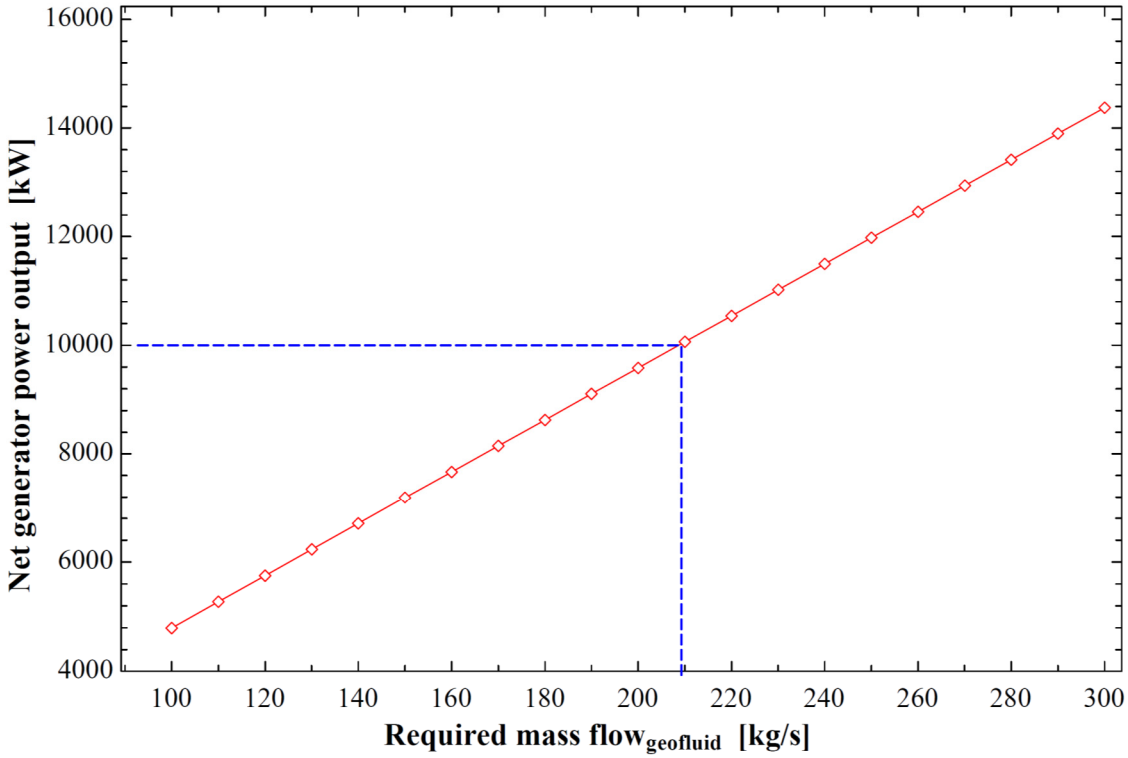

APPENDIX 4: Process flow diagram for dry cooled basic binary plant

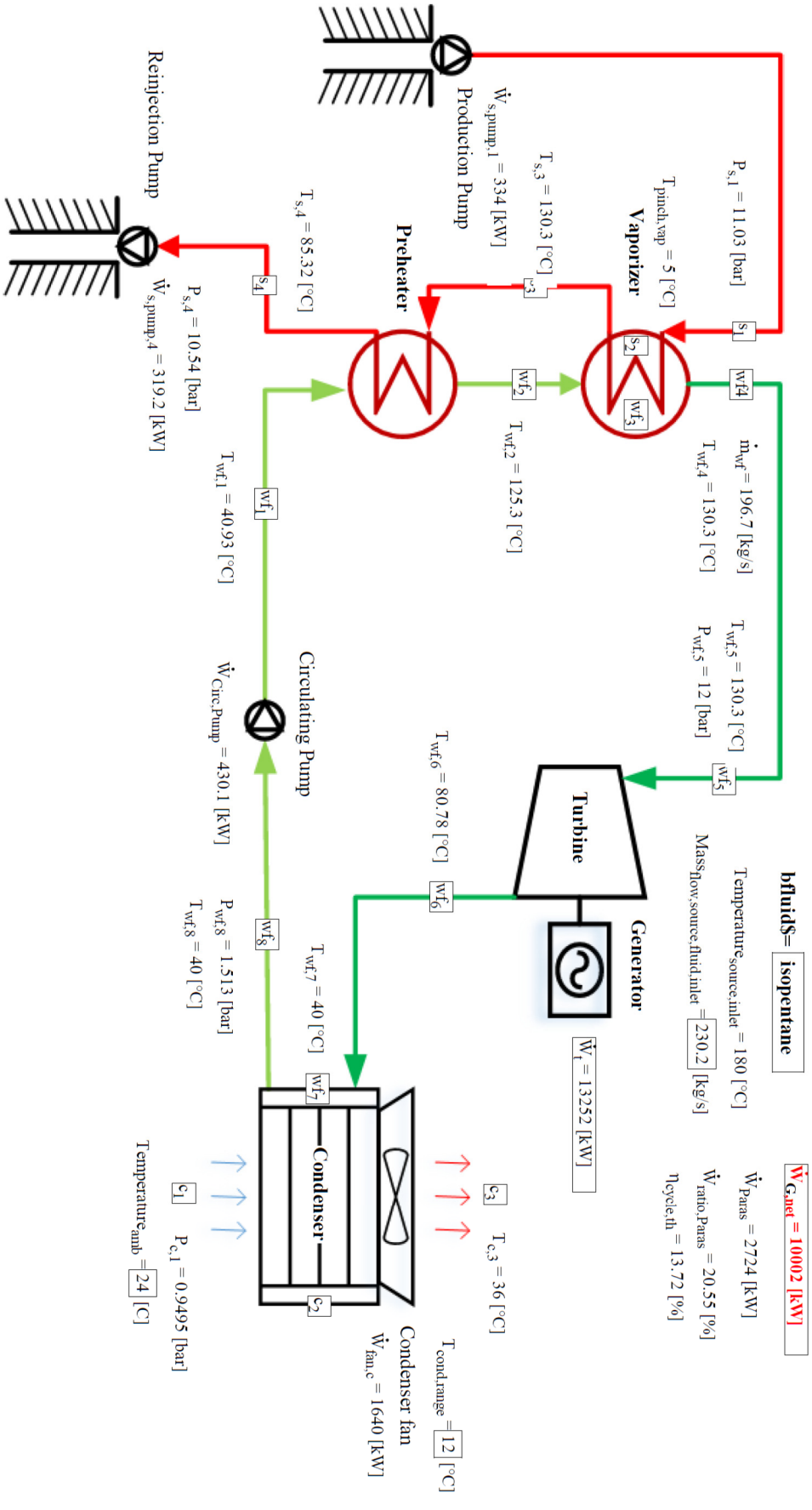

APPENDIX 5: Process flow diagram for wet cooled basic binary plant

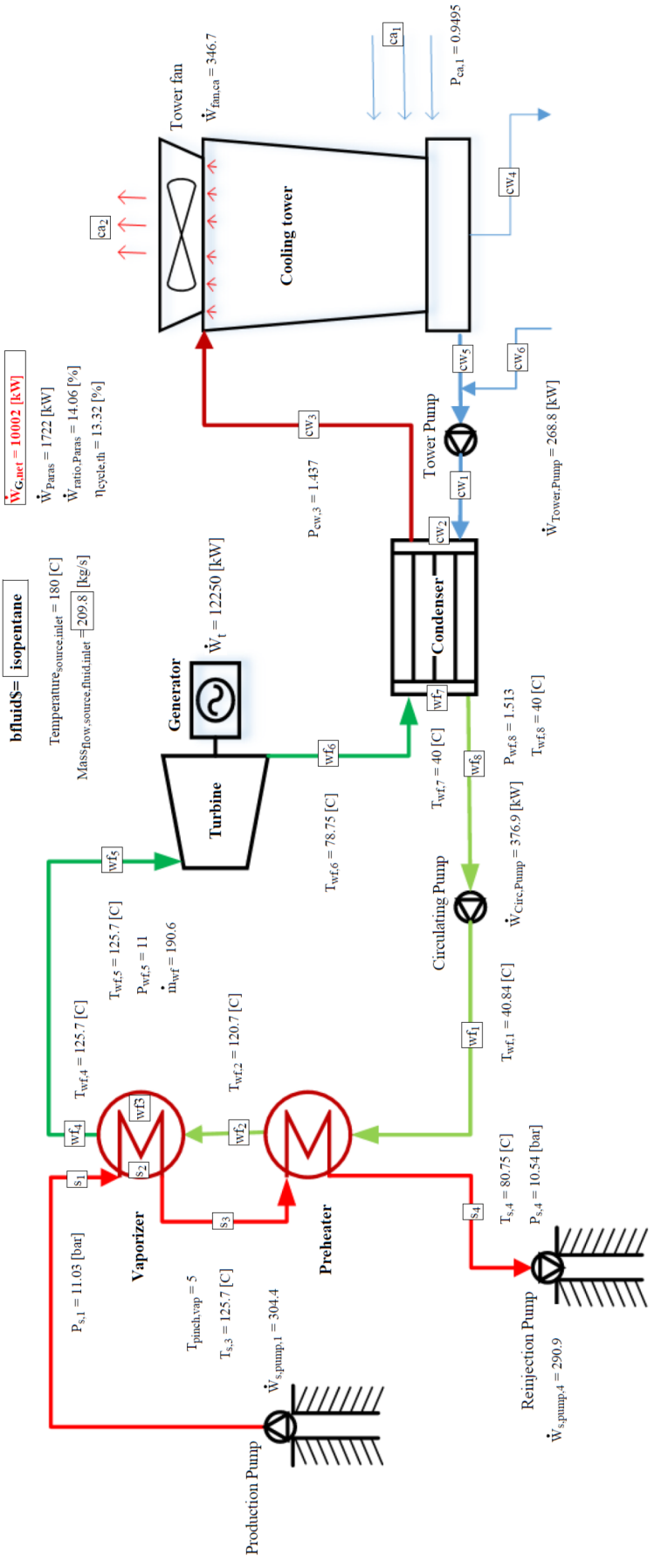

APPENDIX 6: Cycle property diagrams for wet cooled basic binary model

a) T-s diagram for wet cooled basic binary model

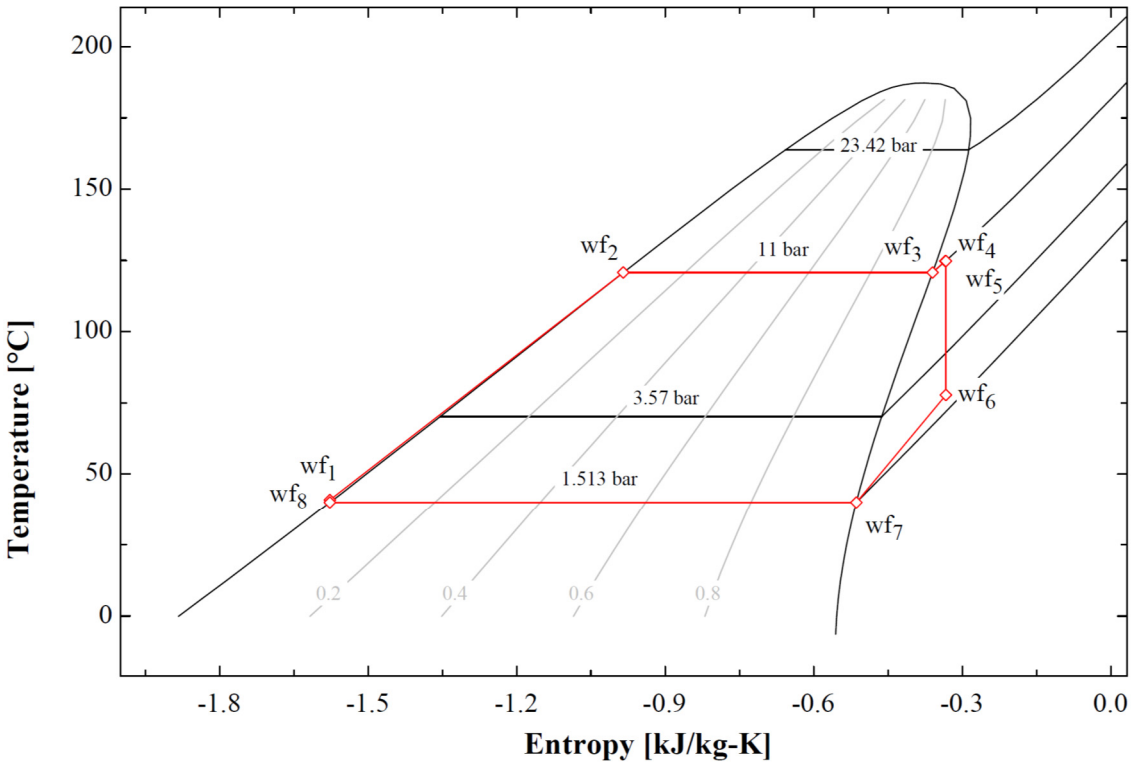

b) T-h diagram for wet cooled basic binary model

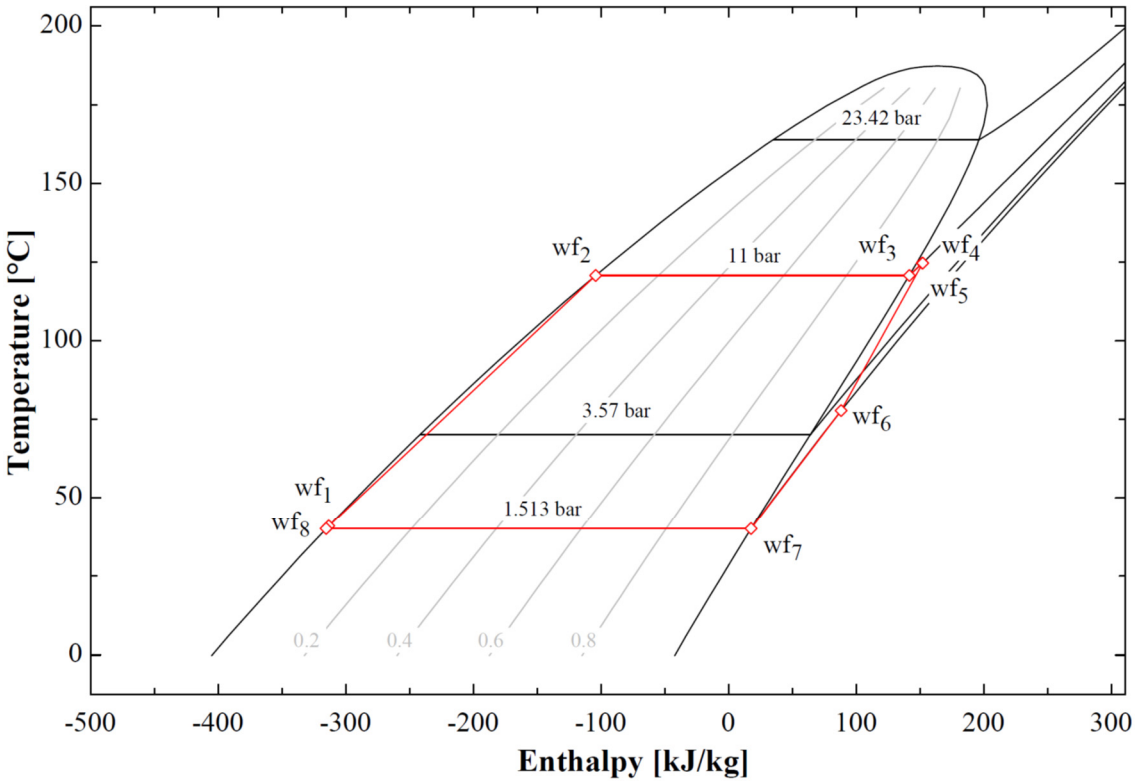

c) P-h diagram for wet cooled basic binary model

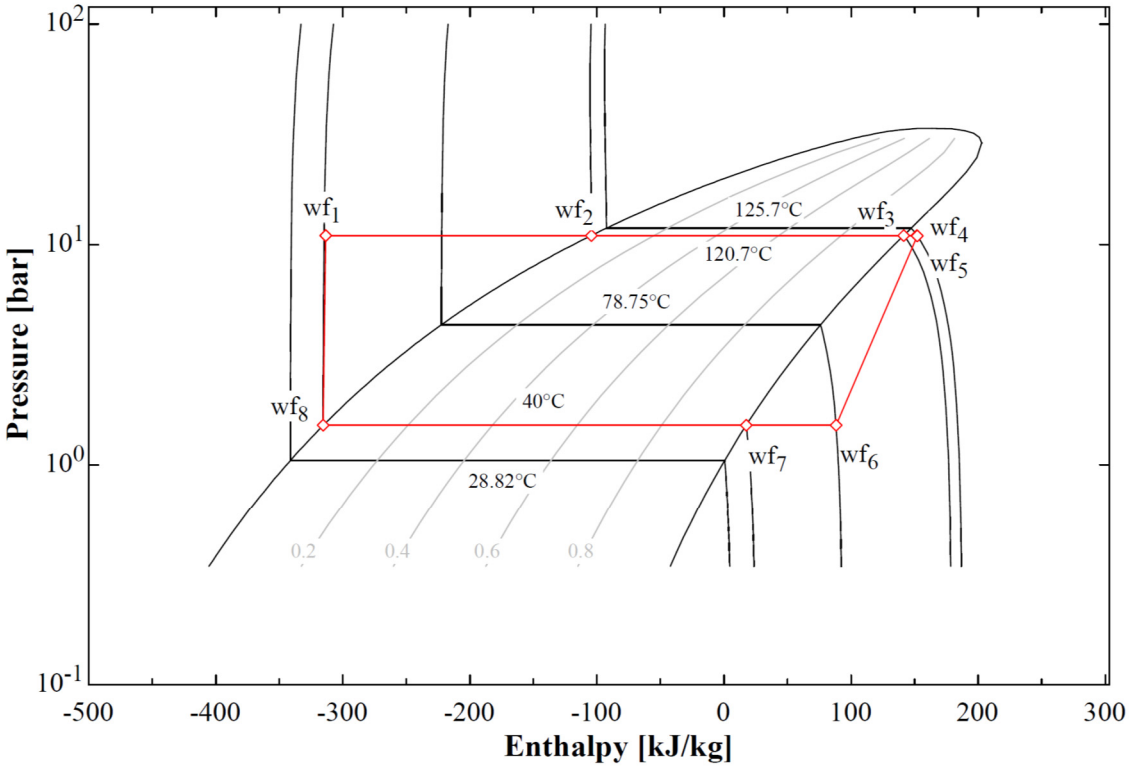

APPENDIX 7: Process flow diagram for dry cooled recuperative binary plant

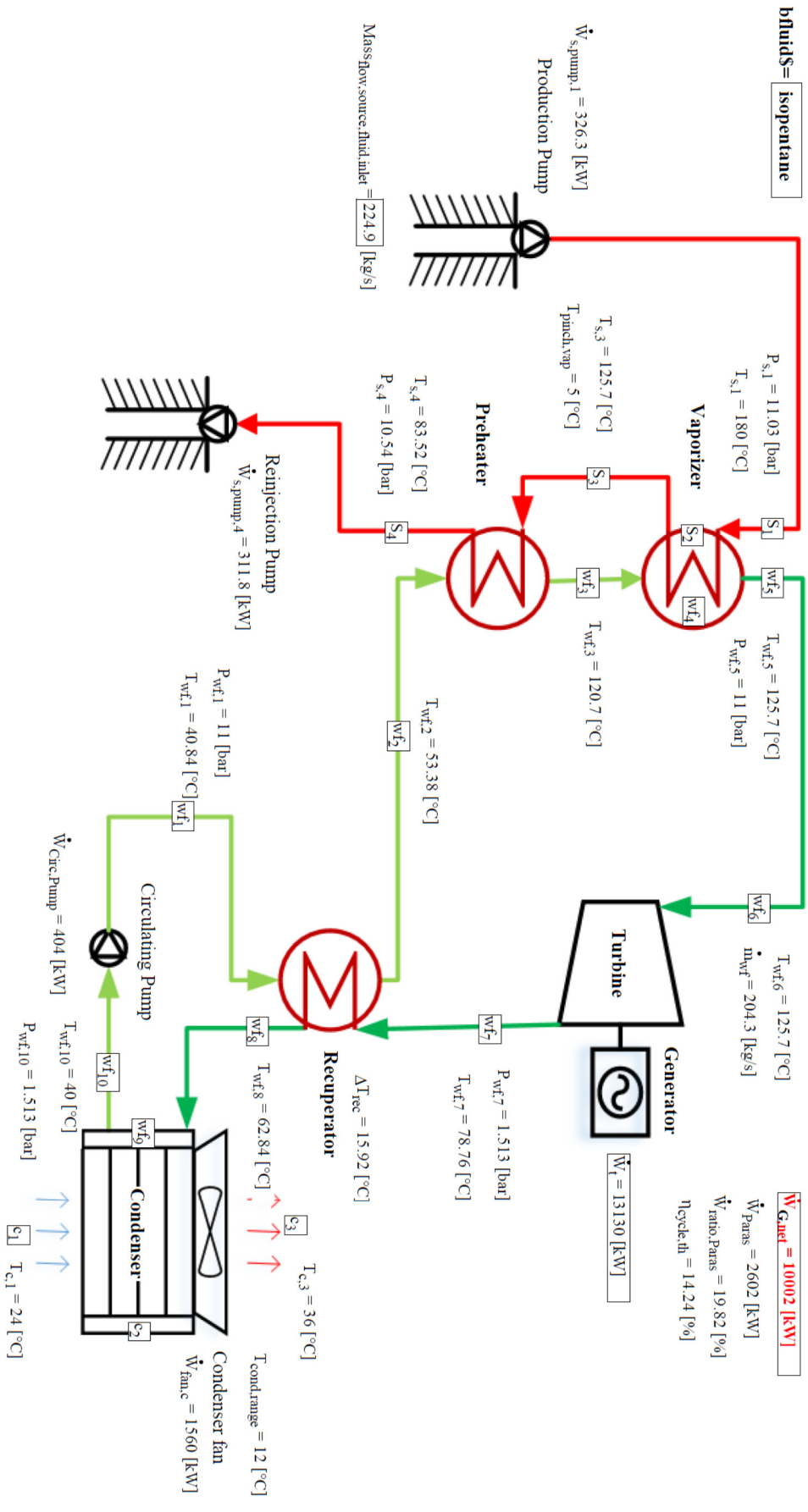

APPENDIX 8: Process flow diagram for wet cooled recuperative binary plant

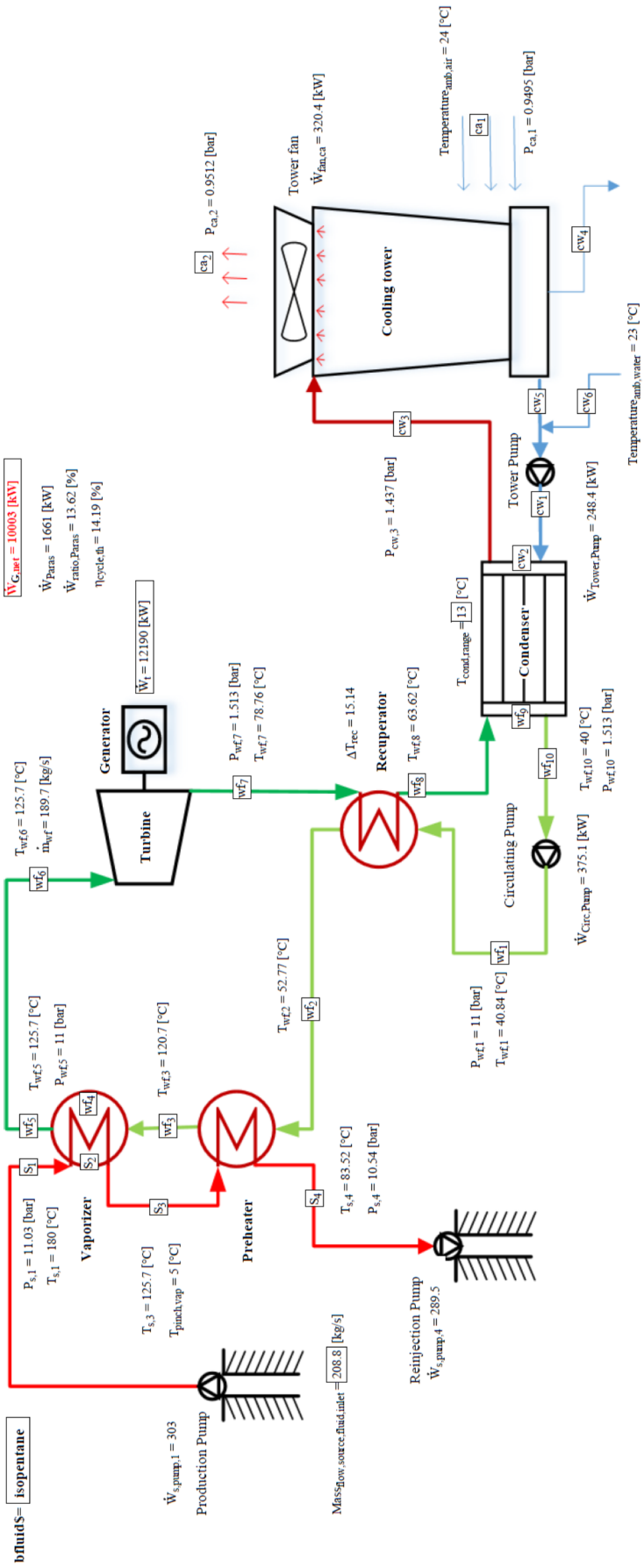

APPENDIX 9: Cycle property diagrams for wet cooled recuperative binary model

a) T-s diagram for Wet cooled recuperative binary plant

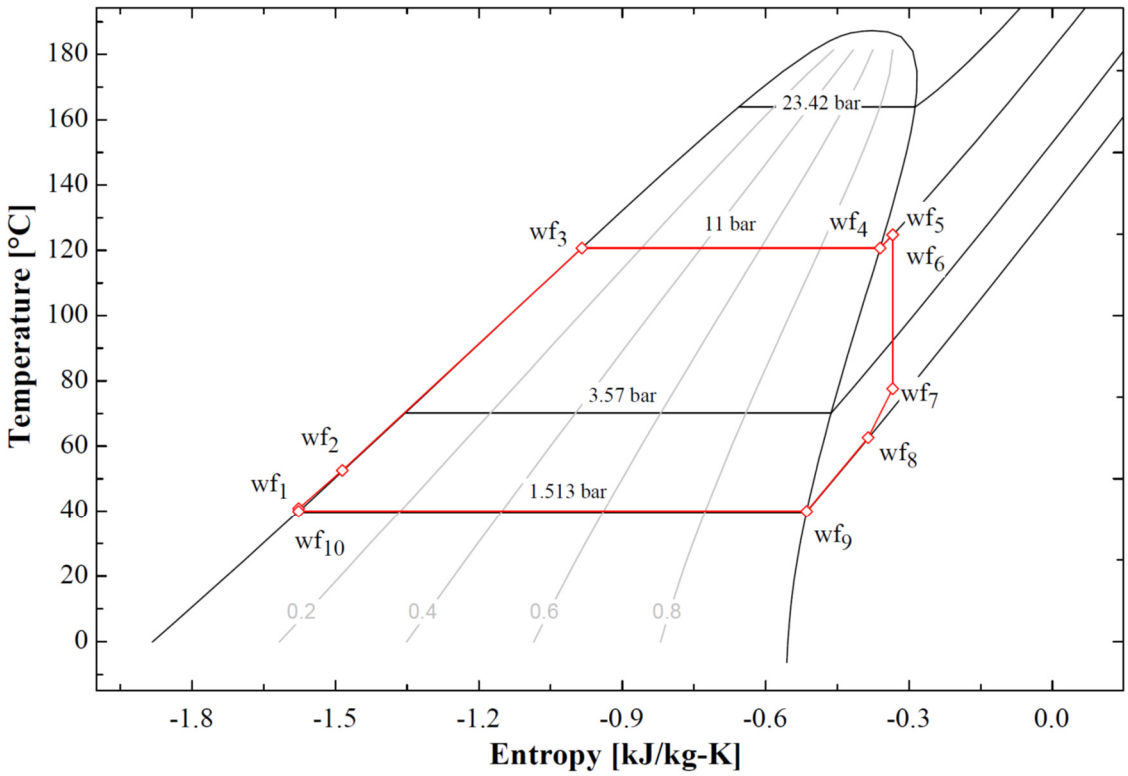

b) T-h diagram for Wet cooled recuperative binary plant

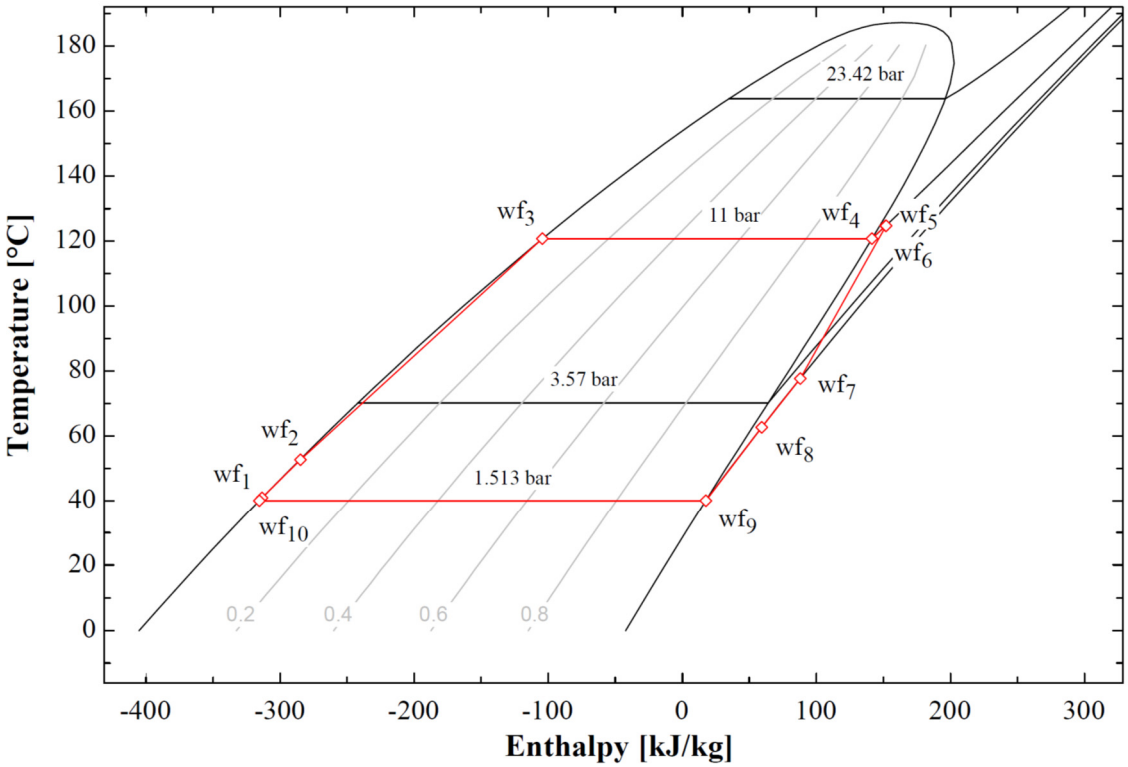

c) P-h diagram for Wet cooled recuperative binary plant

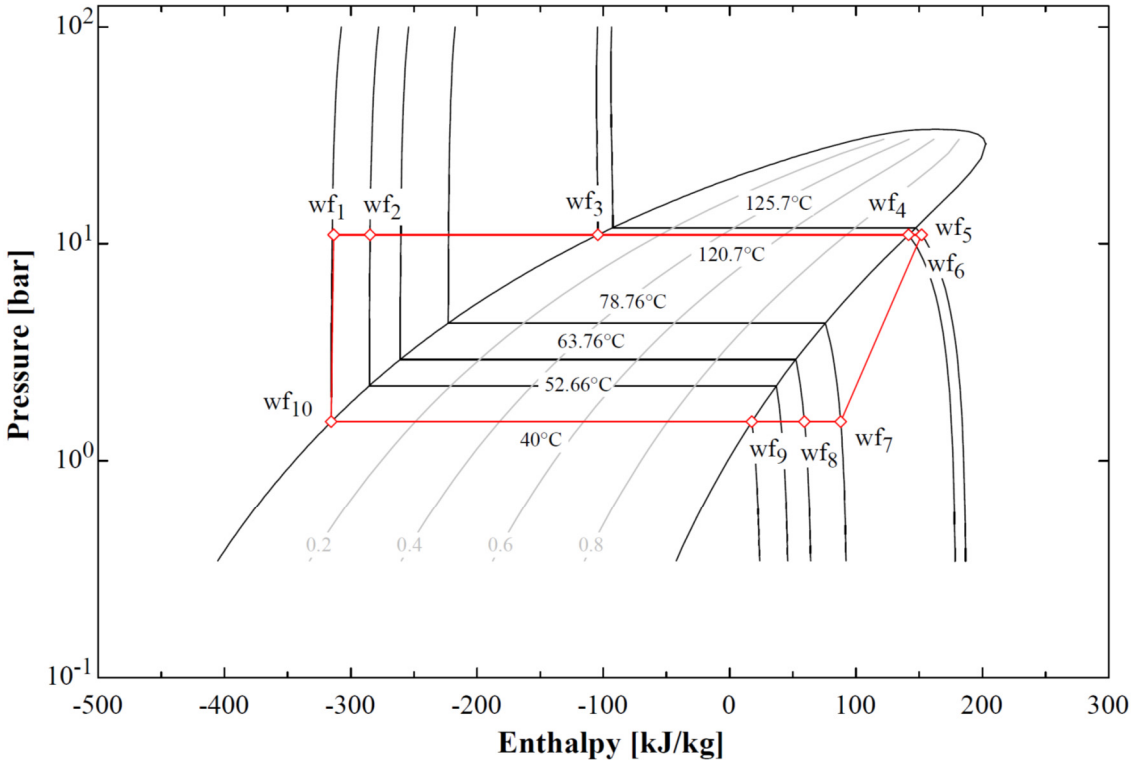

APPENDIX 10: Effect of cooling medium on cycle models

Parameters	Cooling system effect	
	Basic model	Recuperative model
Gross power	-8%	-7%
Parasitic load	-37%	-36%
Parasitic load proportion to gross power	-32%	-31%
Net power	0%	0%
Cycle efficiency	-3%	0%
Preheater area	-2%	-8%
Vaporizer area	-6%	-7%
Recuperator area	0%	-14%
Condenser area	-3%	-11%
Fan power	-79%	-79%
Pump power	27%	29%
Required geothermal fluid mass flow	-9%	-7%
Estimated number of production wells	0%	0%
Working fluid mass flow	-3%	-7%